

University of Windsor

Scholarship at UWindor

Electronic Theses and Dissertations

Theses, Dissertations, and Major Papers

7-7-2020

Development of Low Particle Emission Brake Rotors

Ran Cai

University of Windsor

Follow this and additional works at: <https://scholar.uwindsor.ca/etd>

Recommended Citation

Cai, Ran, "Development of Low Particle Emission Brake Rotors" (2020). *Electronic Theses and Dissertations*. 8349.

<https://scholar.uwindsor.ca/etd/8349>

This online database contains the full-text of PhD dissertations and Masters' theses of University of Windsor students from 1954 forward. These documents are made available for personal study and research purposes only, in accordance with the Canadian Copyright Act and the Creative Commons license—CC BY-NC-ND (Attribution, Non-Commercial, No Derivative Works). Under this license, works must always be attributed to the copyright holder (original author), cannot be used for any commercial purposes, and may not be altered. Any other use would require the permission of the copyright holder. Students may inquire about withdrawing their dissertation and/or thesis from this database. For additional inquiries, please contact the repository administrator via email (scholarship@uwindsor.ca) or by telephone at 519-253-3000ext. 3208.

Development of Low Particle Emission Brake Rotors

By

Ran Cai

A Thesis

Submitted to the Faculty of Graduate Studies
through the Department of Mechanical, Automotive & Materials Engineering
in Partial Fulfillment of the Requirements for
the Degree of Master of Applied Science
at the University of Windsor

Windsor, Ontario, Canada

2020

© 2020 Ran Cai

Development of Low Particle Emission Brake Rotors

by

Ran Cai

APPROVED BY:

G. Zhang

Department of Mechanical, Automotive & Materials Engineering

V. Stoilov

Department of Mechanical, Automotive & Materials Engineering

X. Nie, Co-Advisor

Department of Mechanical, Automotive & Materials Engineering

J. Tjong, Co-Advisor

Department of Mechanical, Automotive & Materials Engineering

May 1, 2020

DECLARATION OF CO-AUTHORSHIP / PREVIOUS PUBLICATION

I. Co-Authorship

I hereby declare that this thesis incorporates material that is result of joint research, as follows:

Chapter 4 of the thesis was co-authored with Chen Zhao under the supervision of Professor Xueyuan Nie. In all cases, the key ideas, primary contributions, experimental designs, data and analysis, interpretation, and writing were performed by the author, and the contribution of co-authors was primarily through the provision of Chen Zhao provided helps on experimental section. Chapter 5 of the thesis was co-authored with Jingzeng Zhang and D.T.A. Matthews under the supervision of Professor Xueyuan Nie and Jimi Tjong. In all cases, the key ideas, primary contributions, experimental designs, data and analysis, interpretation, and writing were performed by the author, and the contribution of co-authors was primarily through the provision of Jingzeng Zhang provided resources and administrated the project; D.T.A. Matthews contributed to the analysis and editing of the manuscript.

I am aware of the University of Windsor Senate Policy on Authorship and I certify that I have properly acknowledged the contribution of other researchers to my thesis, and have obtained written permission from each of the co-author(s) to include the above material(s) in my thesis.

I certify that, with the above qualification, this thesis, and the research to which it refers, is the product of my own work.

II. Previous Publication

This thesis includes two original papers that have been previously published/submitted for publication in peer reviewed journals, as follows:

Thesis Chapter	Publication title/full citation	Publication status
Chapter 4	Cai, Ran , Chen Zhao, and Xueyuan Nie. "Alumina-Based Coating with Dimples as Enabling Sustainable Technology To Reduce Wear and Emission of the Brake System." <i>ACS Sustainable Chemistry & Engineering</i> 8, no. 2 (2019): 893-899. doi:10.1021/acssuschemeng.9b05302.	Published
Chapter 5	Cai, Ran , Jingzeng Zhang, Xueyuan Nie, Jimi Tjong, and D.T.A. Matthews. "Wear Mechanism Evolution on Brake Discs for Reduced Wear and Particulate Emissions." <i>Wear</i> 452-453 (2020): 203283. doi:10.1016/j.wear.2020.203283.	Published

I certify that I have obtained a written permission from the copyright owner(s) to include the above published material(s) in my thesis. I certify that the above material describes work completed during my registration as a graduate student at the University of Windsor.

III. General

I declare that, to the best of my knowledge, my thesis does not infringe upon anyone's copyright nor violate any proprietary rights and that any ideas, techniques, quotations, or any other material from the work of other people included in my thesis, published or otherwise, are fully acknowledged in accordance with the standard referencing practices. Furthermore, to the extent that I have included copyrighted material that surpasses the bounds of fair dealing within the meaning of the Canada Copyright Act, I certify that I have obtained a written permission from the copyright owner(s) to include such material(s) in my thesis.

I declare that this is a true copy of my thesis, including any final revisions, as approved by my thesis committee and the Graduate Studies office, and that this thesis has not been submitted for a higher degree to any other University or Institution.

ABSTRACT

Brake wear has been recognized as one of the most significant non-exhaust traffic-related particulate matter emission sources. Conventional cast iron brake rotors/discs experience substantial wear during the braking and contribute largely to the brake wear debris emissions. To tackle this issue, surface coating on the cast iron rotors represents a trending approach. In this study, a plasma electrolytic aluminating (PEA) process was used for preparing an alumina-based ceramic coating with metallurgical bonding to the cast iron brake rotors. Three different types of brake pads (ceramic, semi-metallic and non asbestos organic (NAO)) were used as the counterparts for tribological tests. The PEA coating with a dimple-like surface promotes the formation of a thin layer transferred from the pad materials to protect the rotor from wear. Compared with uncoated cast iron rotors in the same laboratory test conditions, the coated ones also resulted in a reduced wear rate of the brake pad. The wear debris is likely transported between the secondary plateaus regenerated through compacting wear debris on the pads and the transfer layer on the PEA-coated rotors before the debris is worn off, which would reduce the brake wear emission. The dynamic formation and detachment of the secondary plateaus are responsible to the variation of COFs. The PEA coating could be a promising solution to reduce wear and emission issues and increase longevities of brake rotors for both conventional and electrical vehicles.

DEDICATION

To Mom and Dad,

Hongzeng Zhang and Xinjian Cai,

Thank you for everything you've done and loving me unconditionally.

ACKNOWLEDGEMENTS

I would like to express my sincere gratitude to Dr. Xueyuan Nie and Dr. Jimi Tjong, for providing me with the opportunity to work on this research under their instructive and excellent supervision, as well as their great encouragement and support, kindness and patience.

I would like to express my sincere thanks to the members of my committee Dr. Guoqing Zhang and Dr. Vesselin Stoilov for their invaluable discussions, suggestions and time to this thesis.

I would like to express special thanks to my group members, Mr. Chen Zhao, Mr. Guang Wang, Mr. Jiayi Sun and Miss Yuxian Li for their help and advice. I would also like to acknowledge Miss Yunyun Wu for the XRD analysis. Thanks also to everyone in the MAME Department who has offered me encouragement and support.

TABLE OF CONTENTS

DECLARATION OF CO-AUTHORSHIP / PREVIOUS PUBLICATION	iii
ABSTRACT.....	vi
DEDICATION	vii
ACKNOWLEDGEMENTS	viii
LIST OF TABLES	xiv
LIST OF FIGURES	xv
LIST OF APPENDICES.....	xix
LIST OF ABBREVIATIONS/SYMBOLS.....	xx
CHAPTER 1 INTRODUCTION	1
<i>1.1 Motivation</i>	1
<i>1.2 Objectives of This Study</i>	4
<i>1.3 Organization of the Thesis</i>	4
REFERENCES	6
CHAPTER 2 LITERATURE REVIEW	11
<i>2.1 Brake Wear Emissions</i>	11
<i>2.1.1 Particulate Matter</i>	11
<i>2.1.2 Traffic-related PM Emissions</i>	13
<i>2.1.3 Brake Wear PM Emission</i>	16
<i>2.1.4 Regenerative Braking</i>	18

2.2 Brake Rotor Materials.....	19
2.2.1 Cast Iron Brake Rotor	19
2.2.2 High Carbon Brake Rotor	20
2.2.3 Carbon-carbon and Carbon Ceramic Brake Rotor.....	21
2.3 Brake Pad Materials	22
2.3.1 Frictional Materials	22
2.3.2 Ceramic Pad	24
2.3.3 Semi-metallic Pad.....	24
2.3.4 NAO Pad.....	25
2.4 Coatings on Brake Rotors	26
2.4.1 Hard Chrome Plated Coating.....	26
2.4.2 Laser Cladded Coating.....	27
2.4.3 Thermal Spray Coating	27
2.5 Brake Tests	29
2.5.1 Tribological Tests (Dynamometer vs PoD Tests).....	29
2.5.2 Brake Wear Emission Measurements	29
REFERENCES	31
CHAPTER 3 EXPERIMENTAL DETAILS	47
3.1 Preparation of PEA Coating on Cast Iron.....	47
3.1.1 Cast Iron Materials	47

3.1.2 Preparation of PEA Coating	47
3.2 Tribological Tests.....	49
3.3 Surface Profile Measurement.....	50
3.4 Surface Hardness Measurement	51
3.5 Characterization of Morphology and Elemental Distribution.....	52
REFERENCES	55
CHAPTER 4 ALUMINA-BASED COATING WITH DIMPLES AS ENABLING SUSTAINABLE TECHNOLOGY TO REDUCE WEAR AND EMISSION OF BRAKE SYSTEM	57
4.1 Introduction.....	57
4.2 Experimental Details.....	59
4.3 Results and Discussion.....	60
4.3.1 Alumina-based Coating and Pad Materials	60
4.3.2 Surface Morphology	63
4.3.3 Tribological Behaviors	66
4.3.4 Transformation of Wear Mechanism.....	69
4.4 Conclusions	74
REFERENCES	76
CHAPTER 5 WEAR MECHANISM EVOLUTION ON BRAKE DISCS FOR REDUCED WEAR AND PARTICULATE EMISSIONS.....	80
5.1 Introduction.....	80
5.2 Experimental Details.....	83

5.3 Results and Discussion.....	85
5.3.1 PEA-treated Surface and Pad Material.....	85
5.3.2 Surface Morphology of Wear Tracks.....	89
5.3.3 Tribological Behaviors	94
5.4 Conclusions	102
REFERENCES	103
CHAPTER 6 WEAR PERFORMANCES OF GRAY CAST IRON BRAKE ROTOR WITH PLASMA ELECTROLYTIC ALUMINATING COATING AGAINST DIFFERENT PADS	109
6.1 Introduction	109
6.2 Experimental Details.....	110
6.3 Results and Discussion.....	111
6.3.1 PEA Coating and Pad Materials	111
6.3.2 Surface Morphology of Wear Tracks.....	117
6.3.3 Tribological Behaviors	120
6.4 Conclusions	125
REFERENCES	127
CHAPTER 7 CONCLUSIONS AND FUTURE WORK.....	131
7.1 PEA Coating on Cast Iron	131
7.2 Effects of PEA Coating on Cast Iron Rotors.....	131
7.2.1 Surface Morphology of PEA-coated Cast Iron Rotors.....	131
7.2.2 Wear of PEA-coated Cast Iron Rotors	132

<i>7.3 Effects of PEA Coating on Brake Pads</i>	<i>133</i>
<i>7.3.1 Surface Morphology of Brake Pads.....</i>	<i>133</i>
<i>7.3.2 Wear of Brake Pads.....</i>	<i>134</i>
<i>7.4 Effects of PEA Coating on Wear Particles.....</i>	<i>134</i>
<i>7.5 Tribological Effects of PEA Coating.....</i>	<i>135</i>
<i>7.5.1 Pad Wear Variation and COF Alteration.....</i>	<i>135</i>
<i>7.5.2 Wear Mechanism on PEA Coating.....</i>	<i>135</i>
<i>7.6 Future Work</i>	<i>136</i>
APPENDICES	138
Appendix A	138
Appendix B	139
VITA AUCTORIS	140

LIST OF TABLES

Table 3.1 Chemical composition and properties of cast irons.	47
Table 4.1. Elemental composition of different surfaces as determined using EDX	62
Table 4.2. Surface properties of the samples after tribotests with different sliding distances	65
Table 5.1. Typical surface properties of the samples before and after tribotests....	87
Table 6.1. Main friction materials in ceramic, semi-metallic and NAO brake pads.	117
Table 6.2. Surface roughness of the samples before and after tribotests.	118

LIST OF FIGURES

Figure 2.1 Size comparisons for PM particles [1].	11
Figure 2.2 Deposition potential for PM particles of varying sizes.	12
Figure 2.3 PM _{2.5} emissions from road transport sources according to the UK and German inventories. The scale on the y-axis applies to both countries [10].	15
Figure 2.4 PM ₁₀ emissions from road transport sources according to the UK and German inventories. The scale on the y-axis applies to both countries [10].	16
Figure 2.5 Corrosions on different kinds of commercial automotive brake rotors.	26
Figure 2.6 Porsche Surface Coated Brake (PSCB) disc [88].	28
Figure 2.7 Scheme of the brake dynamometer assembly and measurement instruments [31].	30
Figure 3.1 Schematic drawing of instrument.	48
Figure 3.2 Schematic drawing of Pin-on-Disc test	50
Figure 3.3 Mitutoyo SJ-201P surface profilometer [5].	51
Figure 3.4 Buehler MicroMet II micro-hardness tester [6].	52
Figure 3.5 Tabletop Microscope TM3030 [7].	53
Figure 3.6 Bruker QUANTAX EDS for SEM [8].	53
Figure 3.7 PROTO AXRD BENCHTOP [9].	54

Figure 4.1. SEM images showing morphology of PEA coating: (a) coating surface and (b) cross section.....	61
Figure 4.2. XRD pattern of a PEA coating on cast iron.	61
Figure 4.3. SEM images showing surface morphology of samples: (a) original polished coating; wear track on coating after test sliding distance of (b) 4×50 m and (c) 1000 m; (d) original polished cast iron; wear track on cast iron after test sliding distance of (e) 4×50 m and (f) 1000 m.	64
Figure 4.4. Sectional profile and surface morphology of wear track and polished surface of PEA coating.	66
Figure 4.5. Coefficients of friction of PEA coating and cast iron under different sliding distance: (a) 4×50 m; (b) 1000 m.....	67
Figure 4.6. Wear (upper) and SEM images (lower) of brake pad under different testing condition: (a) cast iron after 4×50 m; (b) PEA coating after 4×50 m; (c) cast iron after 1000 m; (d) PEA coating after 1000 m.	69
Figure 4.7. Cross-sectional SEM images of the frictional surface of PEA-coated brake rotor: (a) mounting material; (b) transfer layer; (c) PEA coating; (d) cast iron.	71
Figure 4.8. Friction process model with regard to PEA-coated and uncoated cast iron brake rotors.	73

Figure 5.1. (a) SEM images showing surface morphology of lightly polished PEA-treated surface; (b) XRD pattern of a PEA-treated surface on cast iron; (c) SEM images showing cross section of PEA-treated cast iron.	86
Figure 5.2. SEM images and EDX of brake pads under different testing conditions: (a, d) original pad surface; (b, e) sliding on cast iron; (c, f) sliding on PEA-treated cast iron, respectively.....	88
Figure 5.3. SEM images: PEA-treated surface - (a) original polished and (b) wear track after test; untreated cast iron - (c) original polished and (d) wear track after test; wear debris collected from (e, f) treated and (g, h) untreated discs.	90
Figure 5.4. SEM images showing: (a-e) surface morphology and related elements detected in the wear track of PEA-treated surface after testing; (f) cross-sectional wear track on the PEA-treated surface after the tribotest.	93
Figure 5.5. (a) Coefficients of friction with insert of sectional profiles of wear tracks, (b) wear of the brake pads, and (c) wear rates of PEA-treated and untreated discs.....	95
Figure 5.6. (a) Friction process model with regards to PEA-treated cast iron brake discs; (b) the schematic of transfer layers on (i) the NAO pad, (ii) a semi-metallic pad, and (iii) a ceramic pad tested at low temperature.	99
Figure 6.1. (a) SEM image showing surface morphology of lightly polished PEA coating; (b) SEM image showing dimples of the PEA coating.	112

Figure 6.2. SEM images of ceramic pad surface (a) before and (b) after tribotests; (c) EDX analysis of original ceramic pad surface.	114
Figure 6.3. SEM images of semi-metallic pad surface (a) before and (b) after tribotests; (c) EDX analysis of original semi-metallic pad surface.	115
Figure 6.4. SEM images of NAO pad surface (a) before and (b) after tribotests; (c) EDX analysis of original NAO pad surface.....	116
Figure 6.5. SEM images of wear tracks on the PEA coatings after tribotests against (a, b) ceramic pad, (c, d) semi-metallic pad and (e, f) NAO pad in (left) back- scattered electrons (BSE) and (right) secondary electrons (SE).	118
Figure 6.6. COFs of 5 repeated tribotests for PEA coating against (a, b) ceramic pad, (c, d) semi-metallic pad and (e, f) NAO pad.....	120
Figure 6.7. Wear of the ceramic, semi-metallic and NAO pads after tribotests against PEA coating in (a) total and (b) average.	121
Figure 6.8. The schematic of the secondary plateaus on (a) the ceramic pad, (b) the semi-metallic pad, and (c) the NAO pad; (d) friction process model with regards to the PEA-coated brake rotor.....	123

LIST OF APPENDICES

Appendix A	138
Appendix B	139

LIST OF ABBREVIATIONS/SYMBOLS

PEA	plasma electrolytic aluminating
NAO	non asbestos organic
COF	coefficients of friction
PM	particulate matter
PEO	plasma electrolytic oxidation
SEM	scanning electron microscope
EDX	energy dispersive X-ray detector
XRD	X-ray diffractometer
R _a	average roughness
R _{pk}	reduced peak height
R _{vk}	reduced valley height
PoD	Pin-on-Disc
APS	atmospheric plasma spray
HVOF	high velocity oxy-fuel
HVAF	high velocity air fuel
SPS	suspension plasma spraying

FAST	friction assessment screening test
CVS	constant volume sampling
HEPA	high-efficiency particulate air
NVH	noise, vibration and harshness
SAE	Society of Automotive Engineers
UNECE	United Nations Economic Commission for Europe
FMVSS	Federal Motor Vehicle Safety Standards
IS	Indian Standard

CHAPTER 1

INTRODUCTION

1.1 Motivation

Particulate matter (PM) is a complex mixture of microscopic solid or liquid particles of organic and inorganic substances suspended in the ambient air [1]. The effects of inhaling PM that have been widely studied in humans include elevated risk of adverse pregnancy outcomes [2], respiratory [3] and cardiovascular diseases [4]. In addition to direct inhalation, the particulates also have impacts on climate and precipitation that adversely affect human health [5]. A significant contributor of directly emitted PM is traffic-related particles, particularly in urban environments and major cities [6]. Traffic-related PM emission can be divided in two main categories according to its source: exhaust traffic-related and non-exhaust traffic-related [7]. Non-exhaust traffic-related PM emissions are predominantly from brake wear, tire wear, road surface wear and resuspended road dust. Considering the increasing strict control on exhaust traffic-related PM emissions, the relative contribution of non-exhaust sources will become increasingly more important for total traffic-related PM emissions [8]. Brake wear is considered to be one of the most significant particulate matter (PM) contributors among non-exhaust traffic-related sources particularly within areas with high traffic density. It can contribute up to 55 % to total non-exhaust traffic-related PM₁₀ emissions by mass and up to 21% of total traffic related PM₁₀ emissions by mass in urban environments [9]. Under growing health, safety and environment (HSE) concerns, manufacturers of both combustion engine and electric vehicles are demanding cleaner braking systems. During a braking event, the brake pad slides against the brake rotor (i.e. brake disc) and transforms the vehicle's kinetic energy

into thermal energy, generating not only mechanical abrasion but also large frictional heat with subsequent wear of both pad and disc. Humps on the surface of brake rotors are pressed into the pads and debris is torn from the friction materials of the pads or sheared off from the brake rotors [10]. About 50% of wear debris generated during braking become airborne while the rest is deposited on the road surface or is attracted to the vehicle [11-13].

Cast iron is the commonly-used material for brake rotors due to its excellent thermophysical properties, high damping capability, good castability and machinability combined with cost-effectiveness [14]. However, the cast iron brake rotor also has excessive wear which leads to wear debris emissions. In these years, surface treatment in forms of coating on cast iron discs represents a trending solution to this problem. Several different types of coating process have been explored to combat problems of wear and corrosion for automotive brake rotor applications including chrome plating [15], laser cladding [16] and thermal spray processes [17]. For instance, both the Porsche Surface Coated Brake (PSCB) disc [18] from Porsche Company and the iDisc [19] from by Bosch Company adopted hard tungsten carbide coatings using a thermal spray process on cast iron substrates. The reported results are remarkable; they claim that the surface modified disc lasts up to 30% longer than its uncoated counterpart, while a 90% reduction in brake dust is also reported. However, such kinds of brake rotors are much more expensive than the normal cast iron discs. A PSCB disc costs around 3500 dollars and a Porsche Ceramic Composite Brake (PCCB) disc from the same company costs even more than 8000 dollars, while a conventional cast iron rotor only expenses around 100 dollars.

In the present study, an alternative cost-effective surface coating process called plasma electrolytic aluminating (PEA) is proposed for improving the durability and environmental performance of brake rotors. PEA is a process born from inspiration of the phosphating process and the plasma-electrolytic oxidation (PEO) process [20]. The PEO process can usually apply for valve metals such as aluminum, magnesium and titanium and their alloys [21]. Succinctly put, the PEO process utilizes a high electric voltage to induce the dielectric breakdown of a passive film on a metal surface. Subsequently, a ceramic oxide film will form on the surface. The ceramic oxide film can be tailored to provide desirable (thermo-) mechanical properties or for biomedical applications [22-24]. Unlike PEO process, PEA is used on ferrous metals and alloys. The PEA can be described as a plasma-assisted electrochemical reaction process in which a composite (hercynite-alumina) ceramic coating is deposited on a ferritic surface from an aluminate-based solution [20]. The PEA coating has a metallurgical bonding to the cast iron substrate, which is different from the thermal spraying approaches emphasizing hard surface coatings with a mechanical bonding on brake rotors.

In this study, the PEA process was utilized to obtain an alumina-based ceramic coating on cast iron brake rotors. In order to assess these tribological performance aspects of brake materials/friction pairs, generally one has a choice between a Pin-on-Disc (PoD) tester and a dynamometer. Some authors compared both the PoD and dynamometer test set-ups in dry sliding conditions and concluded that the specific wear coefficients between the PoD and dynamometer tests were “proportional to the corresponding values obtained with the PoD at room temperature”. [25] This study focused on braking at room temperature conditions and therefore considered tribological tests by PoD methodology.

Three different types of commercial pad materials (ceramic, semi-metallic and non asbestos organic (NAO)) were selected as the counterfaces to the coated disc samples. PoD tests were performed to ascertain the wear and friction performance of the PEA-coated and uncoated cast iron materials in a simulated pad disc contact. The wear rate of brake rotors and pads were measured. The alteration of wear mechanism between PEA-coated cast iron brake rotors and uncoated ones was also investigated. The focus of this work was to study the effect of the PEA coating on friction type of brake system, with the aim of minimizing wear debris emission in a brake system.

1.2 Objectives of This Study

The objectives of this study were:

- 1) To reduce brake particle production through a special surface coating on the face of a brake rotor (i.e. disc).
- 2) To use PEA process to obtain an alumina ceramic coating on a cast iron brake rotor material.
- 3) To alter wear mechanisms through the special coating surface morphology.
- 4) To measure the wear of different brake pads (ceramic, semi-metallic and NAO) for estimating the propensity of dust production of the brake pad/disc system with and without the PEA coating.

1.3 Organization of the Thesis

This thesis includes seven chapters. Chapter 1 introduces the motivation and objectives of this study. Chapter 2 is literature reviews on brake wear emissions, brake rotor and pad

materials, different kinds of coatings on brake rotors and tests of brake system. Chapter 3 describes the test facilities, experimental procedures, and characterization instrumentation. Chapter 4 describes the tribological behavior of ceramic brake pads on the PEA-coated cast iron brake rotors. Chapter 5 describes the wear mechanism of the treated cast iron rotors by PEA process sliding against NAO pads. Chapter 6 describes the wear performances of cast iron brake rotor with PEA coating against three different pads (ceramic, semi-metallic and NAO). For the conclusions and future works, Chapter 7 gives a detailed summary.

REFERENCES

- [1] "Particulate Matter (PM) Basics." *US EPA*. Last modified October 3, 2019.
<https://www.epa.gov/pm-pollution/particulate-matter-pm-basics#PM>.
- [2] Sapkota, Amir, Adam P. Chelikowsky, Keeve E. Nachman, Aaron J. Cohen, and Beate Ritz. "Exposure to particulate matter and adverse birth outcomes: a comprehensive review and meta-analysis." *Air Quality, Atmosphere & Health* 5, no. 4 (2012): 369-381.
doi:10.1007/s11869-010-0106-3.
- [3] Pope Iii, C. Arden, Richard T. Burnett, Michael J. Thun, Eugenia E. Calle, Daniel Krewski, Kazuhiko Ito, and George D. Thurston. "Lung cancer, cardiopulmonary mortality, and long-term exposure to fine particulate air pollution." *JAMA* 287, no. 9 (2002): 1132-1141. doi:10.1001/jama.287.9.1132.
- [4] Brook, Robert D., Sanjay Rajagopalan, C. Arden Pope III, Jeffrey R. Brook, Aruni Bhatnagar, Ana V. Diez-Roux, Fernando Holguin, Yuling Hong, Russell V. Luepker, Murray A. Mittleman, Annette Peters, David S. Siscovick, Sidney C. Smith, Laurie P. Whitsel, and Joel D. Kaufman. "Particulate matter air pollution and cardiovascular disease: an update to the scientific statement from the American Heart Association." *Circulation* 121, no. 21 (2010): 2331-2378. doi:10.1161/CIR.0b013e3181dbee1.
- [5] Wakeling, Dan, Tim Murrells, David Carslaw, John Norris, and Luke Jones. "The contribution of brake wear emissions to particulate matter in ambient air." *FAT-Schriftenreihe* 301 (2017).

- [6] Pierson, William R., and Wanda W. Brachaczek. "Particulate matter associated with vehicles on the road. II." *Aerosol Science and Technology* 2, no. 1 (1982): 1-40. doi:10.1080/02786828308958610.
- [7] Thorpe, Alistair, and Roy M. Harrison. "Sources and properties of non-exhaust particulate matter from road traffic: a review." *Science of the Total Environment* 400, no. 1-3 (2008): 270-282. doi:10.1016/j.scitotenv.2008.06.007.
- [8] Denier van der Gon, Hugo A. C., Miriam E. Gerlofs-Nijland, Robert Gehrig, Mats Gustafsson, Nicole Janssen, Roy M. Harrison, Jan Hulskotte, Christer Johansson, Magdalena Jozwicka, Menno Keuken, Klaas Krijgheld, Leonidas Ntziachristos, Michael Riediker, and Flemming R. Cassee. "The policy relevance of wear emissions from road transport, now and in the future—an international workshop report and consensus statement." *Journal of the Air & Waste Management Association* 63, no. 2 (2013): 136-149. doi:10.1080/10962247.2012.741055.
- [9] Grigoratos, Theodoros, and Giorgio Martini. "Brake wear particle emissions: a review." *Environmental Science and Pollution Research* 22, no. 4 (2015): 2491-2504. doi:10.1007/s11356-014-3696-8.
- [10] Xiao, Xingming, Yan Yin, Jiusheng Bao, Lijian Lu, and Xuejun Feng. "Review on the friction and wear of brake materials." *Advances in Mechanical Engineering* 8, no. 5 (2016): 1687814016647300. doi:10.1177/1687814016647300.
- [11] Mathissen, Marcel, Jaroslaw Grochowicz, Christian Schmidt, Rainer Vogt, Ferdinand H. Farwick Zum Hagen, Tomasz Grabiec, Heinz Steven, and Theodoros

- Grigoratos. "A novel real-world braking cycle for studying brake wear particle emissions." *Wear* 414 (2018): 219-226. doi:10.1016/j.wear.2018.07.020.
- [12] Zum Hagen, Ferdinand H. Farwick, Marcel Mathissen, Tomasz Grabiec, Tim Hennicke, Marc Rettig, Jaroslaw Grochowicz, Rainer Vogt, and Thorsten Benter. "Study of brake wear particle emissions: impact of braking and cruising conditions." *Environmental Science & Technology* 53, no. 9 (2019): 5143-5150. doi:10.1021/acs.est.8b07142.
- [13] Mathissen, Marcel, Theodoros Grigoratos, Tero Lahde, and Rainer Vogt. "Brake wear particle emissions of a passenger car measured on a chassis dynamometer." *Atmosphere* 10, no. 9 (2019): 556. doi:10.3390/atmos10090556.
- [14] Aranke, Omkar, Wael Algenaid, Samuel Awe, and Shrikant Joshi. "Coatings for automotive gray cast iron brake discs: A review." *Coatings* 9, no. 9 (2019): 552. doi:10.3390/coatings9090552.
- [15] Lal, Roop, and Ramesh Chandra Singh. "Experimental comparative study of chrome steel pin with and without chrome plated cast iron disc in situ fully flooded interface lubrication." *Surface Topography: Metrology and Properties* 6, no. 3 (2018): 035001. doi:10.1088/2051-672X/aac60a.
- [16] Liu, Yan, Ying Wu, Yuanming Ma, Wei Gao, Guiying Yang, Hao Fu, Naiyuan Xi, and Hui Chen. "High temperature wear performance of laser cladding Co06 coating on high-speed train brake disc." *Applied Surface Science* 481 (2019): 761-766. doi:10.1016/j.apsusc.2019.02.235.

[17] Federici, Matteo, Cinzia Menapace, Alessandro Moscatelli, Stefano Gialanella, and Giovanni Straffelini. "Pin-on-disc study of a friction material dry sliding against HVOF coated discs at room temperature and 300 °C." *Tribology International* 115 (2017): 89-99. doi:10.1016/j.triboint.2017.05.030.

[18] Elbriggmann, Thorsten. "Porsche Hard Like Diamond." *Porsche HOME - Porsche USA*.
<https://www.porsche.com/usa/aboutporsche/christophorusmagazine/archive/384/articleoverview/article03/>.

[19] "IDisc Brake Disc." *Bosch Mobility Solutions*. <https://www.bosch-mobility-solutions.com/en/highlights/automated-mobility/idisc/>.

[20] Zhao, Chen, Wei Zha, Ran Cai, Xueyuan Nie, and Jimi Tjong. "A New Eco-friendly Anticorrosion Strategy for Ferrous Metals: Plasma Electrolytic Aluminating." *ACS Sustainable Chemistry & Engineering* 7, no. 5 (2019): 5524-5531. doi:10.1021/acssuschemeng.8b06839.

[21] Walsh, Frank C., Chee Tong John Low, Robert James Knoyle Wood, K. T. Stevens, John Archer, A. R. Poeton, and A. Ryder. "Plasma electrolytic oxidation (PEO) for production of anodised coatings on lightweight metal (Al, Mg, Ti) alloys." *Transactions of the IMF* 87, no. 3 (2009): 122-135. doi:10.1179/174591908X372482.

[22] Clyne, Trevor William, and Samuel Christopher Troughton. "A review of recent work on discharge characteristics during plasma electrolytic oxidation of various metals." *International Materials Reviews* 64, no. 3 (2019): 127-162. doi:10.1080/09506608.2018.1466492.

- [23] Yerokhin, Aleksey L., Xueyuan Nie, Adrian Leyland, Allan Matthews, and Stephen J. Dowey. "Plasma electrolysis for surface engineering." *Surface and Coatings Technology* 122, no. 2-3 (1999): 73-93. doi:10.1016/S0257-8972(99)00441-7.
- [24] Nie, Xueyuan, Efsfathios I. Meletis, Jiechao Jiang, Adrian Leyland, Aleksey L. Yerokhin, and Allan Matthews. "Abrasive wear/corrosion properties and TEM analysis of Al₂O₃ coatings fabricated using plasma electrolysis." *Surface and Coatings Technology* 149, no. 2-3 (2002): 245-251. doi:10.1016/S0257-8972(01)01453-0.
- [25] Federici, Matteo, Mattia Alemani, Cinzia Menapace, Stefano Gialanella, Guido Perricone, and Giovanni Straffelini. "A critical comparison of dynamometer data with pin-on-disc data for the same two friction material pairs—A case study." *Wear* 424 (2019): 40-47. doi:10.1016/j.wear.2019.02.009.

CHAPTER 2

LITERATURE REVIEW

2.1 Brake Wear Emissions

2.1.1 Particulate Matter

Particulate matter (PM) is a complex mixture of microscopic solid or liquid particles of organic and inorganic substances suspended in the ambient air [1]. Some particles can be seen with naked eyes and others can only be detected using an electron microscope. The most health-damaging atmospheric particulates are small particles with a diameter between 2.5 and 10 μm (PM_{10}) or less ($\text{PM}_{2.5}$). Figure 2.1 shows the size comparisons for PM_{10} and $\text{PM}_{2.5}$ [1].

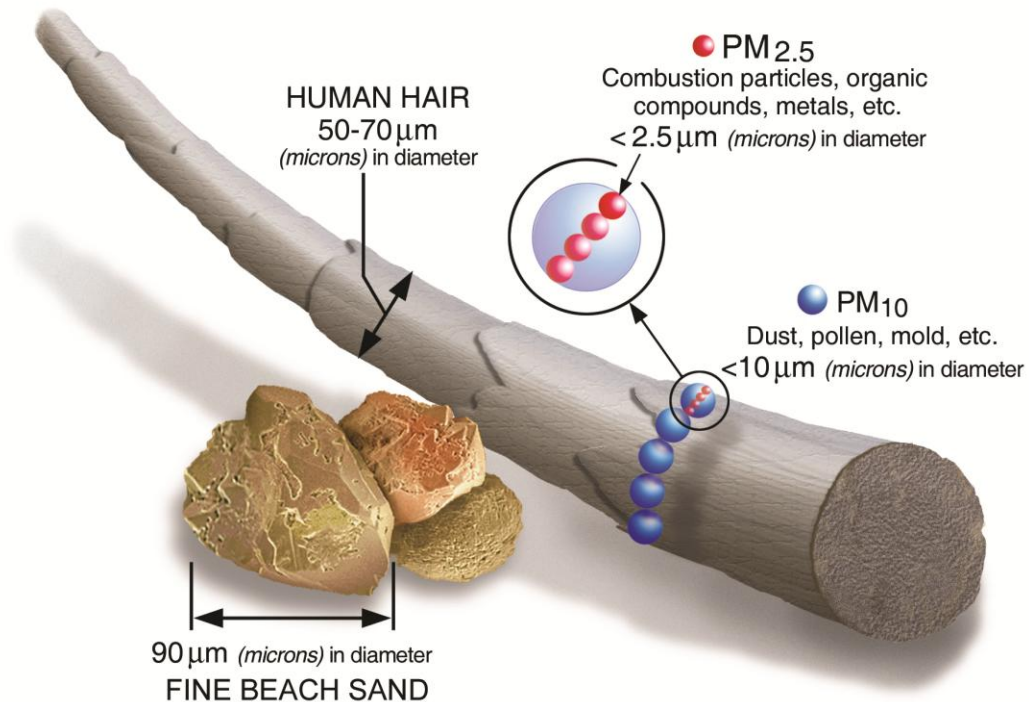


Figure 2.1 Size comparisons for PM particles [1].

Particles with large size ($>10\text{-}50\text{ }\mu\text{m}$) are generally filtered in the nose and throat via cilia and mucus [2]. PM_{10} can penetrate beyond the nasopharynx in the large airways and primarily deposits in the nasal, pharyngeal and laryngeal passages and the trachea, and bronchi region, while $\text{PM}_{2.5}$ primarily tends to deposit in the respiratory bronchioles and alveoli and may pass through the lungs to affect other organs such as blood streams [2, 3]. Figure 2.2 shows the deposition potential for PMs of different sizes.

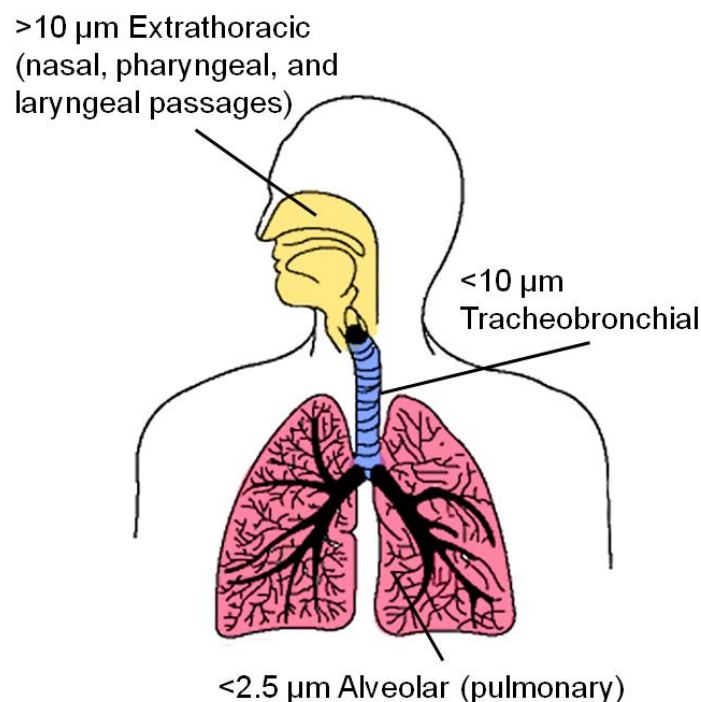


Figure 2.2 Deposition potential for PM particles of varying sizes.

The effects of inhaling PM (in particular $\text{PM}_{2.5}$) that have been widely studied in humans include elevated risk of adverse pregnancy outcomes [4] like premature delivery, birth defects, low birth weight, and premature death, respiratory diseases [5] like asthma and lung cancer [6, 7], cardiovascular diseases [7-9] like vascular inflammation, atherosclerosis and heart attacks. In addition to direct inhalation, the particulates also

have impacts on climate and precipitation that adversely affect human health [10, 11]. It was reported that $PM_{2.5}$ contributed to 4.1 million deaths from heart disease and stroke, lung cancer, chronic lung disease, and respiratory infections worldwide in 2016 [12]. Overall, PM in ambient air ranks as the sixth leading risk factor for the premature death [13, 14].

2.1.2 Traffic-related PM Emissions

Even though some of the particulates are naturally originated from volcanoes, dust storms or forest and grassland fires, human activities such as the burning of fossil fuels or stubbles, road dust and various industrial processes generate significant amounts of particulates [15]. A significant contributor of directly emitted PM is traffic-related particles, particularly in urban environments and major cities [16]. According to the UK's national atmospheric emissions inventory, road transport contributed 12% of total $PM_{2.5}$ emissions in 2018 [17].

PM emitted as a result of road transport activity can be divided in two main categories according to its source: exhaust traffic-related and non-exhaust traffic-related [18].

Exhaust traffic-related particulates (e.g., vehicle tailpipe) are emitted as a result of incomplete fuel combustion and lubricant volatilization during the combustion procedure, and non-exhaust traffic-related particulates are either generated from non-exhaust traffic related sources such as brake, tire, clutch and road surface wear or already exist in the environment as deposited material and become resuspended due to traffic induced turbulence [19].

Exhaust traffic-related particles have been recognized as a significant contributor to ambient PM and for that reason they have been studied and well characterized in the laboratory under well-defined test conditions [19]. Therefore, exhaust traffic-related PM emissions have been declining in recent years, which has been the result of the successful introduction of various abatement technologies driven by ever tighter vehicle emission regulations [10]. One of the strategies adopted by many European countries to improve air quality and reduce greenhouse gas emissions is electrification of vehicles, which removes exhaust traffic-related PM emissions from this source [20]. However, some studies have found that electrification of vehicles may not reduce PM emissions as much as expected, due to the relatively large weight of electric vehicles which could increase non-exhaust emissions [21].

Considering the increasing strict control on exhaust traffic-related PM emissions, the relative contribution of non-exhaust sources will become increasingly more important for total traffic-related PM emissions [22]. There is no related regulation currently in place specifically to limit or reduce non-exhaust traffic-related emissions, so whilst regulation has been effective at driving down exhaust emissions, the non-exhaust emissions have been uncontrolled. A recent report released by the Air Quality Expert Group in the UK recommends as an immediate priority that non-exhaust traffic-related PM emissions are recognized as a source airborne PM, even for vehicles with zero exhaust PM emissions [23]. Data from the UK National Atmospheric Emissions Inventory indicate that the proportion of non-exhaust emissions currently constitute 60% and 73% of total $PM_{2.5}$ and PM_{10} emissions from road transport respectively [24]. Figure 2.2 and Figure 2.3 present traffic-related $PM_{2.5}$ and PM_{10} emissions from the UK and German inventories. The

trends show that exhaust traffic-related PM emissions are estimated to decrease rapidly from 2015 to 2030 and non-exhaust traffic-related PM emissions are estimated to increase steadily over the same period for both the UK and Germany [10]. The inventories for both countries illustrate that the non-exhaust sources will become the dominant sources of traffic-related PM emissions and the trend of increasing dominance is likely to continue until related regulation is introduced.



Figure 2.3 PM_{2.5} emissions from road transport sources according to the UK and German inventories. The scale on the y-axis applies to both countries [10].



Figure 2.4 PM_{10} emissions from road transport sources according to the UK and German inventories. The scale on the y-axis applies to both countries [10].

2.1.3 Brake Wear PM Emission

Non-exhaust traffic-related PM emissions are predominantly from brake wear, tire wear, road surface wear and resuspended road dust. Brake wear has been identified as one of the most significant contributors, being responsible for up to 21% of total urban traffic related PM_{10} emissions by mass [25, 26]. There are two widely used brake system configurations: disc brakes and drum brakes. Standard vehicle brakes function by the

friction between a brake pad and a rotating disc or drum when the two are forced together by application of pressure to the braking system [24].

During a braking event, the brake pad slides against the rotor/disc or the drum and transforms the vehicle's kinetic energy into thermal energy, generating not only mechanical abrasion but also large frictional heat with subsequent wear of both pad and disc or drum. Humps on the surface of disc or drum are pressed into the pad and debris is torn from the pad or sheared off from the disc or the drum. Some of this debris is ejected from the contacting interface. Other debris remains on the disc or drum and pad surfaces and undergoes the cyclic deformation, crushing, fracture, and spalling or peeling [27]. About 50% of wear debris generated during braking become airborne while the rest is deposited on the road surface or is attracted to the vehicle [28-30]. Brake wear emissions are generated not only during braking but also in an acceleration event where the brake wear particles are derived from the detachment of wear particles from the surface of the brake and grooves [31].

The system of drum brakes is more enclosed systems than that of disc brakes, which means that there is a greater proportion of the particles released becoming trapped within the drum brake system instead of getting emitted to the atmosphere. For this reason, PM emissions from drum brakes tend to be lower than that from disc brakes [31, 32].

However, disc brakes offer better stopping performance than drum brakes because the discs are more readily cooled, less prone to the brake fade caused when brake components overheat and recover more quickly from immersion [33]. This thesis will focus on disc brakes.

2.1.4 Regenerative Braking

There are some opportunities to reduce particle emissions from brakes such as optimising the systems and materials already being used including pad work rate, pad materials, rotor work rate, rotor temperature rise and rotor cooling, adapting existing technologies like retracting positive piston or brake pad on both sides of the brake rotor and applying technological advancements including vehicle particulate filters, larger wheel envelopes, brake-by-wire, substituted brake rotors like carbon ceramic rotors and regenerative braking [10]. The brake rotor and pad materials will be discussed in the following sections.

A common idea for electric vehicles and brake emissions is that regenerative braking will remove the brake wear or the need for brakes altogether [34]. During a braking in a conventional vehicle, much of the kinetic energy is converted into heat that is emitted into the environment unused. However, hybrid and electric vehicles with regenerative braking system will recover some kinetic energy by means of the electric motor. When braking, the wheels transfer kinetic energy via the drive train to the generator which transforms part of the kinetic energy into electrical energy, which is then stored in a high-voltage battery [35]. The electric motor can then use this stored energy when driving off or accelerating. At the same time, generator resistance is produced during the creation of the electricity and slows the vehicle. In many situations the braking power from the generator is sufficient, when more braking torque is required than the generator can provide alone the additional braking is accomplished by friction brakes [36]. As a result, regenerative braking can reduce the need to use friction brakes, particularly in urban areas where speeds are lower.

It has been mentioned before that electric vehicle is not free of PM emissions even though it is true that the lack of a tailpipe dramatically improves air quality. Regenerative braking process helps to save fuel in hybrid vehicles and to reduce emissions of CO₂ and pollutants [36]. In addition, regenerative braking does not only rely on frictional brakes so vehicles using generator for braking also totally or partially should have lower brake wear emissions. Unfortunately, regenerative braking will never be able to bring a vehicle to a stop all on its own and the friction brakes are always in play [34]. Furthermore, other non-exhaust traffic-related PM sources like tire and road wear emissions will increase with vehicle mass, which has implications for any vehicle with a power train that is heavier (for example due to additional battery and hardware mass) than the equivalent conventional vehicle it replaces [24].

2.2 Brake Rotor Materials

It has been noted that the materials used to construct the brake systems are important when considering particle emissions from brake wear [10]. The brake discs or rotors are the rotating parts of the brake system of a vehicle against with the applied brake pads. The brake pad materials will be discussed in the next section.

2.2.1 Cast Iron Brake Rotor

For automotive use, brake rotors are the most commonly made from gray cast iron material, a form of cast iron [37]. Gray cast iron has high damping capability and desirable thermophysical properties (melting point, thermal conductivity, and heat storage capacity) which prevent overheating, brake noise, and brake fade [38, 39]. It is also attractive because of its good castability and machinability, combined with its cost-effectiveness [40]. For normal car and light-truck applications, SAE specification J431

G3000 dictates the correct range of hardness, chemical composition, tensile strength, and other properties necessary for the intended use [41]. G3000 disc is a simple but effective general-purpose brake rotor with excellent strength and good wear resistance [42]. The less common G250 is a higher strength material than G3000 with excellent low wear properties, but it has noticeable noise issues. Gray cast iron has some of the major disadvantages: poor corrosion resistance leading to brake judder [43, 44], high weight contributing to increased fuel consumption [45] and relatively large amount of brake wear emissions [46-48]. In order to solving the disadvantages above, some vehicles use brake rotors made from enhanced cast iron materials, other metals or alloys like aluminium and reinforced carbon-carbon or carbon ceramic composites.

2.2.2 High Carbon Brake Rotor

Carbon is a primary element added to gray iron discs to enhance the thermal properties, friction and noise damping ability [49]. The carbon content of G3000 cast iron is approximately 3.25%. When the carbon content of the material falls within the range 3.6 - 3.9%, it is classified as a high carbon iron [42]. When gray cast iron is produced, carbon, and silicon and various other trace elements are added. Some carbon without being absorbed by the metal matrix will be precipitated out into flakes.

Due to carbon's excellent energy conductivity, the carbon flakes in high carbon cast iron brake rotors quickly transfer the heat away from the friction surface. The thermal conductivity of high carbon iron discs is 5~10% higher than G3000 ones [42]. As a result, the higher carbon content improves the thermal stability and reduces thermal brake judder and possible heat cracking of discs in performance driving [50]. In addition, the carbon flakes act like a void within the cast iron disc because of its lower density than iron,

which cause the noise to disperse or dampen [42, 50]. By the way, these properties are not depending so much on the amount of the carbon flakes but the size, shape and orientation [51]. However, the high carbon cast iron rotor sacrifices a little strength for more efficient thermal and noise damping properties. The common G3000 brake rotor has a little higher strength than the high carbon rotor. G250 is a higher strength material with excellent low wear properties but it has noticeable noise issues.

High carbon brake rotors are often used on vehicles with light weight metal which may be more prone to noise issues. High performance vehicles also come standard with high carbon disc rotors due to the potential kinetic energy generated at high speeds [42]. EBC Brakes will use the high carbon cast iron in its new BLADE pattern TGD series image Sport discs and its popular USR and GD sport disc series which will be fitted to many brands such as BMW, Audi, Honda and Ford [50].

2.2.3 Carbon-carbon and Carbon Ceramic Brake Rotor

Carbon-carbon materials have been used in brake rotors for a long time [52]. It is recognized as the optimum brake material and is first introduced in racing cars like F1. The benefits using a carbon-carbon brake rotor include high brake performance and low weight [53]. However, these carbon-carbon brake systems still suffered some disadvantages. Carbon brakes only work effectively at elevated temperatures and do not provide sufficient or consistent levels of friction at low temperatures such as a low coefficient of friction at temperatures below 450 °C [54]. It also has a high rate of wear for the pads. Therefore the brake performance carbon-carbon brake rotors provide is too extreme for everyday use and making them unsuitable for normal road car use [53].

Carbon ceramic brake rotors have many the same benefits as carbon-carbon rotors have but provide consistent coefficient of friction during the range of ever day temperatures. They are constructed in one of two ways: a ceramic material core reinforced with chopped carbon fiber with an additional ceramic layer on the friction surface and a ceramic material core with chopped carbon fiber and no friction layer [53]. The material combines good physical, mechanical and friction properties, such as corrosion resistance, high abrasion and temperature resistance and high and constant friction characteristics in wet, cold and hot conditions [55]. Carbon ceramic rotors are cited as being more durable, increased brake life and less brake wear which would reduce brake wear particulate emissions if these claims are confirmed [53]. However, carbon ceramic rotors are very expensive relative to cast iron standard discs, and are only fitted to premium brands (e.g. Porsche, Bugatti, Lamborghini, Aston Martin, McLaren etc.) [10]. Therefore, although it is adjudged to have the potential to significantly reduce brake particulate emissions it is anticipate that in practice this technology will have only a small penetration into the market [10].

2.3 Brake Pad Materials

Brake pads are an essential component of the brake system. During a braking event, the pressure on the brake pedal given by drivers is translated by way of a hydraulic system to the caliper, and the caliper in turn pushes the brake pad onto the car's brake rotors where the pressure and friction slow down the car or bring it to a complete stop [25].

2.3.1 Frictional Materials

In order to achieve the required properties, most brake pads are not composed of single elements or compounds but rather composites of many materials. More than 2000

different frictional materials are used in commercial brake pads. How the frictional materials shear, break and interact during braking can determine a pad's friction level, noise and wear characteristics [56]. Brake pads generally comprise five main frictional materials components: abrasives, reinforcing fibers, fillers, frictional additives or lubricants and binders [57]. Abrasives are used in order to increase friction, maintain cleanliness between contact surfaces and limit the buildup of transfer films [58]. Aluminum oxide, iron oxides, quartz, silica and zircon are the most common abrasive constituents [59]. Reinforcing fibers provide mechanical strength and structure to the brake pad [25]. They mainly consist of copper, steel, brass, potassium titanate, glass, organic material and Kevlar [60]. Fillers are used to maintain the overall composition of the friction material, and some have other functions as well such as improving thermal and noise pad properties [58]. They usually consist of inorganic compounds (barium and antimony sulphate, magnesium and chromium oxides), silicates, ground slag, stone and metal powders [60]. Frictional additives lubricate, raise the friction, or react with oxygen to help control interfacial films [58]. Graphite is usually employed, but other common materials include ground rubber, metallic particles, carbon black, cashew nut dust and antimony trisulphide [60, 61]. Binders hold the other frictional material components of the brake pad together and ensure the structural integrity of the pad under mechanical and thermal stress [25]. They are usually made of modified phenol-formaldehyde resins while some metallic alloys and modified resins can also be used as binders [58]. The proportions of the abovementioned components vary according to the type of the pad and the manufacturer [25]. Three different lining types are usually found in passenger vehicles: ceramic, semi-metallic and non-asbestos organic (NAO) [62]. When choosing

brake pads for a car, the type of car and the typically drive conditions must be taken into consideration.

2.3.2 Ceramic Pad

Brake pads are made of semi-metallic, NAO, or ceramic materials and each have unique benefits and drawbacks to consider. Ceramic brake pads are mainly made of ceramic fibers and other filling materials, some of which also have metal fibers such as copper fibers. These brake pads are very durable, break down very slowly, perform very well under harsh braking and can dissipate heat quickly. The ceramic content of the brake pads makes them extremely lightweight and they generate less wear debris on friction. Therefore, they work very well in high performance vehicles and racing cars that generate high levels of heat when braking. However, even though the ceramic brake pads do not need to be replaced very often, they are typically very expensive and not well suited for regular driving [62].

2.3.3 Semi-metallic Pad

Semi-metallic brake pads are comprised of metal shavings of copper, steel, graphite, and brass bonded with resin. These brake pads have higher metallic content up to 65% by mass [25]. The high metallic content makes the pads more durable and with excellent heat transfer. As a result, the semi-metallic brake pads perform well, last longer, can tolerate a lot of heat without fading and are tough and economical [62]. On the other hand, because of the high content of metals, the semi-metallic pads are typically heavier than other kinds of brake pads. They are much more prone to squealing and tend to exhibit intrusive noise characteristics [63]. The high weight of the pads can also affect the fuel efficiency of the car to some extent. Semi-metallic brake pads function best when they

are warm. Thus, in colder climates, they need time to warm up and when you brake, you might find a slight delay in the car responding [62]. You can choose brake pads that have ceramic components combined with metals. This could give you the positives of the ceramic brake pads, but at costs that are more economical.

2.3.4 NAO Pad

Organic brake pads had asbestos fibers for many years. These naturally occurring fibers are great structural components that resist heat [56]. However, scientists found that the dust produced by asbestos fibers caused serious health issues like cancer and asbestosis in technicians [64]. This is why manufacturers phased out this material and the newest organic brake pads are often also called non-asbestos organic (NAO) brake pads. NAO brake pads comprise of non-metallic components like glass, rubber, and Kevlar bonded in resin [62]. The NAO pads and also many ceramic pads use more fillers than semi-metallic pads. This helps dampen the vibrations that cause brake squeal by trading off pad life or fade resistance, depending on the friction material used [63]. They are relatively soft and exhibit low noise even after prolonged use compared to other types of pads [25]. They also perform better in high temperature conditions because the heat further binds the components together [62]. However, these brake pads are not very durable and create more dust than the other types even though the debris they produced is relatively eco-friendly and less harmful [18, 65]. These brake pads do not perform as well as semi-metallic brake pads and are thus better suited for lightweight vehicles and lighter traffic conditions where there is no excessive braking [66].

2.4 Coatings on Brake Rotors

Several different types of coatings have been explored to combat not only wear but also corrosion problems (shown in Figure 2.4) for automotive brake rotor applications. A discussion of the coating techniques which have already been extensively investigated for brake-disc applications is provided below.



Figure 2.5 Corrosions on different kinds of commercial automotive brake rotors.

2.4.1 Hard Chrome Plated Coating

Chrome plating has been a traditionally used technology since about 100 years ago for diverse automotive applications such as engine valves and brake rotors [67]. The metallurgical bonding coating prepared by chrome plating has high hardness and a dense microstructure with very low oxide inclusions [68] attributed to excellent resistance to corrosion in harsh environments [69] and very high fracture toughness [70]. The wear resistance of chrome plated coatings has also proven to be superior both in sliding and erosive wear conditions [70, 71]. The chrome plated stainless-steel brake rotor exhibited superior wear resistance, both at low and high temperature, and low mass loss [72]. Similarly, the superior wear resistance with a lower coefficient of friction (COF) as

compared to the bare cast iron rotor of the chrome plated cast iron rotor was also reported [73].

2.4.2 Laser Cladded Coating

Laser cladding is a method that has been increasingly exploited in recent times for various applications [40]. This process enables deposition of pore- and crack-free coatings with a strong substrate-coating metallurgical bonding and minimal heat input into the substrate [74-76]. The laser cladded coating, which can be wide range of Metals alloys, cermets and ceramics, improves wear and corrosion resistance of the matrix [77-79]. However, there are some drawbacks with laser cladding on cast iron brake rotors. Some researchers observed cracking inside the laser cladding coating because of internal stresses gradually built up during the cladding process or residual stresses [75, 80]. It is due to the fact that laser cladded coatings are easily susceptible to cracking due to the mismatch in the coefficient of thermal expansion between the substrate and coating material [81].

2.4.3 Thermal Spray Coating

Thermal spray is a generic term for a technology that involves a group of coating processes capable of depositing diverse metallic, intermetallic, or ceramic layers on component surfaces for varied functional applications, most often as protection against aggressive environments [40]. In its most common form, the technique relies on injection of powder of the material to be coated into a high-temperature, high-velocity zone where the powder particles are fully/partially molten and propelled at a high particle velocity onto the substrate surface to form a splat [82, 83]. These splats serve as building blocks for forming a coating which is mechanically bonded to the substrate [84]. By virtue of its

versatility, thermal spraying is already in commercial use for a wide range of applications including automotive industries. Over the years, several atmospheric plasma spray (APS) and high velocity oxy-fuel (HVOF) coatings have been considered for automotive brake rotor applications to increase the wear and corrosion resistance of the disc material [85, 86]. The relatively new high velocity air fuel (HVAF) spraying and suspension plasma spraying (SPS) have also been gaining rapid attention due to the advantages over the conventional HVOF and APS technologies, respectively [87]. For instance, both the Porsche Surface Coated Brake (PSCB) disc [88] from Porsche Company and the iDisc [89] from by Bosch Company adopted hard tungsten carbide coatings using a thermal spray process on cast iron substrates. The Figure 2.5 shows the Porsche Company's PSCB disc and the hard tungsten carbide coating. The reported results are remarkable, they claim that the surface modified disc lasts up to 30% longer than its uncoated counterpart, while a 90% reduction in brake dust is also reported [88, 89]. However, such a kind of brake rotor is much more expensive than the normal cast iron rotors.



Figure 2.6 Porsche Surface Coated Brake (PSCB) disc [88].

2.5 Brake Tests

2.5.1 Tribological Tests (Dynamometer vs PoD Tests)

Tribological behavior of brakes is often investigated using full-scale dynamometers or small-scale testing rigs. Dynamometer tests are accelerated bench tests and reproduce the real braking conditions since they are carried out on real parts [90]. Small-scale testing rigs, such as the friction assessment screening test (FAST) [91], the Chase machine [92], the reduce-scale dynamometers [93, 94] or the Pin-on-Disc (PoD) tests, are simply used in the initial stage of the development of new brake materials[93]. In particular, PoD tests, carried out using small pins, are rather simplified tests since they are typically carried out under a constant sliding velocity and contact pressure [90]. However, PoD tests have several advantages including shorter testing times, lower costs and the possibility to better relate the tribological behavior to the test parameters such as the sliding velocity and contact pressure [95, 96]. It has been reported that the wear mechanisms observed with the PoD at room temperature turned out to be similar to those observed with the dynamometer tests. As far as the tribological data are concerned, the average COF recorded during the dynamometric tests were similar to the values recorded in the PoD tests, whereas the wear were one order of magnitude lower than the corresponding values obtained with the PoD at room temperature, most probably due to the limited area of contact of the pins [90].

2.5.2 Brake Wear Emission Measurements

The brake wear PM emission can be tested with a brake dynamometer in some previous researches. This measuring system (shown in Figure 2.6) was established with an engine dynamometer, an enclosure (chamber), a constant volume sampling (CVS) system and

real-time mass measurements were made [31]. For a quantitative determination of PM emission, a chamber was placed around the brake assembly, with a blower drawing a constant flow of air through the brake into the constant volume sampling system [47, 97]. The airflow was supplied by a high-efficiency particulate air (HEPA) filtering system. These components were controlled by a data acquisition and control system from a computer [31]. This system allows measuring and investigating airborne brake wear particles and the mass of the wears simultaneously. The real-time mass emission measurements were performed under constant driving, different initial wheel speeds, and acceleration/deceleration conditions [31].

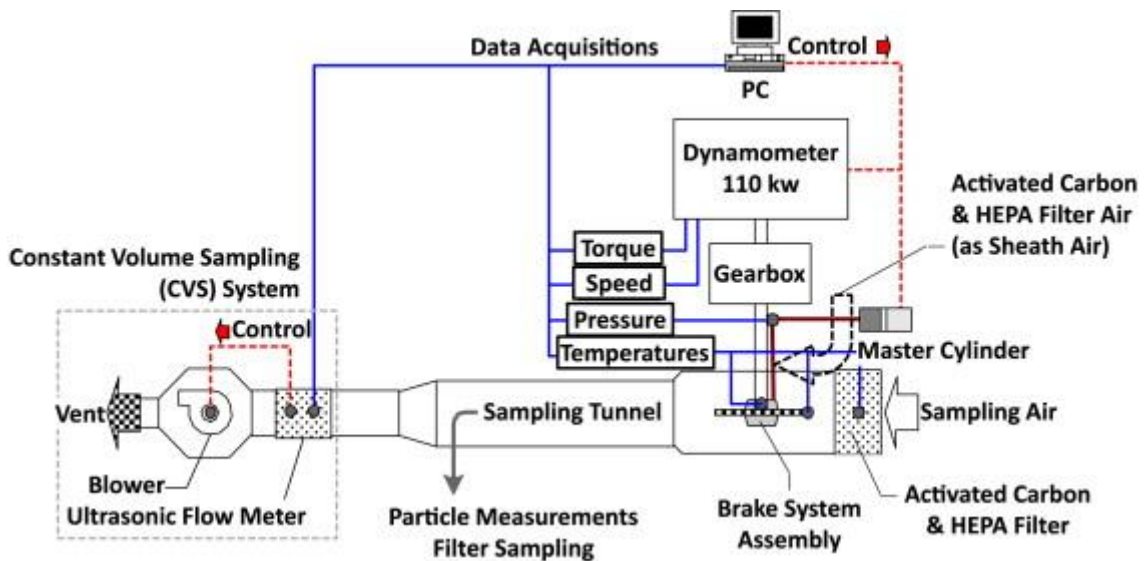


Figure 2.7 Scheme of the brake dynamometer assembly and measurement instruments [31].

REFERENCES

- [1] "Particulate Matter (PM) Basics." US EPA. Last modified October 3, 2019.
<https://www.epa.gov/pm-pollution/particulate-matter-pm-basics#PM>.
- [2] Wasley, Andrew, Alexandra Heal, Fiona Harvey, and Mie Lainio. "Revealed: UK Government Failing to Tackle Rise of Serious Air Pollutant." *The Guardian*. Last modified June 13, 2019. ISSN 0261-3077.
- [3] "Particle Pollution Exposure." US EPA. Last modified June 18, 2019.
<https://www.epa.gov/pmcourse/particle-pollution-exposure>.
- [4] Sapkota, Amir, Adam P. Chelikowsky, Keeve E. Nachman, Aaron J. Cohen, and Beate Ritz. "Exposure to particulate matter and adverse birth outcomes: a comprehensive review and meta-analysis." *Air Quality, Atmosphere & Health* 5, no. 4 (2012): 369-381.
doi:10.1007/s11869-010-0106-3.
- [5] Cohen, Aaron J., H. Ross Anderson, Bart Ostro, Kiran Dev Pandey, Michal Krzyzanowski, Nino Künzli, Kersten Gutschmidt, C. A. Pope, Isabelle Romieu, Jonathan Matthew Samet, and Kirk R. Smith. "The global burden of disease due to outdoor air pollution." *Journal of Toxicology and Environmental Health, Part A* 68, no. 13-14 (2005): 1301-1307. doi:10.1080/15287390590936166.
- [6] Raaschou-Nielsen, Ole, Zorana J. Andersen, Rob Beelen, Evangelia Samoli, Massimo Stafoggia, Gudrun Weinmayr, Barbara Hoffmann et al. "Air pollution and lung cancer incidence in 17 European cohorts: prospective analyses from the European Study of Cohorts for Air Pollution Effects (ESCAPE)." *The Lancet Oncology* 14, no. 9 (2013): 813-822. doi:10.1016/S1470-2045(13)70279-1.

- [7] Pope Iii, C. Arden, Richard T. Burnett, Michael J. Thun, Eugenia E. Calle, Daniel Krewski, Kazuhiko Ito, and George D. Thurston. "Lung cancer, cardiopulmonary mortality, and long-term exposure to fine particulate air pollution." *JAMA* 287, no. 9 (2002): 1132-1141. doi:10.1001/jama.287.9.1132.
- [8] Brook, Robert D., Sanjay Rajagopalan, C. Arden Pope III, Jeffrey R. Brook, Aruni Bhatnagar, Ana V. Diez-Roux, Fernando Holguin, Yuling Hong, Russell V. Luepker, Murray A. Mittleman, Annette Peters, David S. Siscovick, Sidney C. Smith, Laurie P. Whitsel, and Joel D. Kaufman. "Particulate matter air pollution and cardiovascular disease: an update to the scientific statement from the American Heart Association." *Circulation* 121, no. 21 (2010): 2331-2378. doi:10.1161/CIR.0b013e3181dbee1.
- [9] Cesaroni, Giulia, Francesco Forastiere, Massimo Stafoggia, Zorana J. Andersen, Chiara Badaloni, Rob Beelen, Barbara Caracciolo et al. "Long term exposure to ambient air pollution and incidence of acute coronary events: prospective cohort study and meta-analysis in 11 European cohorts from the ESCAPE Project." *BMJ* 348 (2014): f7412. doi:10.1136/bmj.f7412.
- [10] Wakeling, Dan, Tim Murrells, David Carslaw, John Norris, and Luke Jones. "The contribution of brake wear emissions to particulate matter in ambient air." *FAT-Schriftenreihe* 301 (2017).
- [11] Voiland, Adam. "Aerosols: Tiny Particles, Big Impact." *NASA Earth Observatory - Home*. Last modified November 2, 2010.
<https://earthobservatory.nasa.gov/features/Aerosols>.

- [12] Health Effects Institute. "State of Global Air/2018: A Special Report on Global Exposure to Air Pollution and its Disease Burden." State of Global Air 2018. Special Report. Boston, MA:Health Effects Institute (2018).
- [13] Lim, Stephen S., Theo Vos, Abraham D. Flaxman, Goodarz Danaei, Kenji Shibuya, Heather Adair-Rohani, Mohammad A. AlMazroa et al. "A comparative risk assessment of burden of disease and injury attributable to 67 risk factors and risk factor clusters in 21 regions, 1990–2010: a systematic analysis for the Global Burden of Disease Study 2010." *The Lancet* 380, no. 9859 (2012): 2224-2260. doi:10.1016/S0140-6736(12)61766-8.
- [14] "The Weight of Numbers: Air Pollution and PM2.5." Undark Magazine. Last modified July 30, 2018. <https://undark.org/breathtaking/>.
- [15] Omidvarborna, Hamid, Ashok Kumar, and Dong-Shik Kim. "Recent studies on soot modeling for diesel combustion." *Renewable and Sustainable Energy Reviews* 48 (2015): 635-647. doi:10.1016/j.rser.2015.04.019.
- [16] Pierson, William R., and Wanda W. Brachaczek. "Particulate matter associated with vehicles on the road. II." *Aerosol Science and Technology* 2, no. 1 (1982): 1-40. doi:10.1080/02786828308958610.
- [17] Richmond, B., A. Misra, P. Brown, E. Karagianni, T. Murrells, Y. Pang, N. Passant, A. Pepler, R. Stewart, G. Thistlethwaite, L. Turtle, D. Wakeling, C. Walker, and J. Wiltshire. "UK Informative Inventory Report (1990 to 2018)." *UK National Atmospheric Emissions Inventory*, 2020. https://naei.beis.gov.uk/reports/reports?report_id=999.

- [18] Thorpe, Alistair, and Roy M. Harrison. "Sources and properties of non-exhaust particulate matter from road traffic: a review." *Science of the Total Environment* 400, no. 1-3 (2008): 270-282. doi:10.1016/j.scitotenv.2008.06.007.
- [19] Grigoratos, Theodoros, and Giorgio Martini. "Non-exhaust traffic related emissions. Brake and tyre wear PM." *Report no. Report EUR 26648* (2014). doi:10.2790/21481.
- [20] ACEA. "Overview of purchase and tax incentives for electric vehicles in the EU in 2015." (2015).
https://www.acea.be/uploads/publications/Electric_vehicles_overview_2015.pdf.
- [21] Timmers, Victor R. J. H., and Peter A. J. Achten. "Non-exhaust PM emissions from electric vehicles." *Atmospheric Environment* 134 (2016): 10-17.
doi:10.1016/j.atmosenv.2016.03.017.
- [22] Denier van der Gon, Hugo A. C., Miriam E. Gerlofs-Nijland, Robert Gehrig, Mats Gustafsson, Nicole Janssen, Roy M. Harrison, Jan Hulskotte, Christer Johansson, Magdalena Jozwicka, Menno Keuken, Klaas Krijgheld, Leonidas Ntziachristos, Michael Riediker, and Flemming R. Cassee. "The policy relevance of wear emissions from road transport, now and in the future—an international workshop report and consensus statement." *Journal of the Air & Waste Management Association* 63, no. 2 (2013): 136-149. doi:10.1080/10962247.2012.741055.
- [23] "UK Expert Group Focuses Attention on Non-exhaust Emissions from Road Traffic As Regulatory Concern." *Green Car Congress*. Last modified July 20, 2019.
<https://www.greencarcongress.com/2019/07/20190714-nee.html>.

- [24] Air Quality Expert Group. "Non-Exhaust Emissions from Road Traffic." *Home - Defra, UK*. Last modified July 9, 2019. https://uk-air.defra.gov.uk/assets/documents/reports/cat09/1907101151_20190709_Non_Exhaust_Emissions_typeset_Final.pdf
- [25] Grigoratos, Theodoros, and Giorgio Martini. "Brake wear particle emissions: a review." *Environmental Science and Pollution Research* 22, no. 4 (2015): 2491-2504. doi:10.1007/s11356-014-3696-8.
- [26] Alemani, Mattia, Jens Wahlström, and Ulf Olofsson. "On the influence of car brake system parameters on particulate matter emissions." *Wear* 396 (2018): 67-74. doi:10.1016/j.wear.2017.11.011.
- [27] Ostermeyer, Georg Peter, and Michael Müller. "Dynamic interaction of friction and surface topography in brake systems." *Tribology International* 39, no. 5 (2006): 370-380. doi:10.1016/j.triboint.2005.04.018.
- [28] Mathissen, Marcel, Jaroslaw Grochowicz, Christian Schmidt, Rainer Vogt, Ferdinand H. Farwick Zum Hagen, Tomasz Grabiec, Heinz Steven, and Theodoros Grigoratos. "A novel real-world braking cycle for studying brake wear particle emissions." *Wear* 414 (2018): 219-226. doi:10.1016/j.wear.2018.07.020.
- [29] Zum Hagen, Ferdinand H. Farwick, Marcel Mathissen, Tomasz Grabiec, Tim Hennicke, Marc Rettig, Jaroslaw Grochowicz, Rainer Vogt, and Thorsten Benter. "Study of brake wear particle emissions: impact of braking and cruising conditions." *Environmental Science & Technology* 53, no. 9 (2019): 5143-5150. doi:10.1021/acs.est.8b07142.

[30] Mathissen, Marcel, Theodoros Grigoratos, Tero Lahde, and Rainer Vogt. "Brake wear particle emissions of a passenger car measured on a chassis dynamometer."

Atmosphere 10, no. 9 (2019): 556. doi:10.3390/atmos10090556.

[31] Hagino, Hiroyuki, Motoaki Oyama, and Sousuke Sasaki. "Airborne brake wear particle emission due to braking and accelerating." *Wear* 334 (2015): 44-48.

doi:10.1016/j.wear.2015.04.012.

[32] Hagino, Hiroyuki, Motoaki Oyama, and Sousuke Sasaki. "Laboratory testing of airborne brake wear particle emissions using a dynamometer system under urban city driving cycles." *Atmospheric Environment* 131 (2016): 269-278.

doi:10.1016/j.atmosenv.2016.02.014.

[33] Halderman, James D., and Chase D. Mitchell. *Automotive Brake Systems*. Prentice Hall, 1996.

[34] The Brake Report. "EVs: Clean Air and Dirty Brakes." *The BRAKE Report*. Last modified July 2, 2019. <https://thebrakereport.com/clean-air-dirty-brakes/>.

[35] Lampton, Christopher. "How Regenerative Braking Works." *HowStuffWorks.com*. Last modified January 23, 2009. <https://auto.howstuffworks.com/auto-parts/brakes/brake-types/regenerative-braking.htm/printable>.

[36] "Regenerative Braking Systems." *Bosch Mobility Solutions*. <https://www.bosch-mobility-solutions.com/en/products-and-services/passenger-cars-and-light-commercial-vehicles/driving-safety-systems/regenerative-braking-systems/>.

- [37] Ihm, Mark, and TRW Automotive. "Introduction to gray cast iron brake rotor metallurgy." *In TRW Automotive, Seminar*, 2011.
- [38] Cueva, G., Amilton Sinatora, Wilson L. Guesser, and André P. Tschiptschin. "Wear resistance of cast irons used in brake disc rotors." *Wear* 255, no. 7-12 (2003): 1256-1260. doi:10.1016/S0043-1648(03)00146-7.
- [39] Cho, Min-hyung, Seong-jin Kim, Rena Hecht Basch, James W. Fash, and Ho Jang. "Tribological study of gray cast iron with automotive brake linings: The effect of rotor microstructure." *Tribology International* 36, no. 7 (2003): 537-545. doi:10.1016/S0301-679X(02)00260-8.
- [40] Aranke, Omkar, Wael Algenaid, Samuel Awe, and Shrikant Joshi. "Coatings for automotive gray cast iron brake discs: A review." *Coatings* 9, no. 9 (2019): 552. doi:10.3390/coatings9090552.
- [41] "Automotive Gray Iron Castings J431_201801." *SAE International*, 2018. doi:10.4271/J431_201801.
- [42] Gavin, Steve. "Disc Rotor Materials - G3000, G250, High Carbon, What the Flux?" <https://www.mechanic.com.au/news/disc-rotor-materials-g3000-g250-high-carbon-what-the-flux/>.
- [43] Shin, Min-wook, Keun-hyung Cho, Seong-jin Kim, and Ho Jang. "Friction instability induced by corrosion of gray iron brake discs." *Tribology Letters* 37, no. 2 (2010): 149-157. doi:10.1007/s11249-009-9503-x.

- [44] Stanford, Malcolm K., and Vinod K. Jain. "Friction and wear characteristics of hard coatings." *Wear* 251, no. 1-12 (2001): 990-996. doi:10.1016/S0043-1648(01)00719-0.
- [45] Maleque, Md Abdul, Sarker Dyuti, and Md Mustafizur Rahman. "Material selection method in design of automotive brake disc." In proceedings of the world congress on engineering, vol. 3. 2010.
- [46] Hjortenkrans, David S. T., Bo G. Bergbäck, and Agneta V. Höggerud. "Metal emissions from brake linings and tires: case studies of Stockholm, Sweden 1995/1998 and 2005." *Environmental Science & Technology* 41, no. 15 (2007): 5224-5230. doi:10.1021/es070198o.
- [47] Iijima, Akihiro, Keiichi Sato, Kiyoko Yano, Masahiko Kato, Kuniyoshi Kozawa, and Naoki Furuta. "Emission factor for antimony in brake abrasion dusts as one of the major atmospheric antimony sources." *Environmental Science & Technology* 42, no. 8 (2008): 2937-2942. doi:10.1021/es702137g.
- [48] Furusjö, Erik, John Sternbeck, and Anna Palm Cousins. "PM10 source characterization at urban and highway roadside locations." *Science of The Total Environment* 387, no. 1-3 (2007): 206-219. doi:10.1016/j.scitotenv.2007.07.021.
- [49] "Classification of Carbon and Low-Alloy Steels." Total Materia - The World's Most Comprehensive Materials Database. Last modified November 2001. <https://www.totalmateria.com/articles/Art62.htm>.
- [50] "High Carbon Brake Performance Driving." EBC Brakes. <https://ebcbrakes.com/ebc-high-carbon-brake-discs-for-performance-driving/>.

- [51] ASTM A247-10. "Standard Test Method for Evaluating the Microstructure of Graphite in Iron Castings." West Conshohocken, PA: ASTM International, 2010.
doi:10.1520/A0247-10.
- [52] Savage, E. *Carbon-Carbon Composites*. Berlin: Springer Science & Business Media, 2012.
- [53] "Top 10 FAQs on Ceramic Brakes, Pads and Carbon Ceramic Material — Surface Transforms." *Surface Transforms*. Last modified May 22, 2013.
<https://surfacettransforms.com/white-papers/2013/5/22/top-10-faqs-on-ceramic-brakes-pads-and-carbon-ceramic-material>.
- [54] Stadler, Zmago, Kristoffer Krnel, and Tomaz Kosmac. "Friction behavior of sintered metallic brake pads on a C/C–SiC composite brake disc." *Journal of the European Ceramic Society* 27, no. 2-3 (2007): 1411-1417. doi:10.1016/j.jeurceramsoc.2006.04.032.
- [55] Krupka, Mario, and Andreas Kienzle. "Fiber Reinforced Ceramic Composite for Brake Discs." SAE Technical Paper Series, 2000. doi:10.4271/2000-01-2761.
- [56] "Brake Pad Contamination." Know Your Parts. Last modified May 17, 2017.
<https://www.knowyourparts.com/technical-resources/brakes-and-brake-components/brake-pad-contamination/>.
- [57] Chan, D., and Gwidon W. Stachowiak. "Review of automotive brake friction materials." *Proceedings of the Institution of Mechanical Engineers, Part D: Journal of Automobile Engineering* 218, no. 9 (2004): 953-966. doi:10.1243/0954407041856773.

- [58] Blau, Peter J. Compositions, Functions, and Testing of Friction Brake Materials and Their Additives; TOPICAL. No. ORNL/TM--2001/64. Oak Ridge National Lab., 2001. doi:10.2172/788356.
- [59] Eriksson, Mikael, and Staffan Jacobson. "Tribological surfaces of organic brake pads." *Tribology International* 33, no. 12 (2000): 817-827. doi:10.1016/S0301-679X(00)00127-4.
- [60] Jang, Ho, and Seong-jin Kim. "The effects of antimony trisulfide (Sb₂S₃) and zirconium silicate (ZrSiO₄) in the automotive brake friction material on friction characteristics." *Wear* 239, no. 2 (2000): 229-236. doi:10.1016/S0043-1648(00)00314-8.
- [61] Cho, Min-hyung, Jeong Ju, Seong-jin Kim, and Ho Jang. "Tribological properties of solid lubricants (graphite, Sb₂S₃, MoS₂) for automotive brake friction materials." *Wear* 260, no. 7-8 (2006): 855-860. doi:10.1016/j.wear.2005.04.003.
- [62] Aggarwal, Saroj. "What Are Brake Pads Made Of?" YourMechanic. Last modified November 30, 2015. <https://www.yourmechanic.com/article/what-are-brake-pads-made-of>.
- [63] "Disc Brake NVH." Know Your Parts. Last modified November 14, 2017. <https://www.knowyourparts.com/technical-resources/brakes-and-brake-components/disc-brake-nvh/>.
- [64] Lemen, Richard A. "Asbestos in brakes: exposure and risk of disease." *American Journal of Industrial Medicine* 45, no. 3 (2004): 229-237. doi:10.1002/ajim.10334.

[65] Roubicek, Vaclav, Helena Raclavska, Dagmer Juchelkova, and Peter Filip. "Wear and environmental aspects of composite materials for automotive braking industry."

Wear 265, no. 1-2 (2008): 167-175. doi:10.1016/j.wear.2007.09.006.

[66] Liew, Kia Wai, and Umar Nirmal. "Frictional performance evaluation of newly designed brake pad materials." *Materials & Design* 48 (2013): 25-33.

doi:10.1016/j.matdes.2012.07.055.

[67] Tyler, J. M. "Automotive applications for chromium." *Metal Finishing* 93, no. 10 (1995): 11-14. doi:10.1016/0026-0576(96)80425-9.

[68] Mandich, Nenad V., and Donald L. Snyder. "Electrodeposition of chromium." In *Modern electroplating*, edited by Mordechai Schlesinger and Milan Paunovic, 5th ed., 205–241. Hoboken, NJ, USA: Wiley, 2010. ISBN 9781118063149.

[69] Bolelli, Giovanni, Roberto Giovanardi, Luca Lusvarghi, and Tiziano Manfredini.

"Corrosion resistance of HVOF-sprayed coatings for hard chrome replacement."

Corrosion Science 48, no. 11 (2006): 3375-3397. doi:10.1016/j.corsci.2006.03.001.

[70] Bolelli, Giovanni, Valeria Cannillo, Luca Lusvarghi, and Sara Ricco. "Mechanical and tribological properties of electrolytic hard chrome and HVOF-sprayed coatings."

Surface and Coatings Technology 200, no. 9 (2006): 2995-3009.

doi:10.1016/j.surfcoat.2005.04.057.

[71] Houdková, Šarka, František Zahálka, Michaela Kašparová, and Lutz-Michael Berger.

"Comparative study of thermally sprayed coatings under different types of wear

conditions for hard chromium replacement." *Tribology Letters* 43, no. 2 (2011): 139-154.
doi:10.1007/s11249-011-9791-9.

[72] Balamurugan, G. M., Muthukannan Duraiselvam, and V. Anandakrishnan.

"Comparison of high temperature wear behaviour of plasma sprayed WC–Co coated and hard chromium plated AISI 304 austenitic stainless steel." *Materials & Design* 35 (2012): 640-646. doi:10.1016/j.matdes.2011.10.012.

[73] Lal, Roop, and Ramesh Chandra Singh. "Experimental comparative study of chrome steel pin with and without chrome plated cast iron disc in situ fully flooded interface lubrication." *Surface Topography: Metrology and Properties* 6, no. 3 (2018): 035001. doi:10.1088/2051-672X/aac60a.

[74] Van Acker, Karel, Dirk Vanhoyweghen, Retal Persoons, and J. Vangrunderbeek.

"Influence of tungsten carbide particle size and distribution on the wear resistance of laser clad WC/Ni coatings." *Wear* 258, no. 1-4 (2005): 194-202.
doi:10.1016/j.wear.2004.09.041.

[75] Ocelík, Vaclav, Uazir O.B. De Oliveira, M. De Boer, and Jeff Th M. De Hosson.

"Thick Co-based coating on cast iron by side laser cladding: Analysis of processing conditions and coating properties." *Surface and Coatings Technology* 201, no. 12 (2007): 5875-5883. doi:10.1016/j.surfcoat.2006.10.044.

[76] De Oliveira, Uazir O.B., Vaclav Ocelík, and Jeff Th M. De Hosson. "Analysis of

coaxial laser cladding processing conditions." *Surface and Coatings Technology* 197, no. 2-3 (2005): 127-136. doi:10.1016/j.surfcoat.2004.06.029.

- [77] Cadenas, Modesto, Riccardo Vijande, Horacio J. Montes, and Jos é Manuel Sierra. "Wear behaviour of laser clad and plasma sprayed WC-Co coatings." *Wear* 212, no. 2 (1997): 244-253. doi:10.1016/S0043-1648(97)00127-0.
- [78] Gao, Ya-li, Cun-shan Wang, Man Yao, and Hong-bin Liu. "The resistance to wear and corrosion of laser-cladding Al₂O₃ ceramic coating on Mg alloy." *Applied Surface Science* 253, no. 12 (2007): 5306-5311. doi:10.1016/j.apsusc.2006.12.001.
- [79] Subramanian, R., S. Sircar, and Jyoti Mazumder. "Laser cladding of zirconium on magnesium for improved corrosion properties." *Journal of Materials Science* 26, no. 4 (1991): 951-956. doi:10.1007/BF00576771.
- [80] Fernández, Ea, Ma Cadenas, Ra González, Carmen Navas, Ra Fernández, and J. De Damborenea. "Wear behaviour of laser clad NiCrBSi coating." *Wear* 259, no. 7-12 (2005): 870-875.
- [81] Zhou, Shengfeng, Xiaoyan Zeng, Qianwu Hu, and Yongjun Huang. "Analysis of crack behavior for Ni-based WC composite coatings by laser cladding and crack-free realization." *Applied Surface Science* 255, no. 5 (2008): 1646-1653. doi:10.1016/j.apsusc.2008.04.003.
- [82] Herman, Herbert, and Sanjay Sampath. "Thermal spray coatings." In *Metallurgical and Ceramic Protective Coatings*, edited by Kurt H. Stern, 261–289. Dordrecht: Springer, 1996.
- [83] Pawlowski, Lech. *The Science and Engineering of Thermal Spray Coatings*, 2nd ed. Chichester, UK: John Wiley & Sons, 2008. ISBN 9780470754085.

[84] Espallargas, Nuria. *Future Development of Thermal Spray Coatings: Types, Designs, Manufacture and Applications*. Amsterdam: Elsevier, 2015. ISBN 9781845698126.

[85] Gérard, Barbezat. "Application of thermal spraying in the automobile industry." *Surface and Coatings Technology* 201, no. 5 (2006): 2028-2031.
doi:10.1016/j.surfcoat.2006.04.050.

[86] Barbezat, Gerard. "Thermal spray coatings for tribological applications in the automotive industry." *Advanced Engineering Materials* 8, no. 7 (2006): 678-681.
doi:10.1002/adem.200600044.

[87] Killinger, Andreas, Rainer Gadow, Georg Mauer, Alexandre Guignard, Robert Vaßen, and Detlev Stöver. "Review of new developments in suspension and solution precursor thermal spray processes." *Journal of Thermal Spray Technology* 20, no. 4 (2011): 677. doi:10.1007/s11666-011-9639-8.

[88] Elbriggmann, Thorsten. "Porsche Hard Like Diamond." Porsche HOME - Porsche USA.
<https://www.porsche.com/usa/aboutporsche/christophorusmagazine/archive/384/articleoverview/article03/>.

[89] "IDisc Brake Disc." Bosch Mobility Solutions. <https://www.bosch-mobility-solutions.com/en/highlights/automated-mobility/idisc/>.

[90] Federici, Matteo, Mattia Alemani, Cinzia Menapace, Stefano Gialanella, Guido Perricone, and Giovanni Straffelini. "A critical comparison of dynamometer data with

pin-on-disc data for the same two friction material pairs—A case study." *Wear* 424 (2019): 40-47. doi:10.1016/j.wear.2019.02.009.

[91] Anderson, Arnold E., Serge Gratch, and Hayden P. Hayes. "A New Laboratory Friction and Wear Test for the Characterization of Brake Linings." *SAE Technical Paper Series*, 1967. doi:10.4271/670079.

[92] Burkman, Albin J., and Frank H. Hishley. "Laboratory Evaluation of Brake Lining Materials." *SAE Technical Paper Series*, 1967. doi:10.4271/670510.

[93] Sanders, Paul G., Tom M. Dalka, and Rena Hecht Basch. "A reduced-scale brake dynamometer for friction characterization." *Tribology International* 34, no. 9 (2001): 609-615. doi:10.1016/S0301-679X(01)00053-6.

[94] Perzborn, Nils, Carlos Agudelo, and Georg Peter Ostermeyer. "On similarities and differences of measurements on inertia dynamometer and scale testing tribometer for friction coefficient evaluation." *SAE International Journal of Materials and Manufacturing* 8, no. 1 (2015): 104-117. doi:10.4271/2014-01-2523.

[95] Straffelini, Giovanni. *Friction and Wear: Methodologies for Design and Control*. Basingstoke, Switzerland: Springer, Cham, 2015. doi:10.1007/978-3-319-05894-8.

[96] Wahlström, Jens, Anders Söderberg, Lars Olander, Anders Jansson, and Ulf Olofsson. "A pin-on-disc simulation of airborne wear particles from disc brakes." *Wear* 268, no. 5-6 (2010): 763-769. doi:10.1016/j.wear.2009.11.014.

[97] Garg, Bhagwan D., Steven H. Cadle, Patricia A. Mulawa, Peter J. Groblicki, Chris Laroo, and Graham A. Parr. "Brake wear particulate matter emissions." *Environmental Science & Technology* 34, no. 21 (2000): 4463-4469. doi:10.1021/es001108h.

CHAPTER 3

EXPERIMENTAL DETAILS

3.1 Preparation of PEA Coating on Cast Iron

3.1.1 Cast Iron Materials

The substrate materials used in the present study were two common cast irons, a ductile cast iron ASTM A536 (Chapter 4) and a gray cast iron ASTM A247 (Chapters 5 and 6). Their chemical compositions and properties are shown in Table 3.1. The ASTM A536 cast iron was machined into discs with a diameter of 38 mm and a thickness of 5 mm [1], and the ASTM A247 cast iron was machined into discs with a diameter of 25.4 mm and a thickness of 3 mm [2].

Table 3.1 Chemical composition and properties of cast irons.

Materials		ASTM A536	ASTM A247
Element (wt.%)	C	3.50-3.90	2.60-3.75
	Si	2.25-3.00	1.80-3.00
	Mn	0.15-0.35	0.60-0.95
	P	0.05 Max	0.12 Max
	S	0.025 Max	0.07 Max
	Fe	Remainder	Remainder
Vickers Hardness		238	238
Thermal Conductivity (W/ K m)		36	50

3.1.2 Preparation of PEA Coating

A PEA process was used to produce an oxide ceramic coating on the cast iron discs.

During the PEA process, the cast iron discs were polished with abrasive papers and

immersed into an electrolytic solution contained 15-20 g/L sodium aluminate in a stainless steel vessel. The cast iron discs were biased with negative voltage while the stainless vessel was used as cathode. The anode and the cathode were connected to a pulsed direct current (DC) power supply employed a unipolar mode of 40 % duration of 1000 Hz frequency. The schematic drawing of instrument is shown in Figure 3.1. The current density was controlled at 0.15 A/cm^2 , and the treatment time was 5 minutes in Chapter 4 and 15 minutes in Chapters 5 and 6. The temperature of the electrolytic solution was maintained around 300 K by a tap water cooling system. The PEA process has also been reported previously described in detail [3]. After the coating was produced, the coated sample was lightly polished and then cleaned with acetone.

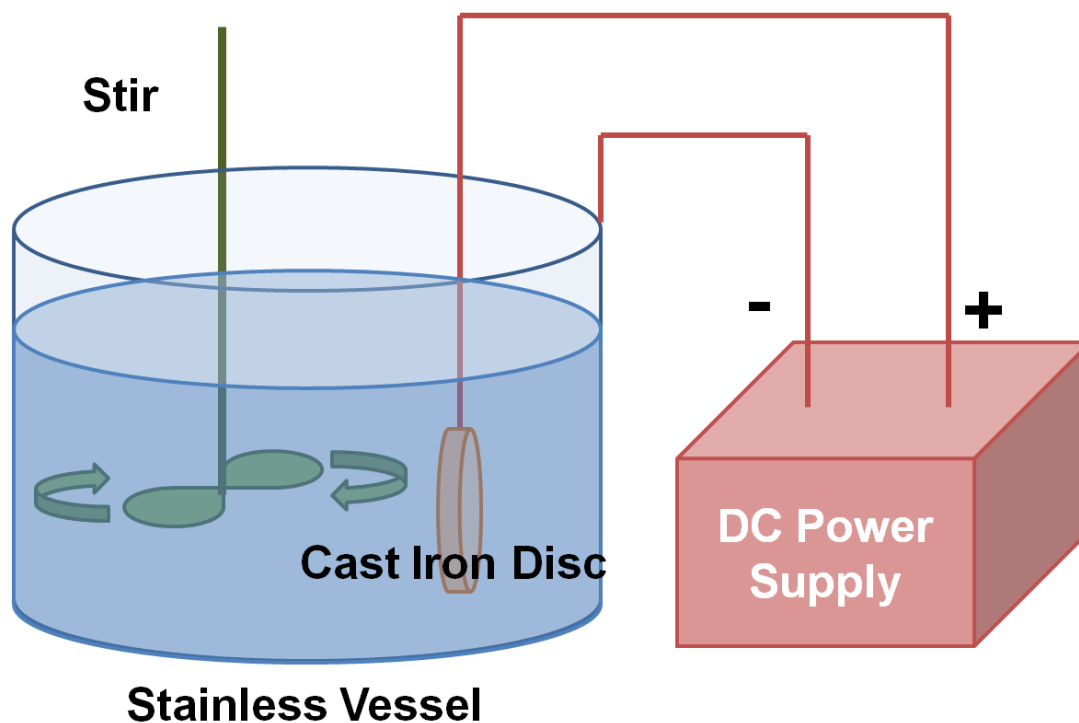


Figure 3.1 Schematic drawing of instrument.

3.2 Tribological Tests

The tribological tests were performed in a Pin-on-Disc tribometer to measure coefficients of friction (COFs) of the PEA-coated discs and uncoated discs for comparison. The tribometer is enclosed by a transparent plastic box. In this test, the brake pad to brake rotor contact pair is replaced by pin and cast iron samples. The pins worked as tribological counterparts were cut out of several different kinds of commercially available brake pads (ceramic, semi-metallic and NAO) and machined into cuboids (5 mm×5 mm×10 mm). The square sides (5 mm×5 mm) contacted the PEA coating in the tests. The schematic drawing of Pin-on-Disc test is shown in Figure 3.2. The Pin-on-Disc tribometer ran with a constant applied normal force of 20 N resulted a nominal contact pressure of 0.8 MPa which was similar to that of a normal braking operation [4]. The ambient air temperature of the tests was at a room temperature of 297 K. The sliding velocity was 0.05 m/s to simulate cold friction of a brake system at low temperature. In Chapter 4, two different testing distances were applied on each sample: at one location, the tribotest was paused every 50 m of sliding distance travelling a total of 4×50 m; at another location, the sample was tested 1000 m without pausing. In Chapter 5, the number of testing rotations for each test was 4000 (equivalent to 50 m sliding distance). In Chapter 5, the sliding distance for every counterpart was 200m at each run of the test and repeated the test for 5 times at the same place of the coated surface. During the tribotests, the COFs were recorded by software. Any changes in the COF curves should be related to the changes in surface morphology. After the tests were completed, the height variations of the pins were determined using a digital dial indicator and these data were then used to calculate the wear of the pads.

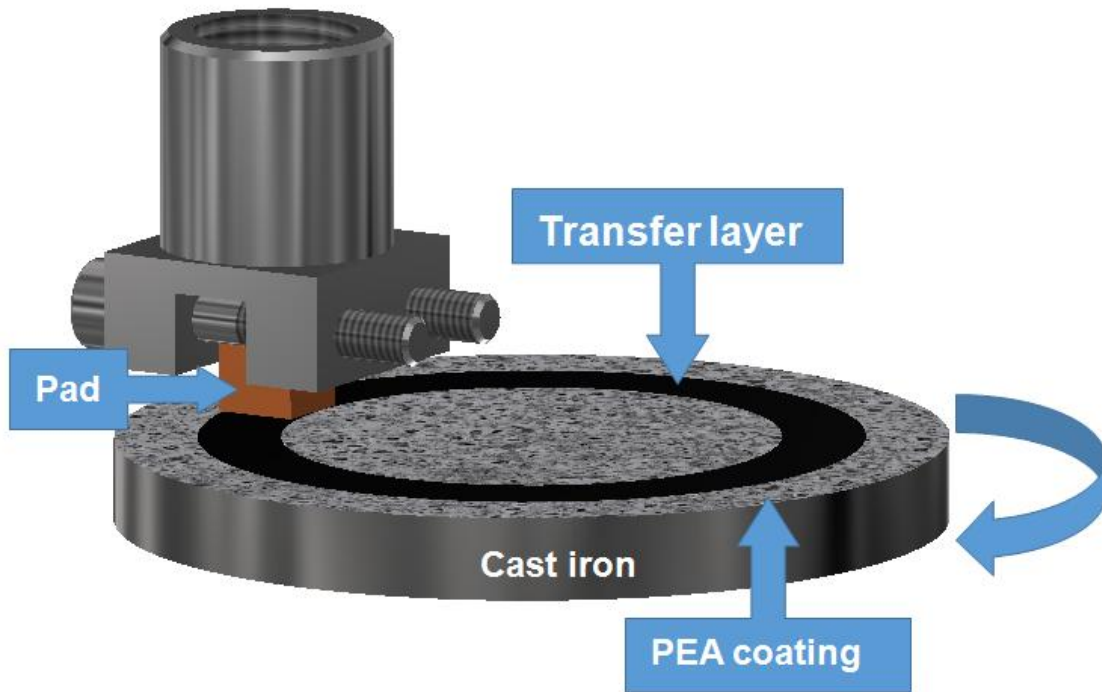


Figure 3.2 Schematic drawing of Pin-on-Disc test

3.3 Surface Profile Measurement

Both the surface roughness (R_a , R_{pk} and R_{vk}) and sectional profiles on the original polished surface and wear tracks of PEA-coated and uncoated cast iron discs were measured and recorded using a surface profilometer (Mitutoyo SJ-201P, shown in Figure 3.3) with a data-summarized system.



Figure 3.3 Mitutoyo SJ-201P surface profilometer [5].

3.4 Surface Hardness Measurement

The hardness of the PEA-coated and untreated cast iron discs was measured by a Vickers hardness tester (Buehler MicroMet II, shown in Figure 3.4).



Figure 3.4 Buehler MicroMet II micro-hardness tester [6].

3.5 Characterization of Morphology and Elemental Distribution

Before the tribological tests, the surface morphology and elemental distribution of the original polished PEA-coated and uncoated cast iron discs and the counterpart pins made from brake pads were observed under a scanning electron microscope (SEM, Hitachi, TM 3030, shown in Figure 3.5) and an energy dispersive X-ray detector (EDX, Bruker, QUANTAX EDS for SEM, shown in Figure 3.6) respectively. The phase structures of the PEA coating were investigated using an X-ray diffractometer (XRD, PROTO, AXRD BENCHTOP, shown in Figure 3.7) with Cu K α radiation. XRD measurements were made from 20-100 °2 theta. After the tests, the SEM and EDX were again utilized to

study the surface morphology and elemental compositions on the wear tracks of PEA-coated and uncoated cast iron discs. The surface morphology of the counterpart pins after sliding tests were also obtained through SEM.



Figure 3.5 Tabletop Microscope TM3030 [7].



Figure 3.6 Bruker QUANTAX EDS for SEM [8].



Figure 3.7 PROTO AXRD BENCHTOP [9].

REFERENCES

- [1] Cai, Ran , Chen Zhao, and Xueyuan Nie. "Alumina-Based Coating with Dimples as Enabling Sustainable Technology To Reduce Wear and Emission of the Brake System." *ACS Sustainable Chemistry & Engineering* 8, no. 2 (2019): 893-899. doi:10.1021/acssuschemeng.9b05302.
- [2] Cai, Ran , Jingzeng Zhang, Xueyuan Nie, Jimi Tjong, and D.T.A. Matthews. "Wear Mechanism Evolution on Brake Discs for Reduced Wear and Particulate Emissions." *Wear* 452-453-453 (2020): 203283. doi:10.1016/j.wear.2020.203283.
- [3] Zhao, Chen, Wei Zha, Ran Cai, Xueyuan Nie, and Jimi Tjong. "A New Eco-friendly Anticorrosion Strategy for Ferrous Metals: Plasma Electrolytic Aluminating." *ACS Sustainable Chemistry & Engineering* 7, no. 5 (2019): 5524-5531. doi:10.1021/acssuschemeng.8b06839.
- [4] Shorowordi, Kazi Md, Abdul S. Md Abdul Haseeb, and Jean-Pierre Celis. "Velocity effects on the wear, friction and tribochemistry of aluminum MMC sliding against phenolic brake pad." *Wear* 256, no. 11-12 (2004): 1176-1181. doi:10.1016/j.wear.2003.08.002.
- [5] "Surftest SJ-201P Portable Surface Roughness Tester." *Advanced Test Equipment Rentals*. https://www.atecorp.com/atecorp/media/pdfs/data-sheets/mitutoyo-sj-201p_datasheet.pdf.
- [6] Zhao, Chen. "Failure Mechanisms of the Protective Coatings for the Hot Stamping Applications." *Electronic Theses and Dissertations* 7311, University of Windsor, 2017. <https://scholar.uwindsor.ca/etd/7311>.

[7] "Tabletop Microscope TM3030 : Hitachi High-Tech GLOBAL." *Hitachi High-Tech in America*. https://www.hitachi-hightech.com/global/product_detail/?pn=em-tm3030.

[8] "QUANTAX for SEM - Overview, X-ray Spectrometer for Scanning Electron Microscopes." *Bruker*. <https://www.bruker.com/products/x-ray-diffraction-and-elemental-analysis/eds-wds-ebsd-sem-micro-xrf-and-sem-micro-ct/quantax-eds-for-sem/overview.html>.

[9] "AXRD BENCHTOP" *PROTO*. <https://www.protoxrd.com/axrd-benchtop-powder.html>.

CHAPTER 4

ALUMINA-BASED COATING WITH DIMPLES AS ENABLING SUSTAINABLE TECHNOLOGY TO REDUCE WEAR AND EMISSION OF BRAKE SYSTEM

4.1 Introduction

Traffic-related particle sources can be distinguished into exhaust and non-exhaust traffic-related particle emissions [1, 2]. Non-exhaust traffic-related sources are estimated to contribute almost the same as exhaust sources to total traffic-related PM₁₀ emissions [3]. Brake wear is considered to be one of the most significant particulate matter (PM) contributors among non-exhaust traffic-related sources particularly within areas with high traffic density. In urban environments, it can contribute up to 55 % by mass to total non-exhaust traffic-related PM₁₀ emissions [4]. These airborne particles have been found to have adverse effects [5] such as weakening pulmonary antimicrobial immune defence [6], inducing heritable mutations [7], and affecting lung function [8]. However, for the brakes to function, the rotors and pads have to wear. When a brake works, humps on the surface of brake rotors are pressed into the pads and debris is torn from the friction materials of the pads or sheared off from the brake rotors [9]. Some debris is thrown out of the contacting interface. Others continue to experience the repeated process, namely, deforming, crushing, breaking, and peeling. Finally, they are adhered onto the pad or even rotor base surface to form a friction film with a thickness of several micrometers to several hundred micrometers [10]. The friction film is greatly beneficial to protect friction materials of the pad from being seriously abraded [9].

In order to reduce brake dust production, a special surface coating on the face of a brake rotor has been proposed. For instance, Porsche Surface Coated Brake (PSCB) rotor

features a cast iron core coated with tungsten carbide. Porsche claims it lasts up to 30 percent longer than its cast iron rotors and reduces brake dust by 90 percent. An alternative method of improving the corrosion and wear resistance of brake rotors can be a ceramic oxide coating prepared using plasma electrolytic aluminating (PEA) process, which is investigated in this paper. In the PEA process, a composite ceramic coating (hercynite–alumina) is deposited on the surface of cast iron or steel with the assistance of plasma discharging in the aluminate-based solutions [11]. It was inspired by both the phosphating and plasma electrolytic oxidation (PEO) processes. PEO is a process whereby a high electric voltage leads to a dielectric breakdown of passive film on a metal surface and subsequent formation of a ceramic oxide film with high hardness, low thermal conductivity, and excellent adhesion to the substrate metal [12-15]. Although the thermal conductivity of the ceramic coating can affect the heat transfer of the brake system, the effect is very little because the thickness of the PEO coating is relatively thin [16].

In this work, the PEA process was utilized to obtain an alumina-based (Al_2O_3) ceramic coating on cast iron brake rotors. The alteration of wear mechanism between PEA-coated cast iron brake rotors and uncoated ones was investigated. A ceramic pad is used as the counterpart of the tribological coupling. The wear rate of brake rotors and pads were also measured to compare the propensity of dust production of PEA-coated brake rotors with uncoated brake rotors. The focus of this work was to study the effect of the PEA coating on friction type of brake system, with the aim of minimizing wear debris emission in a brake system.

4.2 Experimental Details

A ductile cast iron (ASTM A536) plate was machined into discs with a diameter of 38 mm and a thickness of 5 mm. A PEA process was used to produce an oxide ceramic coating on the discs. During the PEA process, the cast iron disc (used as anode) was dipped into an electrolytic solution in a stainless steel vessel (used as cathode). The anode and the cathode were connected to a pulsed DC power supply. The coating was prepared with a unipolar mode of 40 % duration of 1000 Hz. The current density was controlled at 0.15 A/cm^2 , and the treatment time was 5 minutes. The temperature of the solution was maintained around 300 K by a tap water cooling system. The detailed coating formation process was reported previously [16]. After the coating was produced, the coated sample was lightly polished and then cleaned with acetone. The surface morphology and elements of the coated sample were analyzed under a Scanning Electron Microscope (SEM) and an Energy Dispersive X-ray Detector (EDX). An X-ray diffractometer (XRD) with the geometry of $20^\circ - 100^\circ 2\theta$ and CuKalpha radiation was used to investigate the phase structures of the coating. A Mitutoyo surface profiler SJ201P was employed to measure the surface roughness and record the coating surface profiles.

A pin-on-disc tribometer was used to measure coefficients of friction of the coated discs and uncoated discs for comparison. The pins as tribological counterparts were machined from a commercially available ceramic brake pad to have a cuboid geometry (5 mm \times 5 mm \times 10 mm). The testing contact areas were the square sides (5 mm \times 5 mm) of the cuboids. The tests were carried out at a room temperature of 24°C and a humidity of around 50-60 %. The elements' distribution of the brake pad materials was obtained through EDX analysis. The load used for the tribological tests was 20 N, which resulted

in a nominal contact pressure of 0.8 MPa similar to that of a normal braking operation [17, 18]. The sliding speed was 0.05 m/s. Two different testing distances were applied on each sample: at one location, the tribotest was paused every 50 m of sliding distance travelling a total of 4×50 m; at another location, the sample was tested 1000 m without pausing. The coefficients of friction (COF) were recorded by software, and the relationships between the coefficients of friction and surface characteristics were studied and reported in the following section. Any changes in the COF curves should be related to the changes in surface morphology. Since the samples had the same coating thickness, the effect of the coating and substrate (as a system) on frictional behavior can be assumed to be the same for all cases. After the tribological tests, the Mitutoyo surface profiler was also utilized to obtain the sectional profiles of the wear tracks. The surface morphology and elemental compositions on the wear tracks of each sample were studied for better understanding of wear and friction mechanism.

4.3 Results and Discussion

4.3.1 Alumina-based Coating and Pad Materials

The base materials of the tribological test coupling samples were obtained from commercial brake rotor and pad, respectively. The brake rotor was made of ductile cast iron. Through the PEA process, an alumina-based coating was grown on the top surface of the cast iron samples as shown in Figure 4.1 where images of the coating surface and cross section were presented. The coating has a dimple-like surface morphology, Figure 4.1a. The interfacial region between the substrate and the coating exhibits small pores, and larger pores appear at the upper region in the coating, Figure 4.1b. Figure 4.2 shows a XRD pattern of the PEA coating, indicating that the coating mainly comprises Al_2O_3

phase with some FeAl_2O_4 . The peaks of iron (Fe) detected are from the cast iron substrate. A similar result was reported previously [11].

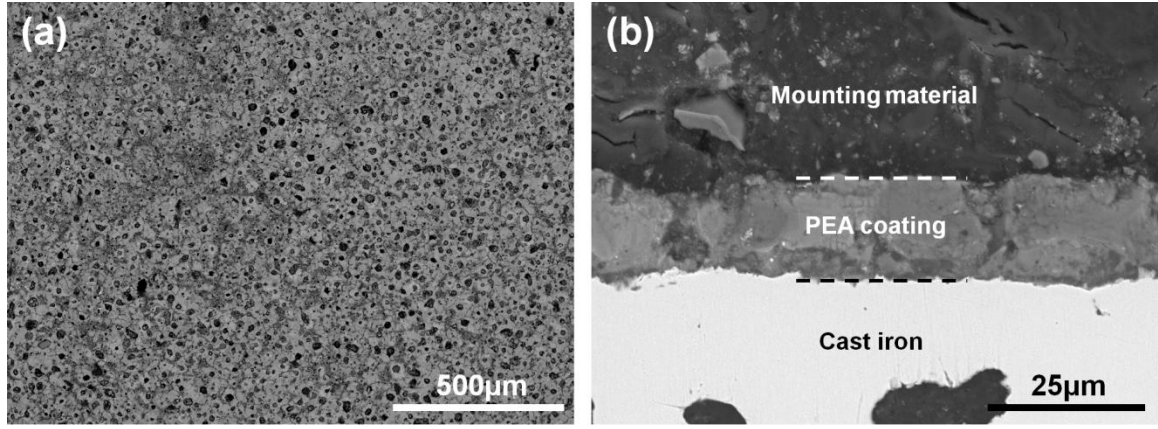


Figure 4.1. SEM images showing morphology of PEA coating: (a) coating surface and (b) cross section.

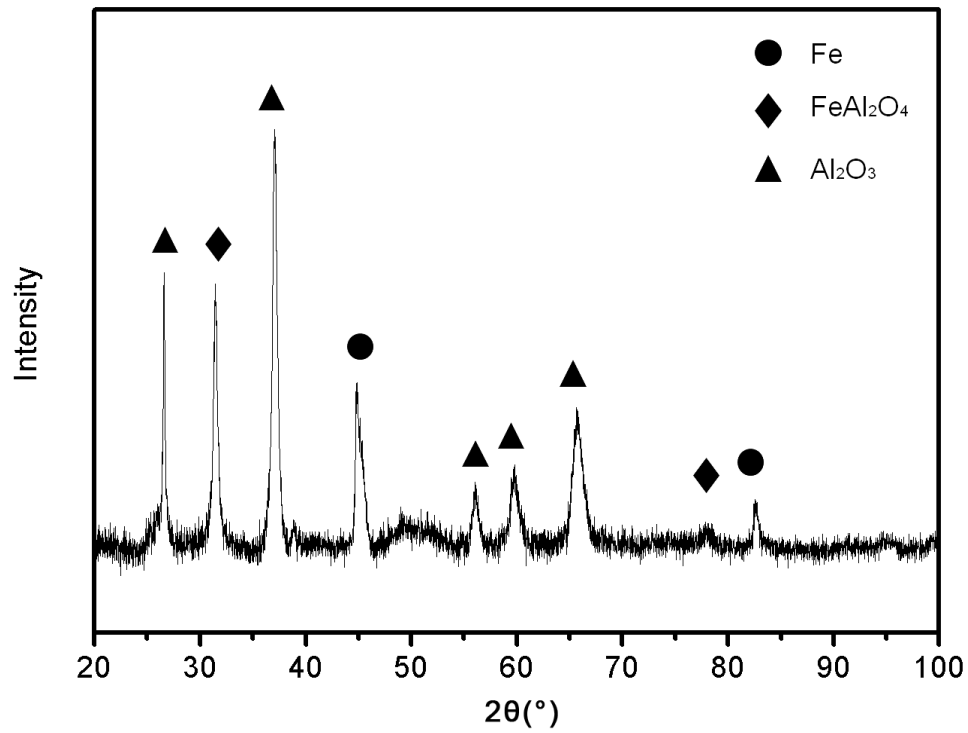


Figure 4.2. XRD pattern of a PEA coating on cast iron.

Friction materials in the pad play important roles in the brake system since brakes use friction to brake. A brake pad may require no less than 10 to 20 different raw materials. Depending on their specific roles, the raw materials are divided into three categories; "bonding material", "stiffener" (reinforcement), and "friction adjustment material." The bonding material holds the raw materials of the pad together and ensures the structural integrity of the pad under mechanical and thermal stresses. The stiffener provides mechanical strength and structure to the pad. The friction adjustment material mainly regulates the tribological characteristics of the pad. It is used for stabilizing the performance of friction.

Table 4.1. Elemental composition of different surfaces as determined using EDX

Material Element	Ceramic pad	PEA-coated cast iron		Cast iron	
		Polished surface	Wear track	Polished surface	Wear track
C	○	○	○	○	○
O	○	○	○	-	○
Na	-	○	-	-	-
Mg	○	-	○	-	-
Al	○	○	○	-	-
Si	○	○	○	○	○
S	○	-	○	-	-
K	○	-	○	-	-
Ca	○	-	○	-	-
Ti	○	-	○	-	-
Fe	○	○	○	○	○
Cu	○	-	○	-	-
Zn	○	-	○	-	-
Ba	○	-	○	-	-

○ the element included; - the element excluded.

The elements distribution of the brake pad materials was obtained through EDX analysis.

Table 4.1 shows the elements of the pad. Ba, Ti and S were from the stiffener and worked

as fillers in friction materials. Fe, Ca and brass (Cu and Zn) fibers were reinforcements and used to increase both thermal conductivity and material mechanical strength. C, Si, K, Mg and Al were from friction adjustment materials, where Si, Mg and Al worked as abrasives and helped to improve friction levels; Al could also improve heat conductivity and help to polish and clean the metallic counterface enhancing friction stability; and carbon was used as a lubricate component to lower the friction coefficient. An unexpectedly high friction would cause overheating of a brake system.

4.3.2 Surface Morphology

The surface morphology of the original as-polished samples and wear tracks after tribotests is shown in Figure 4.3. The Roughness Average (R_a), Reduced Peak Height (R_{pk}) and Reduced Valley Height (R_{vk}) of sample surfaces before and after the tests were measured and shown in Table 4.2. Due to its dimple-like texturing surface, the polished coating (Figure 4.3a) had a comparatively rougher surface than uncoated polished original cast iron (Figure 4.3d). Figures 4.3b and 4.3c show that there are thin films formed on the coating in the wear track after the pin-on-disc tribotest while the cast iron sample showed only scratches in the wear track (Figures 4.3e and 4.3f). The dimple-like surface seems to promote the formation of a transferred layer on the top of the coating, compared to the uncoated cast iron case. The chemical composition of the transfer layer was detected using EDX and listed in Table 4.1, showing that the layer materials were from the brake pad. For the uncoated cast iron sample, oxidation might occur on its wear track because of the frictional heat generated between the rotor and the pad materials during the sliding, since oxygen element was massively found on the wear track as shown in Table 4.1. Table 4.2 records surface properties of the coated and uncoated cast iron

samples after the tribotests with different sliding distances. From the table, it can be seen that the coating surface became smoother on its wear track area due to coverage of the transferred layer. However, the surface of the uncoated cast iron sample roughened; and the depth of valley R_{vk} significantly increased as well because wear grooves were formed after the sliding wear test.

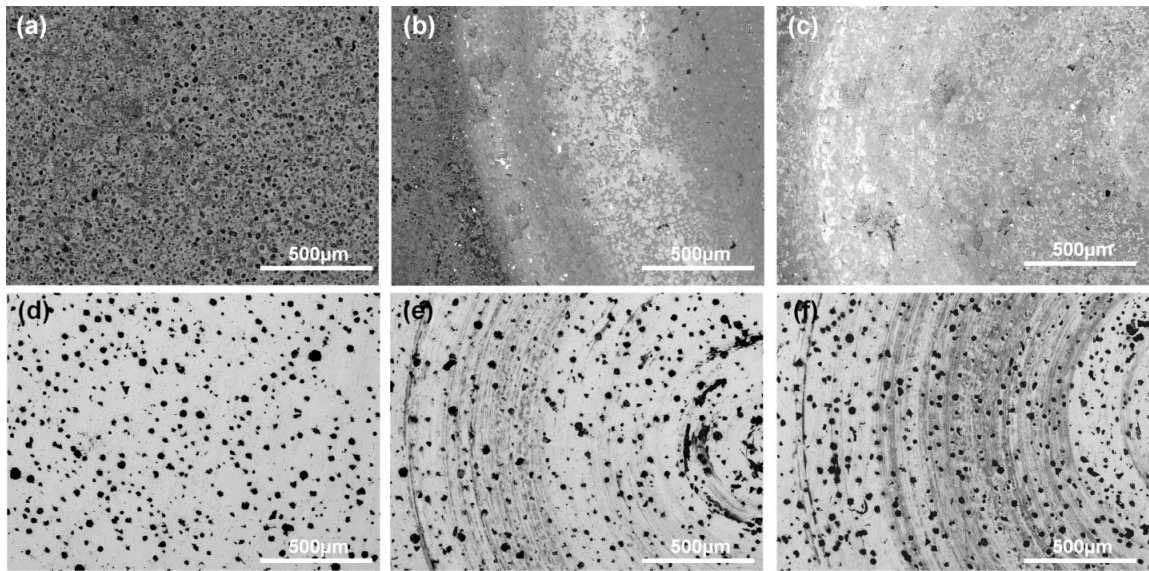


Figure 4.3. SEM images showing surface morphology of samples: (a) original polished coating; wear track on coating after test sliding distance of (b) 4×50 m and (c) 1000 m; (d) original polished cast iron; wear track on cast iron after test sliding distance of (e) 4×50 m and (f) 1000 m.

Table 4.2. Surface properties of the samples after tribotests with different sliding distances

Sample	Material	PEA coating		Cast iron	
	Testing distance	4 ×50 m	1000 m	4 ×50 m	1000 m
Polished surface	R _a (μm)	2.65		0.10	
	R _{pk} (μm)	0.37		0.17	
	R _{vk} (μm)	3.51		0.56	
Wear track	R _a (μm)	1.17	1.39	0.21	0.20
	R _{pk} (μm)	0.77	0.41	0.17	0.18
	R _{vk} (μm)	3.75	3.56	1.14	1.36

Figure 4.4 illustrates in detail the sectional profile and surface morphology inside and outside the wear track on PEA coating after the tribotest. Unlike large and deep dimples on the original coating (shown in very right side of the sectional profile in Figure 4.4), the wear track shown on the left side has quite even surface. A thin layer filled in the dimples and covered the original coating. The thin layer adhered well to the dimpled surface. When the sliding distance of the test increased, the transfer layer became thicker to some extent and a secondary transfer layer seemingly formed on the top of the first thin layer. Some cracks and chippings can be found locally on the new accumulated layer. Additionally, there are some variations along the transversal direction on the wear track in terms of surface morphology and profile of the transfer layer. The differences were attributed to uneven distributions of friction materials in the brake pad which led to non-uniformity of the transfer layer formed on the coated rotor material.

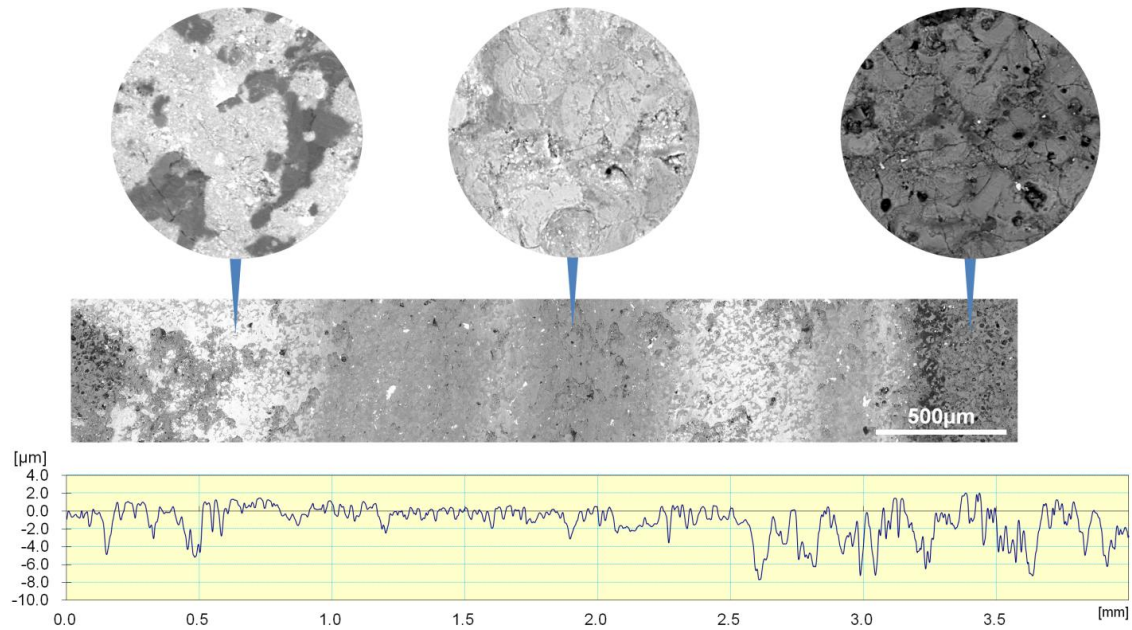


Figure 4.4. Sectional profile and surface morphology of wear track and polished surface of PEA coating.

4.3.3 Tribological Behaviors

The pad-on-disc tests were conducted on the PEA-coated and uncoated cast iron brake rotor coupons. The tests were either interrupted every 50 m sliding distance for 200 m in total or were continued up to 1000 m. Their coefficients of friction were plotted in Figures 4.5a and 4.5b, respectively. The height variation of each tested brake pad was measured with a digital dial indicator. Generally speaking, the frictions are slightly higher for interrupted brake sliding operation (in Figure 4.5a) than for continuously sliding testing (in Figure 4.5b). The repeating operation of braking and releasing would be helpful to have a higher friction force. Figure 4.5 also illustrates the comparison of the dynamic COFs of PEA-coated vs. uncoated base cast iron coupons. In the tribotests, the coefficient of friction is relatively low for the coated cast iron test samples. A cast iron brake disc sample exhibits a consistently higher COF level. As for the case with the

sliding distance of 4×50 m (Figure 4.5a), the COF of both coating and cast iron increased at the first and the second 50 m. The coefficients of friction decreased at the third 50 m for the coating and cast iron to varying degrees. However, the friction coefficient of the coating reached its maximum in the last 50 m sliding, while the friction of cast iron at the end was lower than its maximum shown at the second 50 m. Consequently, the coated and uncoated brake rotors are approaching almost the same COF of 0.15. When the friction reached a steady stage during the continuously sliding with 1000 m distance, the coefficient of friction was 0.10-0.12 (for PEA coating) or 0.13-0.14 (for cast iron).

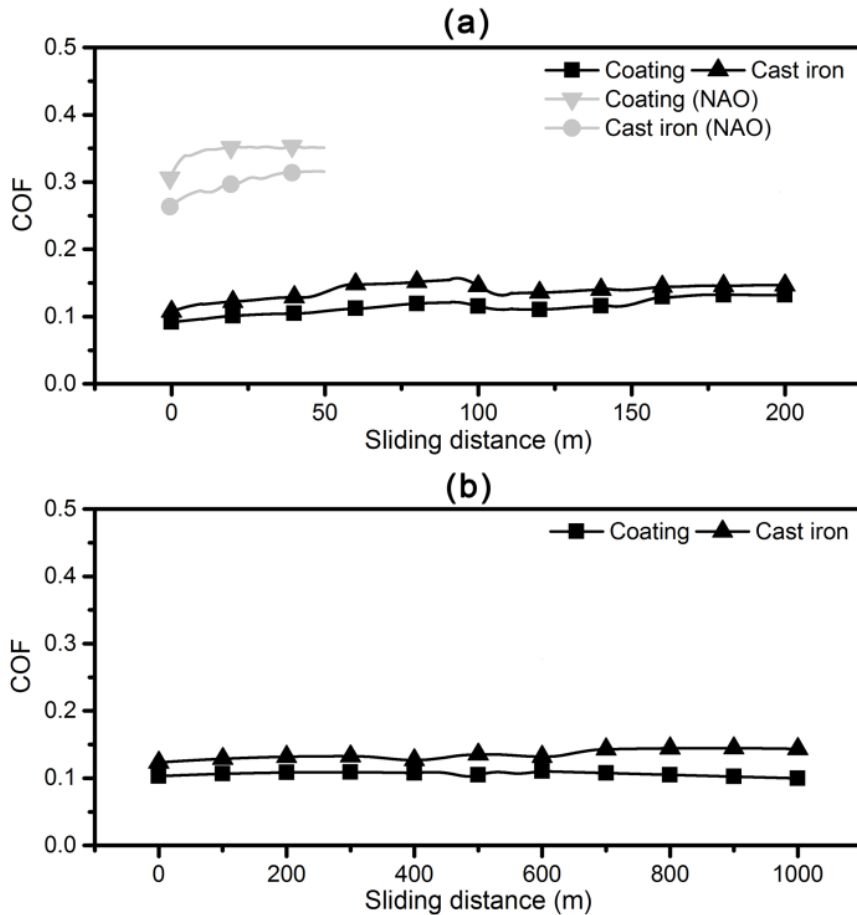


Figure 4.5. Coefficients of friction of PEA coating and cast iron under different sliding distance: (a) 4×50 m; (b) 1000 m.

It should be noted that the coefficients of friction are lower than a normal value of a rotor-pad friction which is 0.30-0.42 [9, 19]. The low COFs obtained should be attributed to ceramic pad's low cold bite performance (i.e., at ambient temperature). Another tribotest under the same test conditions was conducted using a commercial non asbestos organic (NAO) brake pad as the counterpart of the tribological coupling [20]. From the test with the sliding distance of 50 m, the NAO pad showed a much better cold bite than the ceramic pad. When its friction reached a steady stage, the COF was around 0.3 for coated and uncoated cast iron samples. The COFs of coated and uncoated rotors against the NAO pad are shown by gray lines in Figure 4.5a.

Figure 4.6 shows wear rates of the brake pads under different testing conditions.

Obviously, the coating caused a significantly lower wear to the brake pads. For the interrupted brake testing condition (4×50 m), a 40 % less wear occurred on the brake pad materials when the pads were running against the coating instead of against the bare cast iron. After the non-stop test with 1000 m sliding distance, a 30 % less wear on the pads can be observed for the tests with the coating case vs. the uncoated rotor material.

This is believed to be the results of changes of friction modes, that is, from an abrasive-like friction sliding to an adhesive-like friction sliding. The SEM images on the bottom of Figure 4.6 show the surfaces of the brake pad segments after the sliding tests. The pads tested against the coating (Figures 4.6b and 4.6d) looks smoother than those against uncoated cast iron rotor (Figures 4.6a and 4.6c). It can be seen that there is a foreign material patch transferred from cast iron rotor onto the pad surface after 1000 m sliding distance (Figure 4.6c).

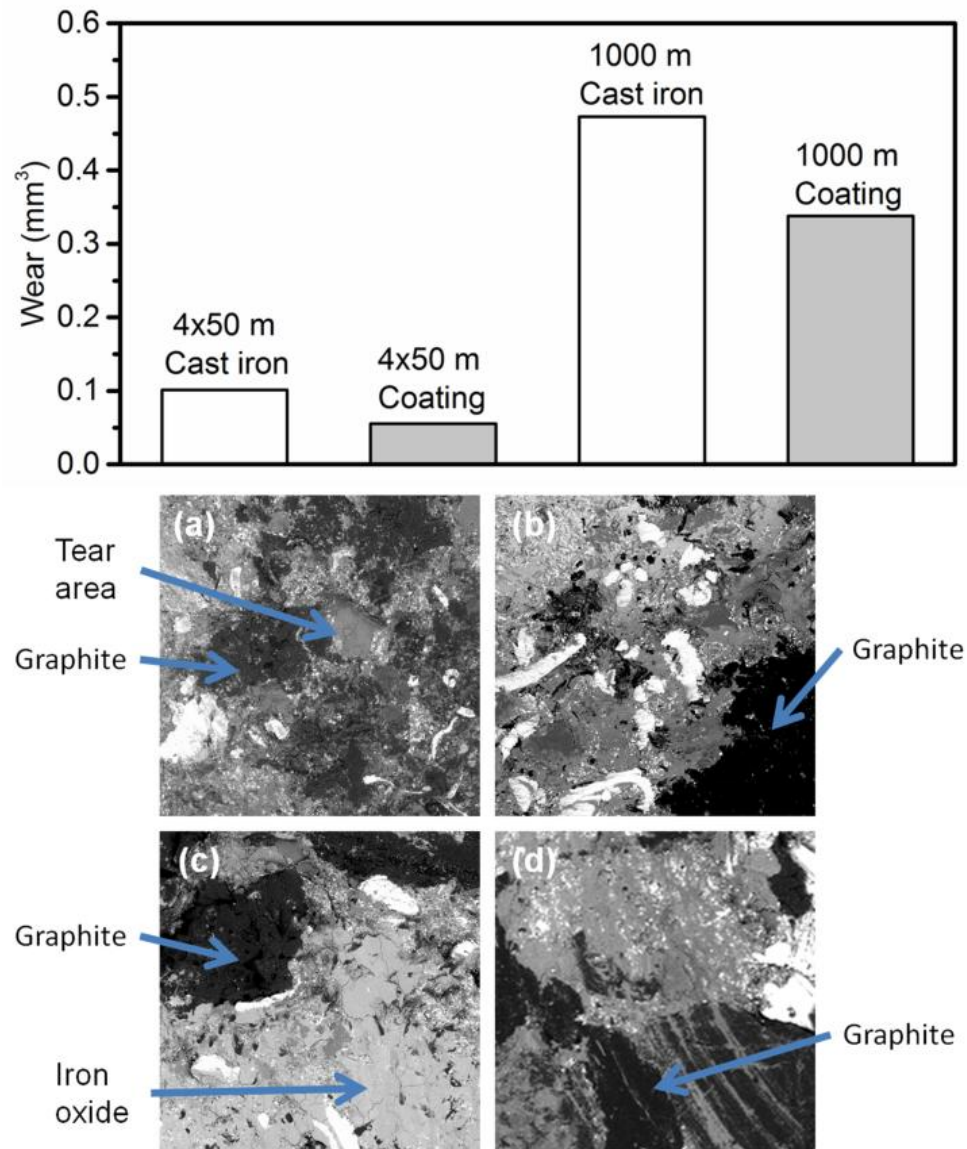


Figure 4.6. Wear (upper) and SEM images (lower) of brake pad under different testing condition: (a) cast iron after 4×50 m; (b) PEA coating after 4×50 m; (c) cast iron after 1000 m; (d) PEA coating after 1000 m.

4.3.4 Transformation of Wear Mechanism

There are two types of friction mechanism when it comes to brakes: abrasive friction and adhesive (adherent) friction. The cast iron rotors likely lead to abrasive friction as also

shown in this study. This type of friction involves the breaking of bonds of both the pad material and the rotor's cast iron when the caliper pushes them together; however, both of the coupling components experience wear. However, after the PEA coating process was applied on the original cast iron brake rotors, the type of friction changed from abrasive friction to adhesive friction. In adhesive friction, the pad materials were transferred onto the coated surface of the rotor forming a thin protective layer.

Figure 4.7 is SEM images of the cross-sectional frictional surfaces of the PEA-coated rotors after the test. As shown in Figures 4.3, 4.4 and 4.7, substances transferred from the brake pad is accumulated on the surface of the PEA-coated cast iron rotor to form a film. This is because the alumina-based ceramic coating had a dimple-like texture on the surface of the coated cast iron rotor and the substances transferred from the brake pad were to fill up the dimples first. Then, the substances in the dimples of PEA coating protruded from the surface of the coated rotor, and subsequently more transferred materials were accumulated between the protrusions. Thus it is thought that the dimple-like texture would function like keys or tree pits. When a brake system uses adhesive friction, the two contact surfaces are the same or similar materials and generate friction by breaking or shearing the bonds that are the same in the pad. The transfer layer is firmly bonded to the rotor's surface and cannot be washed away by water or wheel cleaners. While the first thin layer was adherent to the coating surface as a primary protective film, the second additional layer can be worn and replenished by the brake pad during the braking. These pads still produce dusts but with a much less amount.

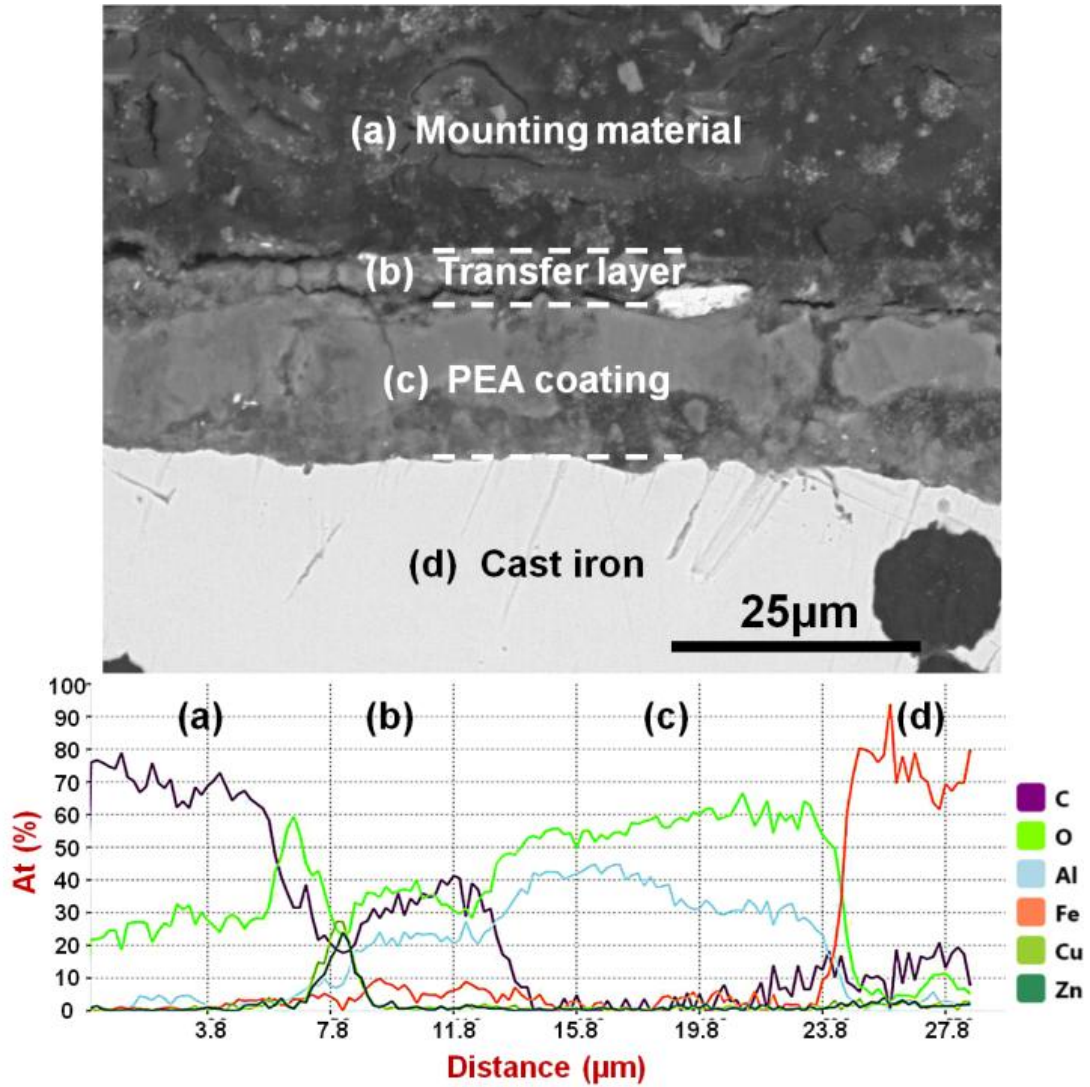


Figure 4.7. Cross-sectional SEM images of the frictional surface of PEA-coated brake rotor: (a) mounting material; (b) transfer layer; (c) PEA coating; (d) cast iron.

The friction mechanism model with regard to the PEA-coated brake rotor can be proposed as shown in Figure 4.8. In the case of the PEA-coated brake rotor, the coating surface was harder than the pad, and the wear debris would mainly come from the brake pad and fill in dimples (pores) and recess areas on the surface of the brake rotor to form a film. The film accumulates over the whole frictional surface. The hard particle inclusions

in the brake pad then scratch off a part of accumulated film on the brake rotor. As the accumulation and scratch-off of the film are repeated in this manner, the thickness of the film is kept substantially constant through the repeated braking operations. The brake pad is accordingly worn in an almost constant manner, which leads to a relatively stable friction coefficient in long braking distances (Figure 4.5b). In the case of the cast iron brake rotor, the initial smooth surface is scratched out by the hard particles in the brake pad where the particles have a higher hardness than the cast iron base material. During the sliding contact of pad and rotor, the shear force is generated on the pad surface materials, which causes wear to the brake pad. There was no transferred layer formed on the wear track of cast iron brake rotor (Figures 4.3e and 4.3f). The darkened areas near the wear scratches and grooves in Figures 4.3e and 4.3f were attributed to the friction-induced heat resulting in oxidation of iron elements in the cast iron rotor. The abrasive-like wear mechanism would increase the coefficient of friction to the degree where an intensive wear could occur to both pad and rotor.

It is worth mentioning that Figure 4.5 also suggests a stable friction and good durability. Figure 4.5a presents the results of tribotests repeated by 4 times with the total sliding distance of 200 m; Figure 5b shows the results after the 1000 m continuously sliding. The transfer layer's morphology (Figures 4.4 and 4.7) was almost the same after the test of 50 m, 200 m or 1000 m. The transfer layer was very durable at the test conditions. To investigate the effect of the sliding speed on the transfer layer, a high speed sliding tribometer [21] was used. When the sliding velocity went up to 5.62 m/s (maximum allowable speed of the tester), the transfer layer from the pad was still firmly attached on the coating surface. Thus, it is reasonable to believe that the dimples on the coating

surface would provide the transfer layer with excellent anchor sites for enhanced durability of brake rotor against friction wear.

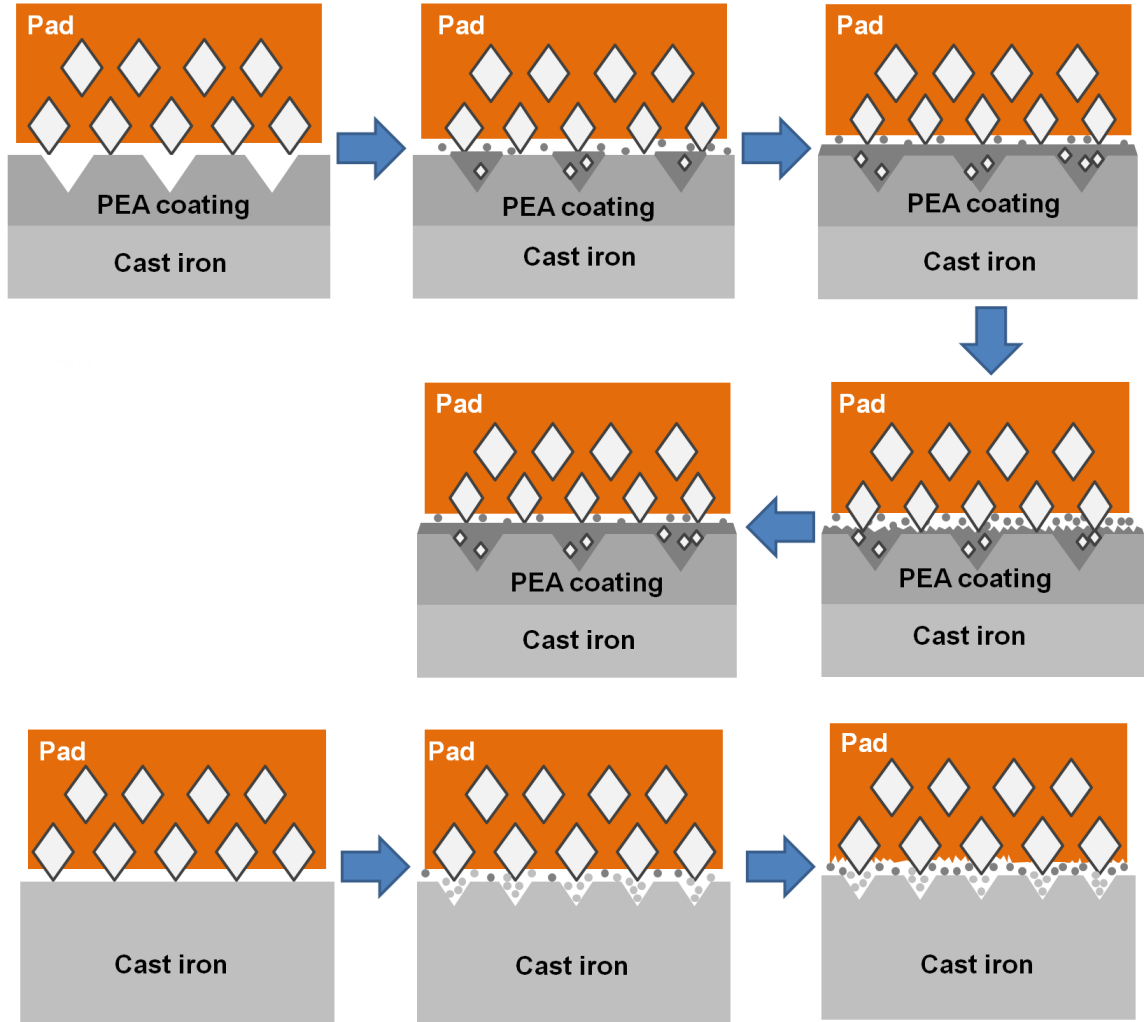


Figure 4.8. Friction process model with regard to PEA-coated and uncoated cast iron brake rotors.

Certainly, to reach the stage of real applications for the PEA-coated rotor, more research would be needed, including brake dynamometer test, R90 standard certificate tests [22], and others. However, this work has demonstrated a new environmental-friendly strategy potentially for better sustainability and lower emission of transportation industry.

Since there is almost no wear on the coated brake rotor, the rotor may last as long as a whole life of a vehicle if this proposed strategy can hold true in the further validation tests. Otherwise, 2-3 more brake rotors are needed for maintenance of each vehicle during its lifetime. The coated rotor also results in 30-40 % less wear to the brake pad, meaning there is only a need for one more pad (instead of 3 more pads) for the lifetime of a car. These results are very significant in tackling sustainability of the transportation industry potentially for natural resource preservation and environmental protection, considering that more than 70 million vehicles are produced worldwide every year.

4.4 Conclusions

Alumina-based coating on cast iron discs can be obtained by a PEA (plasma electrolytic aluminating) process. Unlike the uncoated cast iron surface, the hard coating has dimple-like surface morphology which can provide anchoring sites for formation of a transfer layer. With the coating, the wear behavior between rotor and pad changed from abrasive friction to adhesive friction. Substances transferred from the friction materials of brake pad are accumulated on the surface of the PEA-coated cast iron rotor to form a film when the brake system functions. The transferred substances are firstly stored in the dimples then protruded from the surface and more transferred materials are accumulated between the protrusions leading to a continuous film covering the whole frictional surface. The accumulated film is always being worn and replenished by the brake pad during braking, thus almost only pads produce dust and become the primary wear component. Contrarily the conventional cast iron rotor surface is scratched out by friction materials from brake pad during the braking and produces debris also from rotor without formation of transferred film. Compared with a conventional cast iron brake rotor, the PEA-coated cast

iron rotor causes much less wear to the brake pad material under the tested conditions. The PEA-coated cast iron has a slightly lower coefficient of friction than uncoated cast iron, while the friction level is more stable for the coating case. This work demonstrates an alumina-based coating strategy that can minimize wear debris emission in a brake system for sustainable and environmental benefit. Further studies including brake dynamometer tests are necessary to verify of the findings obtained in the current study.

REFERENCES

- [1] Grigoratos, Theodoros, and Giorgio Martini. "Brake wear particle emissions: a review." *Environmental Science and Pollution Research* 22, no. 4 (2015): 2491-2504. doi:10.1007/s11356-014-3696-8.
- [2] Boulter, P. G. "A review of emission factors and models for road vehicle non-exhaust particulate matter. TRL Limited, Wokingham, UK. (TRL Report PPR065)." *Atmospheric Environment* 77 (2005): 283-300.
- [3] Amato, Fulvio, Flemming Ralph Cassé, Hugo A. C. Denier Van Der Gon, Robert Gehrig, Mats Gustafsson, Wolfgang Hafner, Roy M. Harrison, Magdalena Jóźwicka, Frank J. Kelly, Teresa Moreno, André Stephan Henry Prévôt, Martijn Schaap, J. Sunyer, and Xavier Querol. "Urban air quality: the challenge of traffic non-exhaust emissions." *Journal of Hazardous Materials* 275 (2014): 31-36. doi:10.1016/j.jhazmat.2014.04.053.
- [4] Harrison, Roy M., Alan M. Jones, Johanna Gietl, Jianxin Yin, and David C. Green. "Estimation of the contributions of brake dust, tire wear, and resuspension to nonexhaust traffic particles derived from atmospheric measurements." *Environmental Science & Technology* 46, no. 12 (2012): 6523-6529. doi:10.1021/es300894r.
- [5] Lyu, Yezhe, Jens Wahlström, Minghui Tu, and Ulf Olofsson. "A Friction, Wear and Emission Tribometer Study of Non-Asbestos Organic Pins Sliding Against AlSiC MMC Discs." *Tribology in Industry* 40, no. 2 (2018): 274-282. doi:10.24874/ti.2018.40.02.11.
- [6] Zelikoff, Judith T., Lung Chi Chen, Mitchell D. Cohen, Kaijie Fang, Terry Gordon, Yun Li, Christine Nadziejko, and Richard B. Schlesinger. "Effects of inhaled ambient

particulate matter on pulmonary antimicrobial immune defense." *Inhalation Toxicology* 15, no. 2 (2003): 131-150. doi:10.1080/08958370304478.

[7] Samet, Jonathan M., David M. DeMarini, and Heinrich V. Malling. "Do airborne particles induce heritable mutations?." *Science* 304, no. 5673 (2004): 971-972. doi:10.1126/science.1097441.

[8] Zhou, Yun, Yuewei Liu, Yuanchao Song, Jungang Xie, Xiuqing Cui, Bing Zhang, Tingming Shi, Jing Yuan, and Weihong Chen. "Short-term effects of outdoor air pollution on lung function among female non-smokers in China." *Scientific Reports* 6 (2016): 34947. doi:10.1038/srep34947.

[9] Xiao, Xingming, Yan Yin, Jiusheng Bao, Lijian Lu, and Xuejun Feng. "Review on the friction and wear of brake materials." *Advances in Mechanical Engineering* 8, no. 5 (2016): 1687814016647300. doi:10.1177/1687814016647300.

[10] Ostermeyer, Georg Peter, and Michael Müller. "Dynamic interaction of friction and surface topography in brake systems." *Tribology International* 39, no. 5 (2006): 370-380. doi:10.1016/j.triboint.2005.04.018.

[11] Zhao, Chen, Wei Zha, Ran Cai, Xueyuan Nie, and Jimi Tjong. "A New Eco-friendly Anticorrosion Strategy for Ferrous Metals: Plasma Electrolytic Aluminating." *ACS Sustainable Chemistry & Engineering* 7, no. 5 (2019): 5524-5531. doi:10.1021/acssuschemeng.8b06839.

- [12] Yerokhin, Aleksey L., Xueyuan Nie, Adrian Leyland, Allan Matthews, and Stephen J. Dowey. "Plasma electrolysis for surface engineering." *Surface and Coatings Technology* 122, no. 2-3 (1999): 73-93. doi:10.1016/S0257-8972(99)00441-7.
- [13] Chang, Feng-Chuan, Chaur-Jeng Wang, Jyh-Wei Lee, and Bih-Show Lou. "Microstructure and mechanical properties evaluation of molybdenum disulfide-titania nanocomposite coatings grown by plasma electrolytic oxidation." *Surface and Coatings Technology* 303 (2016): 68-77. doi:10.1016/j.surfcoat.2016.03.078.
- [14] Walsh, Frank C., Chee Tong John Low, Robert James Knoyle Wood, K. T. Stevens, John Archer, A. R. Poeton, and A. Ryder. "Plasma electrolytic oxidation (PEO) for production of anodised coatings on lightweight metal (Al, Mg, Ti) alloys." *Transactions of the IMF* 87, no. 3 (2009): 122-135. doi:10.1179/174591908X372482.
- [15] Nie, Xueyuan, Efsfathios I. Meletis, Jiechao Jiang, Adrian Leyland, Aleksey L. Yerokhin, and Allan Matthews. "Abrasive wear/corrosion properties and TEM analysis of Al₂O₃ coatings fabricated using plasma electrolysis." *Surface and Coatings Technology* 149, no. 2-3 (2002): 245-251. doi:10.1016/S0257-8972(01)01453-0.
- [16] Shen, Xinwei, Xueyuan Nie, and Jimi Tjong. "Effects of electrolytic jet plasma oxidation (EJPO) coatings on thermal behavior of engine cylinders." *Heat and Mass Transfer* 55, no. 9 (2019): 2503-2515. doi:10.1007/s00231-019-02600-6.
- [17] Shorowordi, Kazi Md, Abdul S. Md Abdul Haseeb, and Jean-Pierre Celis. "Velocity effects on the wear, friction and tribochemistry of aluminum MMC sliding against phenolic brake pad." *Wear* 256, no. 11-12 (2004): 1176-1181. doi:10.1016/j.wear.2003.08.002.

- [18] Sallit, I., Caroline S. Richard, R. Adam, and François Robbe-Valloire. "Characterization methodology of a tribological couple: metal matrix composite/brake pads." *Materials Characterization* 40, no. 3 (1998): 169-188. doi:10.1016/S1044-5803(98)00007-2.
- [19] Österle, Werner, and Ingrid Urban. "Friction layers and friction films on PMC brake pads." *Wear* 257, no. 1-2 (2004): 215-226. doi:10.1016/j.wear.2003.12.017.
- [20] Cai, Ran, Chen Zhao, Jiayi Sun, and Xueyuan Nie. "Wear Mechanism of Cast Iron Brake Rotor Altered by Plasma Electrolytic Oxidation Coating for Reduction of Wear and Emission." Paper presented at TACT 2019 International Thin Films Conference, Taipei, Taiwan, November 17-20, 2019.
- [21] Wang, Guang, Xueyuan Nie, and Jimi Tjong. "Investigation into mixed and hydrodynamic frictions of PEO coatings and cast iron." *SAE International Journal of Fuels and Lubricants* 9, no. 1 (2016): 23-31. doi:10.4271/2016-01-0491.
- [22] Economic Commission for Europe–Inland Transport Committee. "Regulation No 90 of the Economic Commission for Europe of the United Nations (UN/ECE) — Uniform provisions concerning the approval of replacement brake lining assemblies and drum brake linings for power-driven vehicles and their trailers." *Official Journal of the European Union* (2010): 19-49.

CHAPTER 5

WEAR MECHANISM EVOLUTION ON BRAKE DISCS FOR REDUCED WEAR AND PARTICULATE EMISSIONS

5.1 Introduction

Up to 55% by mass of particulate matter (PM) emissions in the automotive sector come from non-exhaust traffic related emissions. Brake wear has been identified as one of the most significant contributors, being responsible for up to 21% of total urban traffic related PM₁₀ emissions by mass [1-3]. About 50% of wear debris generated during braking become airborne while the rest is deposited on the road surface or is attracted to the vehicle [4-6]. Such particle emission has a strong adverse effect on air, water and ground quality. Additionally, some constituents of airborne particles have been recognized as having potentially dangerous effects on human health, such as weakening pulmonary antimicrobial immune defence, inducing heritable mutations, and affecting lung function [7-9]. Under growing health, safety and environment (HSE) concerns, manufacturers of both combustion engine and electric vehicles are demanding cleaner braking systems.

For brakes to function, the rotating discs and pads have to press against each other, causing wear and tear. During a braking event, the pad slides against the disc and transforms the vehicle's kinetic energy into thermal energy, generating not only mechanical abrasion but also large frictional heat with subsequent wear of both pads and discs. Humps on the surface of disc are pressed into the pad and debris is torn from the pad or sheared off from the disc. Some of this debris is ejected from the contacting interface. Other debris remains on the disc and pad surfaces and undergoes the cyclic

deformation, crushing, fracture, and spalling or peeling. This debris can adhere onto the pad or disc base surface to form a friction film with a thickness of up to several hundred micrometers [10]. Commonly used brake pads are based on non asbestos organic (NAO), ceramic or semi-metal as friction materials, which have different characteristics of friction at low and high operating temperatures [1]. A semi-metallic brake pad often appears to have a higher average friction level and unfortunate propensity to generate more noise and dust. A ceramic brake pad is quiet with less dust generation; however, the ceramic pad is inferior to the NAO pad in frictional performance at low brake temperatures. The NAO pad does however show a higher tendency in brake fade if excessive heat is generated by aggressive braking. On balance of these properties, NAO pads are the preferred choice for millions of passenger vehicles.

There is an urgent need to reduce brake particle production and several approaches have been assessed to achieve reduced wear in a variety of (high temperature) tribological contacts including thermal spraying or laser cladding. These can also be realized on the brake disc face [11-15]. A prime example is the Porsche Surface Coated Brake (PSCB) disc, which adopts a coating of tungsten carbide on a cast iron substrate. The reported results are remarkable, with claims that the surface modified disc lasts up to 30% longer than its uncoated counterpart, while a 90% reduction in brake dust is also reported [16]. However, to tackle wear and emission issues, the previous research has so far been emphasized on disc surface hardening or hard coatings based on a strategy applied to prevent abrasive wear. In the present work, an alternative surface modification is proposed for improved durability and environmental performance of a brake disc. Specifically, an interlocking surface is prepared using plasma electrolytic aluminating

(PEA) process. PEA is a process very recently born from inspiration of the phosphating process and the plasma-electrolytic oxidation (PEO) process. The PEO process is commonly used to improve the corrosion resistance and tribological performance of aluminium (Al) and magnesium (Mg) alloys. Succinctly put, the PEO process utilizes a high electric voltage to induce the dielectric breakdown of a passive film on a metal surface. Subsequently, a ceramic oxide film will form on the surface. The ceramic oxide film can be tailored to provide desirable (thermo-) mechanical properties or for biomedical applications [17-22]. The PEA process is a plasma discharge-assisted process in which a composite (hercynite-alumina) ceramic coating is deposited on a ferritic surface from an aluminate-based solution [23]. Most significantly, the PEA-treated surface has a dimple-like interlocking morphology which is considered a key factor for transitioning the wear mechanism of a brake disc away from abrasive wear in this study.

Important aspect in testing of friction pairs for simulated brake contacts, are the frictional response to pad/disc, the wear mechanisms and the wear rates. In order to assess these tribological performance aspects of brake materials/friction pairs, generally one has a choice between a pin-on-disc (PoD) tester and a dynamometer. Recently, Federici et al [24] provided a comparative case study for friction pairs of NAO brake pad materials in contact with pearlitic cast iron, similar to the reference situation in our study thus. In that critical comparison, the authors compare both the PoD and dynamometer test set-ups in dry sliding conditions and conclude importantly that the specific wear coefficients between the PoD and dynamometer tests were “proportional to the corresponding values obtained with the PoD at room temperature”. [24] In addition, similar friction values, wear mechanisms and limited disparity between friction layers produced in both tests are

reported at room temperature. In this research, we focus on “cold” braking conditions and therefore here also consider tribo-testing by pin-on-disc methodology, a decision supported by the aforementioned research. Specifically, tribological testing was performed to ascertain the wear and friction performance of the PEA-treated and untreated cast iron materials in a simulated pad disc contact. To achieve this, a commercial NAO pad material was selected as the counterbody to the treated and untreated samples. The reason for this was due to its expected superior friction performance compared to ceramic brake pads at room temperature [1, 25]. The difference in wear mechanisms between a PEA-treated and untreated discs was investigated. In addition, the debris productions caused by the treated and untreated disc are compared by virtue of analysis of the wear rates.

5.2 Experimental Details

Gray cast iron (ASTM A247) was cut into 3 mm thick coupon samples with a diameter of 25.4 mm. The cast iron coupon discs were treated using the PEA process. During the PEA process, the cast iron sample was immersed into an electrolytic solution and biased with negative voltage. The electrolyte contained 15% ~ 20% sodium aluminate. The pulsed DC power supply was employed with a 40% duration of 1000Hz. The samples were treated for 15 minutes at current density of 0.15 A/cm^2 . A cooling system maintained the electrolytic solution temperature around 300 K. The PEA process has been reported previously described in detail [23]. After the process, we lightly polished the PEA-treated samples and cleaned them with compressed air and acetone. A scanning electron microscope (SEM) was used to observe the surface morphology of the PEA-treated surface and the elements of which were analyzed under an energy dispersive X-

ray detector (EDX). The phase structures of the treated sample were investigated using an X-ray diffractometer (XRD) with Cu K α radiation. XRD measurements were made from 20-100 °2 theta. Both the surface roughness and surface profiles were measured using a Mitutoyo surface profiler SJ201P. The hardness of the PEA-treated samples and the untreated cast iron samples was measured by Vickers hardness tester (Wilson VH1102). The tests were performed in a pin-on-disc tribometer to measure coefficients of friction (COF) of the treated and untreated brake discs. The tribometer is enclosed by a transparent plastic box. In this test, the pad to disc contact pair is replaced by pin and cast iron coupon sample. The pins worked as tribological counterparts were cut out of a commercially available NAO brake pad and machined into cuboid samples (5 mm \times 5 mm \times 10 mm) in which the square sides (5 mm \times 5 mm) were the testing contact areas. The elemental distribution of the NAO pad materials was analyzed through an EDX. The pin-on-disc tribometer ran with a constant applied normal force of 20 N resulted in 0.6-0.9 MPa contact pressure which was similar to that of a normal braking operation [26]. The ambient air temperature was at a room temperature of 297 K and the relative humidity was around 50-60% during the tests. The sliding speed was 0.05 m/s to simulate cold friction of a brake system at low temperature. The number of testing rotations for each test was 4000 (equivalent to 50 m sliding distance), during which the COF was recorded. After the tests, the sectional profiles of the wear tracks were obtained using the Mitutoyo surface profiler, and the wear loss was calculated based on the cross-sectional area multiplied by the circumference of the wear track. The wear rate is a wear loss per unit load and sliding distance. For a better comprehension of the wear and friction mechanism,

the SEM and EDX were again utilized to study the surface morphology and elemental compositions on the wear tracks of treated and untreated cast iron samples.

5.3 Results and Discussion

5.3.1 PEA-treated Surface and Pad Material

Brake discs are commonly made of gray cast iron due to its high thermal conductivity, low cost and easy casting. Figure 5.1a shows the surface image of the PEA-treated gray cast iron disc with a ceramic coating. The treated surface topography exhibits a characteristic dimple-like morphology with a porosity of 10-12 %, while Figure 5.1b shows the same surface's XRD pattern. The XRD data reveals the main constituent phase of surface coating is Al_2O_3 phase, coupled with a smaller fraction of FeAl_2O_4 . Iron (Fe) peaks are present due to the reflections from the cast iron substrate. Figure 5.1c presents the cross section of the PEA-treated cast iron, showing the coating includes dense ceramic microstructures and pores. The coating thickness is 15-20 μm . The phase FeAl_2O_4 identified in the XRD analysis indicates that there is a metallurgical bonding between the PEA coating and the cast iron substrate [25]. Table 5.1 lists the average Vickers hardness of both the PEA-treated surface (795 $\text{HV}_{0.05}$) and the untreated cast iron (310 $\text{HV}_{0.05}$). The treated surface was 2-3 times harder than the untreated one. The cross-sectional hardness of the PEA-treated surface was reported to be in a range of 750-800 HV, depended on the locations away from the surface [23]. These results are in line with results reported in the previous study [23].

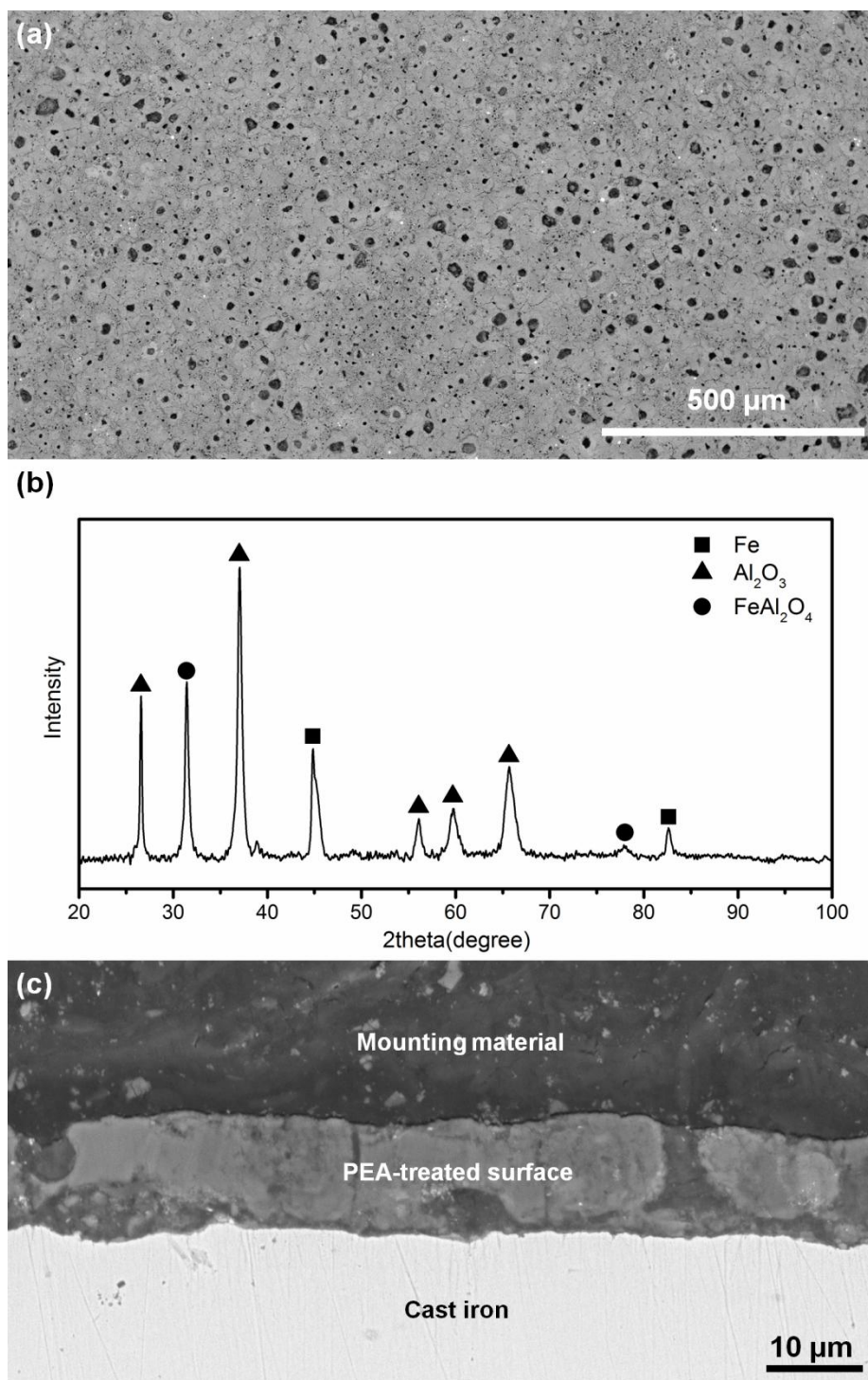


Figure 5.1. (a) SEM images showing surface morphology of lightly polished PEA-treated surface; (b) XRD pattern of a PEA-treated surface on cast iron; (c) SEM images showing cross section of PEA-treated cast iron.

Table 5.1. Typical surface properties of the samples before and after tribotests.

Sample	Material	PEA-treated surface	Cast iron
Polished surface	R_a (μm)	2.33	0.15
	R_{pk} (μm)	0.72	0.10
	R_{vk} (μm)	3.26	0.45
	Hardness (HV)	795	310
Wear track	R_a (μm)	1.65	0.29
	R_{pk} (μm)	0.76	0.09
	R_{vk} (μm)	3.95	1.14

NAO is one of the commonly used brake pad types in passenger vehicles as its friction materials are less abrasive, have excellent noise, vibration and harshness (NVH) behavior and cause lower disc wear than other pads. Figure 5.2 presents SEM images and elemental distribution maps of the NAO pads before and after the tribotests. The NAO pad in this study contains many friction materials which play different roles in the brake system. Depending on their specific roles, the friction materials are divided into five main categories: binders, reinforcing fibers, fillers, frictional additives or lubricants, and abrasives [1]. Binders are usually made of modified phenol-formaldehyde resins and hold the components of the brake pad together to ensure the structural integrity of the pad under mechanical and thermal stress [1]. Of the elements detected in the EDX mapping, copper (Cu) is present as Cu fibers and these are an example of reinforcing fibers. Such fibers increase both the thermal conductivity and mechanical strength of the material. Barium sulphate (Ba and S) and antimony sulphate (Sb and S) act as fillers in friction materials. Graphite (C) acts as lubricant to lower the friction coefficient. An unexpectedly

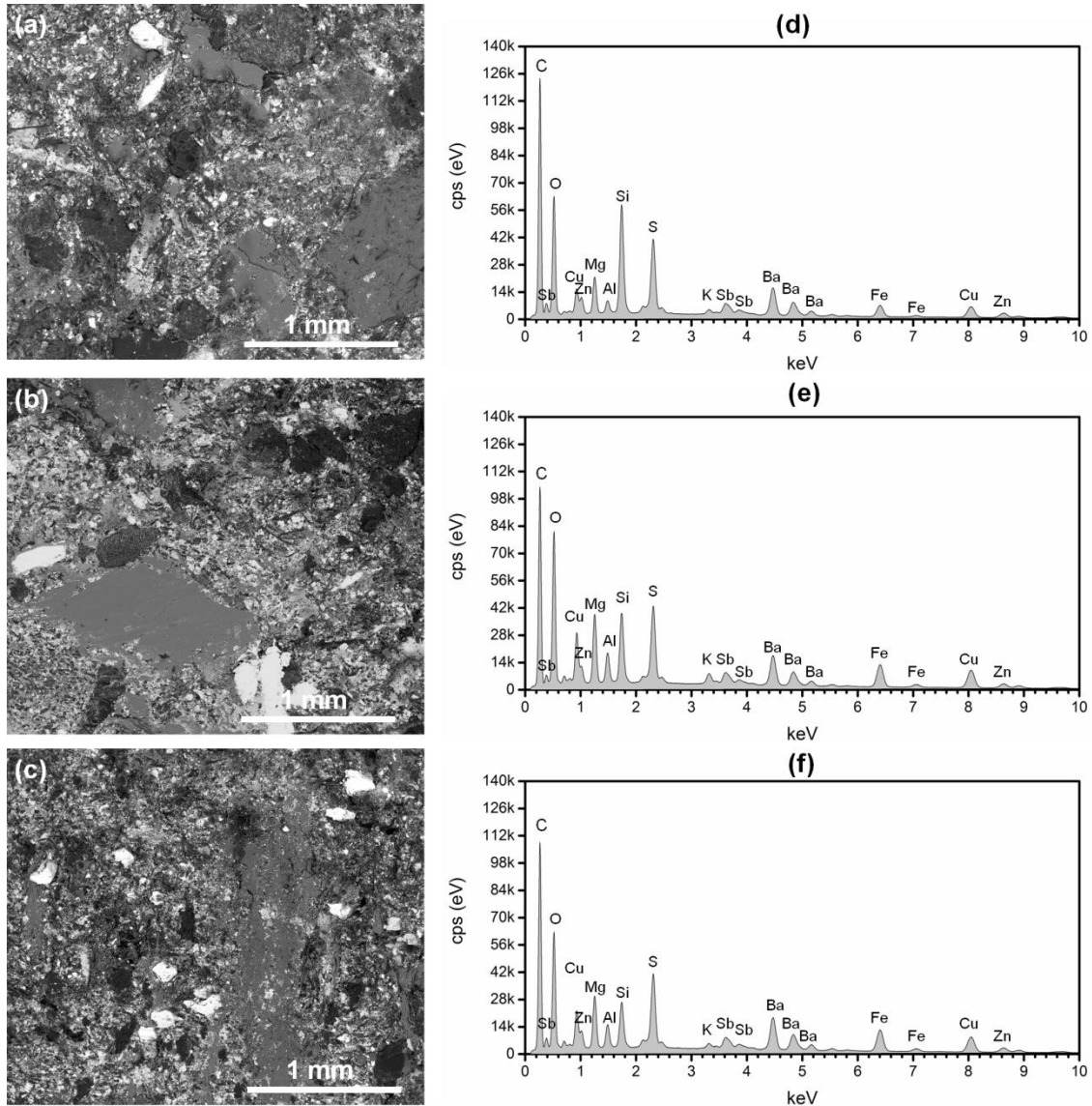


Figure 5.2. SEM images and EDX of brake pads under different testing conditions: (a, d) original pad surface; (b, e) sliding on cast iron; (c, f) sliding on PEA-treated cast iron, respectively.

high friction may cause overheating of a brake system and the graphite addition aims thus to combat this phenomenon. Iron (Fe) oxide, magnesium (Mg) oxide, silicon (Si) oxide and vermiculite (Si, Mg, Al, K and Fe containing mineral) are used as abrasives: iron oxide for regulating the coefficient of friction and increasing cold friction, magnesium

oxide and silicon oxide for increasing the friction coefficient, and vermiculite for noise reduction. The chemical compositions of the brake pad surfaces were quite similar to each other before and after the tribotests, irrespective of the counter material. That is to say, the pad after testing against treated (Figure 5.2e) or untreated cast iron (Figure 5.2f) had almost the same EDX spectrum, which suggests that there was no material transfer from the PEA-treated surface or the cast iron surface to the pad material.

5. 3.2 Surface Morphology of Wear Tracks

The surface morphology of the wear tracks after tribotesting is shown in Figure 5.3. The surfaces have been characterised by their average Roughness (R_a), their Reduced Peak Height (R_{pk}) and Reduced Valley Height (R_{vk}) values in order to quantify the surface topography. The results of these measurements, taken both before and after tribological testing, are shown in Table 5.1. The mildly polished PEA-treated surface (Figure 5.3a) is characterised by higher roughness values than the untreated polished original cast iron (Figure 5.3c). This can be attributed to the dimple-like PEA-treated surface. Figure 5.3b shows that a thin film formed and attached on the treated surface in the wear track (bright areas) during the pin-on-disc tribotest, while no material build-up was identified on the cast iron sample. This tribo-contact was instead characterised by scratch marks in the wear track (Figure 5.3d), indicating typical abrasive wear. It can be stated therefore that the dimple-like surface promotes the formation of a transfer layer from the brake pad, in a manner similar to compaction galling [27], while the pore-free surface of the gray cast iron, combined with the free carbon (graphite) prevents material sticking [28]. The chemical compositions of the respective tribo-tracks were characterised using EDX. Large amounts of oxygen were identified in the wear track of the untreated cast iron

sample. It is reasonable to postulate that this oxidation was the result of frictional heat produced during sliding [28]. The EDX mapping identified increased dark areas in Figure 5.3d compared to Figure 5.3c as carbon, which was believed come from the pad through material transfer.

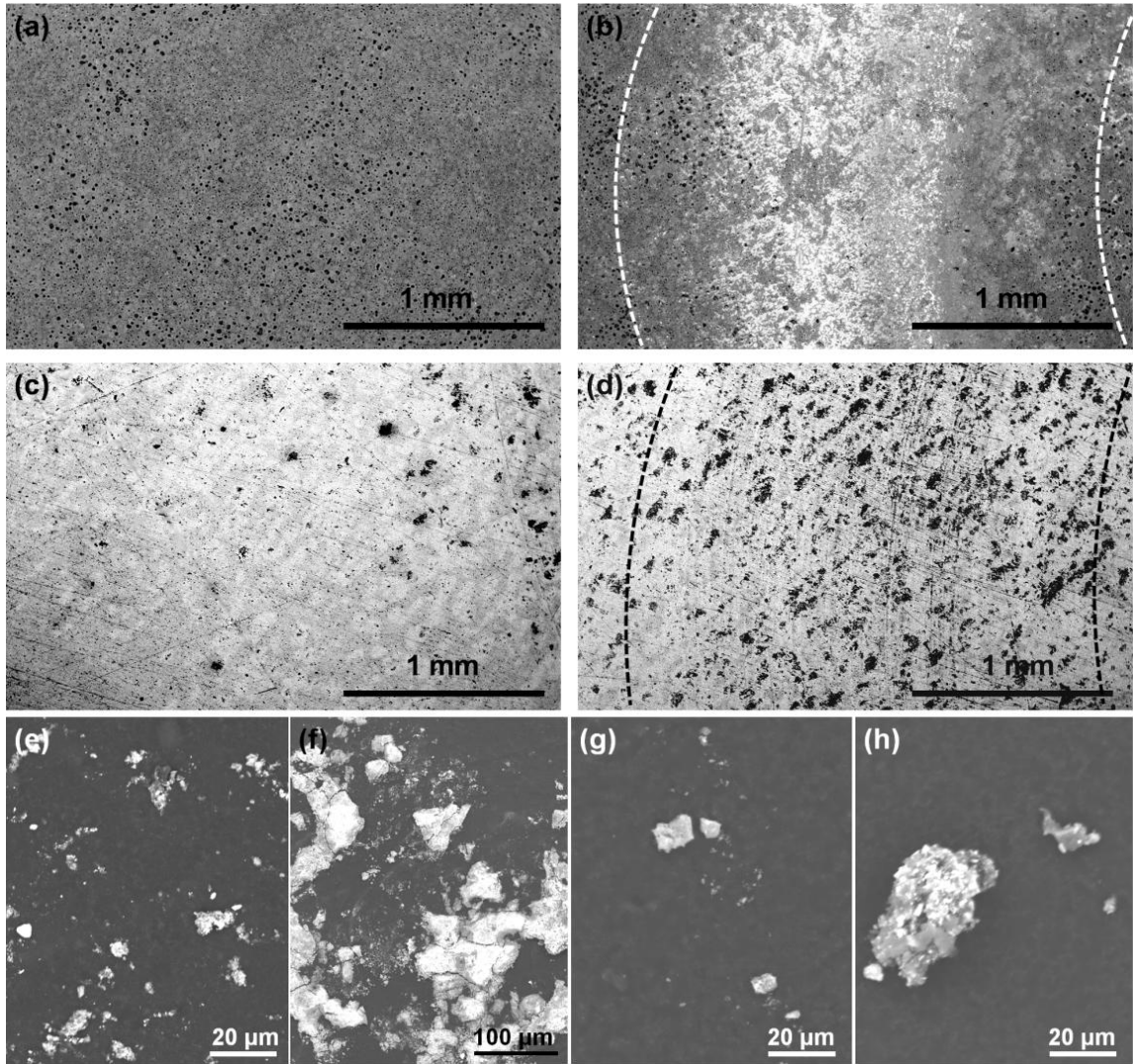


Figure 5.3. SEM images: PEA-treated surface - (a) original polished and (b) wear track after test; untreated cast iron - (c) original polished and (d) wear track after test; wear debris collected from (e, f) treated and (g, h) untreated discs.

From Table 5.1, it can be seen that the characteristic roughness values of the treated surface are lower following the tribotests than prior to testing. That is, the surface becomes smoother within the tribological contact. We attribute this loss of roughness not to material loss or asperity flattening [20], but in fact due to the aforementioned material transfer. This also supports a hypothesis that debris build-up in the dimples of the treated sample will lead to local contact areas for the initiation of material transfer due to the galling induced overlayer [25] as will be discussed in more detail hereafter. On the other hand, the surface of the untreated cast iron sample became rougher following the tribotest. It is particularly interesting to note that the R_{vk} value increased greatly and this is attributed to the scratch marks identified previously (Figure 5.3d). Figure 5.3e-h shows the particle matters collected from the wear track surfaces at the early testing stage of 5 m sliding distance to visualize the particle size generation in the early contact phase. The particle collection is achieved through pressing SEM conductive carbon tapes on the wear tracks where the particles were picked up by the tapes. When the wear process proceeds for longer than 5 m sliding distance, the increased number of particles are already found to compact together, which in turn also makes observation of individual particles difficult. Figure 5.3e-f presents images of the wear particles obtained from the PEA-treated cast iron surface. For the case of the treated cast iron disc, PM2.5 and PM10 wear debris can be seen in Figure 3e on the one hand. On the other hand, a significant portion of large wear debris has a particle size of 100-200 μm (Figure 5.3f). The wear debris collected from the wear track of the untreated cast iron disc appears to have both PM2.5 and PM10 particles (Figure 5.3g). The particles can be as large as 20 μm (Figure 5.3h) which was much smaller than the case in Figure 5.3f. It is noteworthy that the more particles shown

in Figure 5.3e vs. Figure 5.3g are due to collective behavior of dimple-like PEA-treated surface. In this case, the dimples act as reservoirs (having sizes of 1-50 μm as shown in Figure 5.1a) and accommodate the fine particles to reduce airborne emission. After the stable transfer layer was formed, the wear particle sizes increased before the non-exhaust emission could occur. The large size and local compaction of PM seen in the case of PEA treated surfaces would cause less harm to human health [2, 8, 29]. We can also confer that the small wear debris on the untreated cast iron disc was generated from both the worn pad friction materials and the disc itself and then centrifugally ejected from the wear track, which is the reason why the fewer particles were picked up by the SEM carbon tape as shown in Figure 3g and 3h, and also indication of a higher airborne emission.

To address our previously mentioned hypothesis on the wear mechanisms involved in the sliding of the treated sample against a NAO pad, we consider in Figure 4a detailed electron microscopy analysis of the sample's wear track. While the transfer layer is not homogeneous under high magnifications, it can be seen to cover the original treated surface and fill the pores on the surface, as highlighted for example in the area of circle (b) in Figure 5.4a. The thin layer appears to be well adhered dimpled surface, mostly likely due to mechanical interlocking where the material collects in the surface dimples initially as local islands (Figure 5.4b). As mentioned, the transferred layer is not homogeneous, with some areas being thicker than others, with a secondary transfer layer apparently developing over the first transfer layer. This supports our hypothesis that the build-up takes the form of compaction galling. Other morphological features, such as cracks (Figure 5.4c) and local spalling (Figure 5.4d) are identified in the second layer.

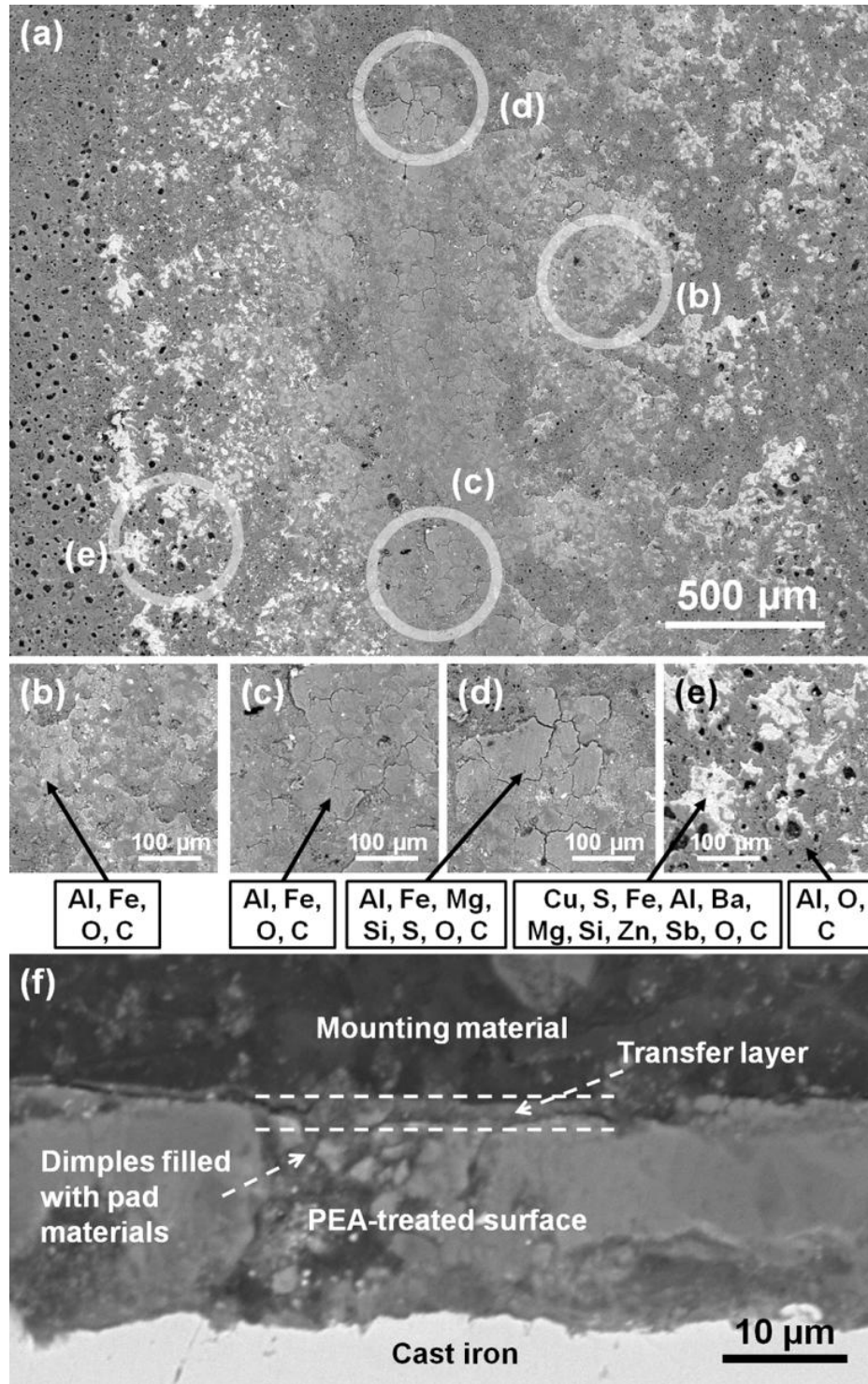


Figure 5.4. SEM images showing: (a-e) surface morphology and related elements detected in the wear track of PEA-treated surface after testing; (f) cross-sectional wear track on the PEA-treated surface after the tribotest.

Furthermore, morphological variations are also identified transverse to the sliding direction. These differences and inhomogeneities can be related to the uneven distributions of friction materials in the brake pad (Figure 5.4e, see also Figure 5.2) which is reflected in the non-uniform development of the transfer layer – an observations supported also by discrepancies in both surface morphology and chemical compositions at different locations of the disc material surface (Figure 5.4). Figure 4f is a cross-sectional SEM image of the wear track on the PEA-treated surface after the tribotest, which also shows existence of the transfer layer on the top of the treated surface. It should be noted that surface topology of the transfer layer varied only in a few micrometers range approximately indicated by R_{vk} of the wear track on the PEA-treated surface in Table 5.1, which did not cause vibration and noise during the tribotest.

5. 3.3 Tribological Behaviors

Figure 5.5a relays the dynamic coefficients of friction (COFs) for samples treated by the PEA process as well as the untreated gray cast iron variants. It is evident that the coefficient of friction for the treated sample is higher than the bare cast iron. The COFs of both test samples increased during the run-in period, and then gradually reached a stable level. When the friction reached a steady state, the COFs were 0.31-0.32 for the PEA-treated cast iron and 0.25-0.26 for the untreated cast iron. The average COFs obtained from 3 repeated tests were 0.31 ± 0.04 and 0.25 ± 0.07 for treated and untreated discs, respectively.

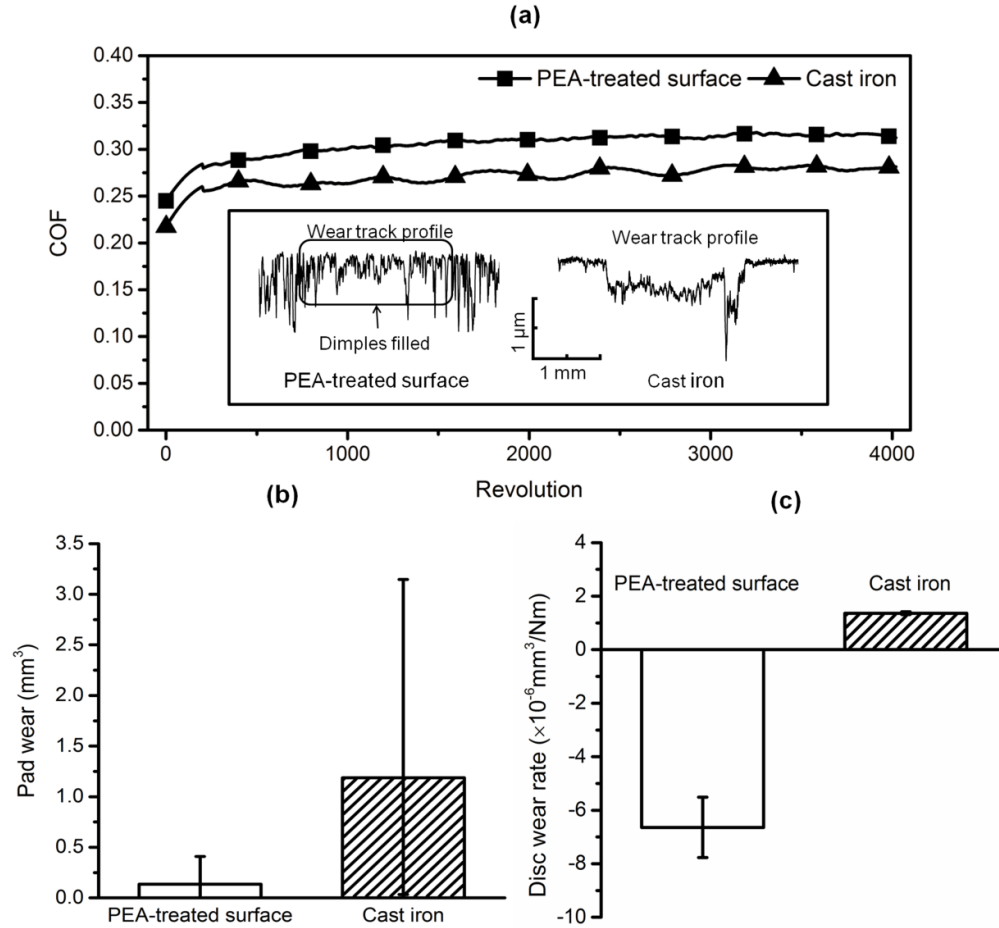


Figure 5.5. (a) Coefficients of friction with insert of sectional profiles of wear tracks, (b) wear of the brake pads, and (c) wear rates of PEA-treated and untreated discs.

After the test program was completed, a digital dial indicator was used to determine the height variation of the brake pad sample and this data was then used to calculate the wear of the pads. Figure 5.5b reveals these results as the wear of the brake pads after comparative sliding distances against the various disc surfaces prepared in this study. Despite the differences in surface morphologies seen in section 5.3.2 and the related observation that material is transferred to the PEA-treated sample during sliding, the PEA-treated cast iron is actually found to result in a significantly lower (up to 75%)

brake pad wear, compared to bare cast iron. In Figure 5.5b, the large measurement error calculated from tribotests repeated at least 5 times was caused by uncertainty during each of the repeated tests when dynamic formation or detachment of a transfer layer (or so-called secondary plateaus [1]) on the pad surfaces arbitrarily occurred. Some of the wear debris was compacted and attached back to the pad contacting surfaces before emitting to the air.

To increase the precision of measurements for the wear rates of the treated and untreated cast iron discs, each tribotest was repetitively performed four times. In other words, 50 m sliding distance (i.e. 4000 revolutions) was repeated four times on the same wear track before the wear tracks were measured using a surface profilometer. By doing so, the wear tracks were obviously shown from their surface profile curves. This also increases the certainty of the wear measurements. Such a tribotest series was repeated at least 3 times on different disc surfaces against virgin pad surfaces for both untreated and PEA-treated discs. The average wear rate of the untreated cast iron disc is $1.36 \times 10^{-6} \text{ mm}^3 / (\text{N m})$, while the wear rate of PEA-treated cast iron is negative, as shown in Figure 5.5c where the error bars are also given. The negative value indicates that a transfer layer was formed on the PEA-treated surface, which confirms the observation in Figure 5.4. The wear profiles (insets Figure 5.5a) suggest that the negative wear rate is predominantly due to the material transfer to the surface dimples, resulting in a stable surface layer.

Subsequently, the transfer layer thickness hardly increased with sliding distances; newly generated wear debris from the brake pad is added to the disc's transfer layer through compaction galling as fine PM and sequentially released to the air as large PM at a similar rate in terms of mass or volume loss [25].

Recollecting the previous observations, we can relate this to be the result of a disparity in friction mode. More specifically, in the tribological contacts investigated here, the cast iron material undergoes an abrasive-like friction sliding while the PEA-treated surface produces a contact characterized by adhesive-like friction sliding combined with compaction galling. The SEM images in Figure 5.2, showing the surfaces of the brake pad segments before and after the sliding tests, demonstrate that after being tested against the PEA-treated surface, the pad has a smoother surface (Figure 5.2b) compared to not only the original pad (Figure 5.2a) but also the pad tested against the untreated cast iron disc (Figure 5.2c). Small surface cracks can be seen on the pad after it was tested against untreated cast iron. Thus, we can conclude that the effect of PEA-treated surfaces lead to a less aggressive tribological degradation of the NAO pad.

These observations of course have practical implications in materials and surface design in brake tribology and can pave the way for further developments. We know that there are two main types of friction mechanism associated with disc-pad contacts, namely abrasive friction and adhesive friction [30]. It is well documented that gray cast iron discs usually undergo abrasive friction [25, 31]. One characteristic of abrasive friction is the breaking of bonds in both the pad material and the disc when they are brought into contact with one another. In other words, both the pad and the disk experience wear.

However, through the application of a dimpled surface, produced by PEA processing on the cast iron disc, a step change in brake performance is seen, and more significantly a transition to adhesive-like friction is observed. This is driven by the transfer layer development due to compaction galling. In this contact type and friction state, the pad materials were seen to transfer onto the surface of the treated disc, forming a compact,

thin layer without any loss in friction performance. We can now translate this information to a friction mechanism model as in Figure 5.6 wherein we show schematically the wear coupling. The wear debris – initially present as abrasive particles generated from the pad materials – fills firstly the dimples in the surface and other depressed areas and compacts to form a film as in compaction galling [27]. The transferred film then accumulates over the whole frictional surface and a transition away from abrasive friction mode occurs. The development of the transfer film, in turn means that both surfaces in the contact are effectively the same or similar materials. The friction generated in this contact is now achieved by rupture or shear of bonds identical to those in the pad material. As the film repeatedly accumulates and is worn off in this manner it leads to a relatively high and stable COF (Figure 5.5a). When the secondary transfer layer reaches to a certain thickness, which is apparently developing over the first transfer layer anchored by the dimple-like disc surface, the formation and disruption of the friction layer would dynamically occur due to stress-induced cracks (Figure 5.4c) and local spalling (Figure 5.4d) of the secondary transfer layer mainly. It should be noticed that the thickness of the transfer layer seldom changed even though the test ran 1000 m sliding distance [25].

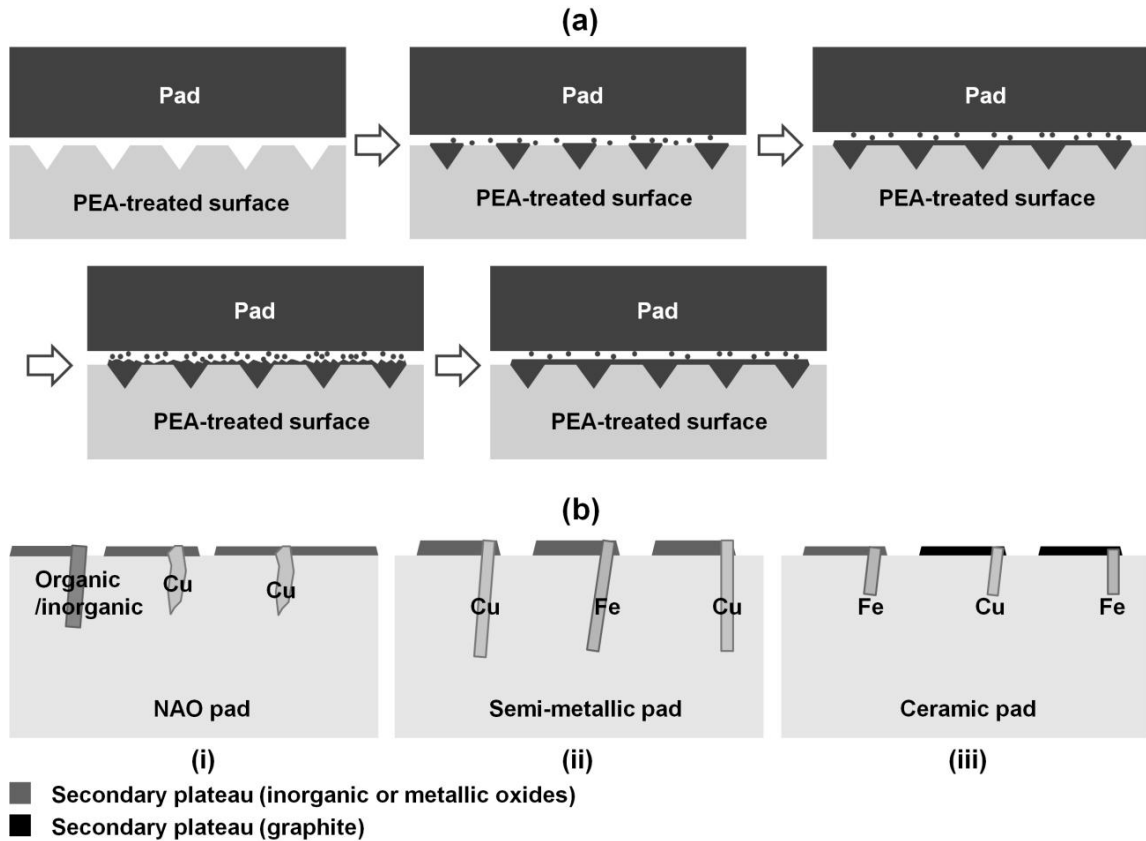


Figure 5.6. (a) Friction process model with regards to PEA-treated cast iron brake discs; (b) the schematic of transfer layers on (i) the NAO pad, (ii) a semi-metallic pad, and (iii) a ceramic pad tested at low temperature.

Figure 5.6b-i is the schematic of tribo-film formation on the NAO pad where there is no obvious secondary plateau. The shapes of Fe and Cu are of small irregular pieces, instead of fibres as shown in Figure 5.6b-ii and 5.6b-iii. The thin tribo-film comprises inorganic oxides which are partially from accumulated wear debris of the pad friction materials followed by the compaction and densification under the applied mechanical and thermal stresses.

A few researchers [32, 33] have studied thermal spraying a WC-Co-Cr coating on brake discs and tested these against a low-metal pad. A typical contact plateau is found to form on the pad contact surface where the copper fiber acts as a primary plateau and worn materials from both the pad and the coating pile up and create a secondary plateau [1] as shown depicted in Figure 5.6b-ii. A transfer layer is also generated from the pad onto the treated disc. The contact surfaces of both the pad and treated disc can accommodate worn material, which results in a relatively low wear rate and a low level of particle emissions. Their study also shows that it takes a longer time to reach steady state in temperature (from 25 to 150 °C) and COF (from 0.2 to 0.48) for the treated disc than untreated one during the PoD tests. At low temperatures (25-50 °C), the COF is 0.2, which is lower than the COF reported in this work. This could be due to transient effects in relation to the development of the transfer layer on the treated disc. Specifically, the transfer layer takes longer to build up on the WC/Co-treated disc than the PEA-treated disc. For a typical thermal spray, coating for anti-wear applications, high hardness and low porosity are desired for low wear of the disc on one hand. On the other hand, the dense and smooth coating likely makes the transfer layer uneven and nonuniform [32]. Contrary to the dense surface coating prepared by the thermal spraying technology, this work has proposed a different approach: utilize the dimple-like hard coating surface to provide firm mechanical interlocking anchor sites for the promotion of the quick formation of a transfer layer on the disc which leads to a shortening in the process of reaching a steady stage in COF even at the low or room temperature. The transfer layer prevents the treated disc from experiencing abrasive wear, and the results show almost no wear for the treated sample and much less wear for the counter pad.

The COF at low temperatures (or so-called cold friction performance) is quite dependent on the material composition of the secondary plateau on the pad contact surface. In previous research [25, 34] where a ceramic pad instead of a NAO pad is used, the low COF level is due to formation of many carbon graphite patches as the secondary plateau at the low testing temperature ($\sim 25^\circ\text{C}$), Figure 5.6b-iii. Metallic oxides (Fe-Cu-Zn-O) would become the main composition of the secondary plateaus at high friction temperatures [32, 35], which results in a higher COF at a level of 0.4-0.5 at elevated temperatures [32, 33, 36]. It is well-known that the friction performance of a ceramic pad is inferior in cold environments and superior at high operating temperatures, when compared to a NAO pad. Interestingly, the compaction galling-induced transfer layers on the treated discs in this and previous works [25] have no major differences in chemical compositions for those friction-decisive formulations, such as O, Fe, Cu, Zn and Mg [32, 36]. The difference in COF at low temperature is mainly determined by the possible evolution in chemical compositions of the pad top surface during the sliding contact.

These insights also indicate not only the fact that it is highly desirable to generate a stable transfer layer by compaction galling, but also why there is a lack of formation of a stable transfer layer on the cast iron surface. This can be attributed firstly to the presence of free carbon (graphite), which, as mentioned previously, prevents material sticking [28].

Secondly, it can be attributed to the lack of dimples, to entrap third body wear debris developed during the wear process, which promotes compaction galling, as evidenced for the PEA coated surfaces.

This PoD study showed that, due to the initiation and evolution of compaction galling in the tribological contact, a PEA-treated disc exhibits negligible wear on its own surface

and can result in up to 75% less wear of its corresponding brake pad. Also considering the wear debris from the PEA-treated disc can be as large as 200 μm in size, the PM emission would be less detrimental to human health, compared to the treated cast iron case. The PEA-treated disc thus represents a promising solution for reduction of both wear and non-exhaust emission of a brake system.

5.4 Conclusions

A dimple-like ceramic surface on cast iron brake disc can be generated by a PEA process. This dimple-like morphology provides a mechanical key for the initiation and growth of a transfer layer by compaction galling. The materials transferred from the friction materials of a brake pad first accumulate in the dimples and eventually result in a replenishable film over the entire frictional surface. As the transfer layer was anchored by the PEA-induced surface, the wear behavior of the brake disc and NAO pad changed away from abrasive. The result of this transition is that there was no wear observed on the PEA-treated sample. Furthermore, the pad materials also experienced significantly reduced wear when compared to standard brake disc material. In the boundaries of this investigation, we found that a PEA-treated cast iron shows a slightly higher COF than the variant without PEA treatment. This work therefore underlines the potential importance of a PEA-induced surface strategy for minimizing wear and in turn debris emissions in future brake systems. Further tests such as brake dynamometer tests will help confirm the validity of PEA applications in actual automotive brake systems.

REFERENCES

- [1] Grigoratos, Theodoros, and Giorgio Martini. "Brake wear particle emissions: a review." *Environmental Science and Pollution Research* 22, no. 4 (2015): 2491-2504. doi:10.1007/s11356-014-3696-8.
- [2] Timmers, Victor R. J. H., and Peter A. J. Achten. "Non-exhaust PM emissions from electric vehicles." *Atmospheric Environment* 134 (2016): 10-17. doi:10.1016/j.atmosenv.2016.03.017.
- [3] Alemani, Mattia, Jens Wahlström, and Ulf Olofsson. "On the influence of car brake system parameters on particulate matter emissions." *Wear* 396 (2018): 67-74. doi:10.1016/j.wear.2017.11.011.
- [4] Mathissen, Marcel, Jaroslaw Grochowicz, Christian Schmidt, Rainer Vogt, Ferdinand H. Farwick Zum Hagen, Tomasz Grabiec, Heinz Steven, and Theodoros Grigoratos. "A novel real-world braking cycle for studying brake wear particle emissions." *Wear* 414 (2018): 219-226. doi:10.1016/j.wear.2018.07.020.
- [5] Zum Hagen, Ferdinand H. Farwick, Marcel Mathissen, Tomasz Grabiec, Tim Hennicke, Marc Rettig, Jaroslaw Grochowicz, Rainer Vogt, and Thorsten Benter. "Study of brake wear particle emissions: impact of braking and cruising conditions." *Environmental Science & Technology* 53, no. 9 (2019): 5143-5150. doi:10.1021/acs.est.8b07142.
- [6] Mathissen, Marcel, Theodoros Grigoratos, Tero Lahde, and Rainer Vogt. "Brake wear particle emissions of a passenger car measured on a chassis dynamometer." *Atmosphere* 10, no. 9 (2019): 556. doi:10.3390/atmos10090556.

[7] Greater London Authority. "London Environment Strategy Appendix 2: Evidence Base." Mayor of London.

https://www.london.gov.uk/sites/default/files/appendix_2_evidence_base.pdf.

[8] Southern Ontario Centre for Atmospheric Aerosol Research (SOCAAR). "Near-Road Air Pollution Pilot Study Summary Report Fall 2019." University of Toronto, Toronto, 2019. <https://www.socaar.utoronto.ca/wp-content/uploads/2019/10/SOCAAR-Near-Road-Air-Pollution-Pilot-Study-Summary-Report-Fall-2019-web-Final.pdf>.

[9] Air Quality Expert Group. "Non-Exhaust Emissions from Road Traffic." *Home - Defra, UK*. Last modified July 9, 2019. https://uk-air.defra.gov.uk/assets/documents/reports/cat09/1907101151_20190709_Non_Exhaust_Emissions_typeset_Final.pdf

[10] Ostermeyer, Georg Peter, and Michael Müller. "Dynamic interaction of friction and surface topography in brake systems." *Tribology International* 39, no. 5 (2006): 370-380. doi:10.1016/j.triboint.2005.04.018.

[11] Aranke, Omkar, Wael Algenaid, Samuel Awe, and Shrikant Joshi. "Coatings for automotive gray cast iron brake discs: A review." *Coatings* 9, no. 9 (2019): 552. doi:10.3390/coatings9090552.

[12] Federici, Matteo, Cinzia Menapace, Alessandro Moscatelli, Stefano Gialanella, and Giovanni Straffelini. "Effect of roughness on the wear behavior of HVOF coatings dry sliding against a friction material." *Wear* 368 (2016): 326-334. doi:10.1016/j.wear.2016.10.013.

- [13] Liu, Yan, Ying Wu, Yuanming Ma, Wei Gao, Guiying Yang, Hao Fu, Naiyuan Xi, and Hui Chen. "High temperature wear performance of laser cladding Co06 coating on high-speed train brake disc." *Applied Surface Science* 481 (2019): 761-766. doi:10.1016/j.apsusc.2019.02.235.
- [14] Rahman, Naveed Ur, Luigi Capuano, Matthijn B. De Rooij, David T. A. Matthews, Andrea Garc ía-Junceda, Melkamu Awoke Mekicha, Laura Cordova, Gis èle Walmag, Mario Sinnaeve, and G. R. B. E. Römer. "Laser metal deposition of vanadium-rich high speed steel: Microstructural and high temperature wear characterization." *Surface and Coatings Technology* 364 (2019): 115-126. doi:10.1016/j.surfcoat.2019.02.044.
- [15] Rahman, Naveed Ur, Matthijn B. De Rooij, David T. A. Matthews, Gis èle Walmag, Mario Sinnaeve, and G. R. B. E. Römer. "Wear characterization of multilayer laser clad high speed steels." *Tribology International* 130 (2019): 52-62. doi:10.1016/j.triboint.2018.08.019.
- [16] Elbriggmann, Thorsten. "Hard like Diamond." *Christophorus Porsche Magazine* 384 (2017): 17.
- [17] Yerokhin, Aleksey L., Xueyuan Nie, Adrian Leyland, Allan Matthews, and Stephen J. Dowey. "Plasma electrolysis for surface engineering." *Surface and Coatings Technology* 122, no. 2-3 (1999): 73-93. doi:10.1016/S0257-8972(99)00441-7.
- [18] Nie, Yining, Carol Kalapos, Xueyuan Nie, Monica Murphy, Riyad Hussein, and Jing Zhang. "Superhydrophilicity and antibacterial property of a Cu-dotted oxide coating surface." *Annals of Clinical Microbiology and Antimicrobials* 9, no. 1 (2010): 25. doi:10.1186/1476-0711-9-25.

- [19] Clyne, Trevor William, and Samuel Christopher Troughton. "A review of recent work on discharge characteristics during plasma electrolytic oxidation of various metals." *International Materials Reviews* 64, no. 3 (2019): 127-162. doi:10.1080/09506608.2018.1466492.
- [20] Cai, Ran, Chen Zhao, and Xueyuan Nie. "Effect of plasma electrolytic oxidation process on surface characteristics and tribological behavior." *Surface and Coatings Technology* 375 (2019): 824-832. doi:10.1016/j.surfcoat.2019.06.104.
- [21] Lou, Bih-Show, Jyh-Wei Lee, Chuan-Ming Tseng, Yi-Yuan Lin, and Chien-An Yen. "Mechanical property and corrosion resistance evaluation of AZ31 magnesium alloys by plasma electrolytic oxidation treatment: effect of MoS₂ particle addition." *Surface and Coatings Technology* 350 (2018): 813-822. doi:10.1016/j.surfcoat.2018.04.044.
- [22] Shen, Xinwei, Xueyuan Nie, and Jimi Tjong. "Effects of electrolytic jet plasma oxidation (EJPO) coatings on thermal behavior of engine cylinders." *Heat and Mass Transfer* 55, no. 9 (2019): 2503-2515. doi:10.1007/s00231-019-02600-6.
- [23] Zhao, Chen, Wei Zha, Ran Cai, Xueyuan Nie, and Jimi Tjong. "A New Eco-friendly Anticorrosion Strategy for Ferrous Metals: Plasma Electrolytic Aluminating." *ACS Sustainable Chemistry & Engineering* 7, no. 5 (2019): 5524-5531. doi:10.1021/acssuschemeng.8b06839.
- [24] Federici, Matteo, Mattia Alemani, Cinzia Menapace, Stefano Gialanella, Guido Perricone, and Giovanni Straffelini. "A critical comparison of dynamometer data with pin-on-disc data for the same two friction material pairs—A case study." *Wear* 424 (2019): 40-47. doi:10.1016/j.wear.2019.02.009.

- [25] Cai, Ran, Chen Zhao, and Xueyuan Nie. "Alumina-Based Coating with Dimples as Enabling Sustainable Technology To Reduce Wear and Emission of the Brake System." *ACS Sustainable Chemistry & Engineering* 8, no. 2 (2019): 893-899. doi:10.1021/acssuschemeng.9b05302.
- [26] Shorowordi, Kazi Md, Abdul S. Md Abdul Haseeb, and Jean-Pierre Celis. "Velocity effects on the wear, friction and tribochemistry of aluminum MMC sliding against phenolic brake pad." *Wear* 256, no. 11-12 (2004): 1176-1181. doi:10.1016/j.wear.2003.08.002.
- [27] Venema, Jenny, Javad Hazrati, David T. A. Matthews, R. A. Stegeman, and A. H. Van Den Boogaard. "The effects of temperature on friction and wear mechanisms during direct press hardening of Al-Si coated ultra-high strength steel." *Wear* 406 (2018): 149-155. doi:10.1016/j.wear.2018.04.006.
- [28] Österle, Werner, and Andrey I. Dmitriev. "The role of solid lubricants for brake friction materials." *Lubricants* 4, no. 1 (2016): 5. doi:10.3390/lubricants4010005.
- [29] Grigoratos, Theodoros, and Giorgio Martini. "Non-exhaust traffic related emissions. Brake and tyre wear PM." *Report no. Report EUR 26648* (2014). doi:10.2790/21481.
- [30] Hu, Bo. "Friction and Wear of Automotive and Aircraft Brakes." In *ASM handbook. Vol. 18, Friction, lubrication, and wear technology*, edited by George E. Totten, 969-982. Materials Park, Ohio: ASM International, 2017. ISBN 978-1-62708-141-2.

- [31] Mohammadnejad, Ali, Abbas Bahrami, Majid Goli, Hossein Dehbashi Nia, and Peyman Taheri. "Wear Induced Failure of Automotive Disc Brakes—A Case Study." *Materials* 12, no. 24 (2019): 4214. doi:10.3390/ma12244214.
- [32] Wahlström, Jens, Yezhe Lyu, Vlastimil Matjeka, and Anders Söderberg. "A pin-on-disc tribometer study of disc brake contact pairs with respect to wear and airborne particle emissions." *Wear* 384 (2017): 124-130. doi:10.1016/j.wear.2017.05.011.
- [33] Menapace, Cinzia, Alessandro Mancini, Matteo Federici, Giovanni Straffelini, and Stefano Gialanella. "Characterization of airborne wear debris produced by brake pads pressed against HVOF-coated discs." *Friction* (2019): 1-12. doi:10.1007/s40544-019-0284-4.
- [34] Jin, Hongyun, Keke Zhou, Zhengjia Ji, Xiaocong Tian, Ying Chen, Luhua Lu, Yazhou Ren, Chunhui Xu, Shanshan Duan, Jiangyu Li, and Shu'en Hou. "Comparative tribological behavior of friction composites containing natural graphite and expanded graphite." *Friction* (2019): 1-11. doi:10.1007/s40544-019-0293-3.
- [35] Eriksson, Mikael, Filip Bergman, and Staffan Jacobson. "On the nature of tribological contact in automotive brakes." *Wear* 252, no. 1-2 (2002): 26-36. doi:10.1016/S0043-1648(01)00849-3.
- [36] Lyu, Yezhe, Mara Leonardi, Jens Wahlström, Stefano Gialanella, and Ulf Olofsson. "Friction, wear and airborne particle emission from Cu-free brake materials." *Tribology International* 141 (2020): 105959. doi:10.1016/j.triboint.2019.105959.

CHAPTER 6

WEAR PERFORMANCES OF GRAY CAST IRON BRAKE ROTOR WITH PLASMA ELECTROLYTIC ALUMINATING COATING AGAINST DIFFERENT PADS

6.1 Introduction

Gray cast iron is the commonly-used material for brake rotors due to its excellent thermophysical properties, high damping capability, good castability and machinability combined with cost-effectiveness [1]. However, the gray cast iron brake rotor also has excessive wear during braking which leads to wear debris emissions like particulate matter (PM) that have adverse effects on human health [2]. In these years, surface treatment in forms of coating on gray cast iron rotors represents a trending solution to this problem. Several different approaches explored to combat the wear problems for brake rotors include chrome plating [3, 4], laser cladding [5, 6] and thermal spray processes [7-9]. Bosch Company adopted a hard tungsten carbide coating on the cast iron substrate of its iDisc using a thermal spray process and claims that it produces 90% less brake dust compared with a conventional brake rotor and lasts twice as long as a normal brake rotor [10]. However, such a kind of brake rotor is much more expensive than the normal cast iron rotor.

In the present work, an alternative cost-effective surface coating process called plasma electrolytic aluminating (PEA) is proposed for improved durability and environmental performance of a brake rotor. The PEA is specially developed for coating ferrous alloys [11], which is different from conventional plasma-electrolytic oxidation (PEO) process [12-15]. The PEO process can usually apply for valve metals such as aluminum, magnesium and titanium and their alloys [14]. The PEA can be described as a plasma-

assisted electrochemical reaction process in which a composite (hercynite-alumina) ceramic coating is deposited on a ferritic surface from an aluminate-based solution [11]. It is noteworthy that the PEA coating has a metallurgical bonding to the cast iron substrate, which is different from the thermal spraying approaches emphasizing hard surface coatings with a mechanical bonding on brake rotors.

In this study, tribological tests were performed to evaluate the wear and friction performance of the PEA-coated gray cast iron materials in a simulated pad-on-disc contact. Three different types of commercial pad material (ceramic, semi-metallic and non asbestos organic (NAO)) were selected as the counterfaces to the coated disc samples. Performances of alumina-based ceramic coatings vs. different brake pad materials were comparatively investigated in this study. Their COFs and wear were measured. The COFs influenced by pad wear or pad transfer layer (secondary plateau) behaviors were discussed.

6.2 Experimental Details

Gray cast iron (ASTM A247) was cut into 3 mm thick disc-shaped samples with a diameter of 25.4 mm. The cast iron samples were polished with abrasive papers and coated using the PEA process. During the PEA process, the samples were immersed into an electrolyte contained 15-20 g/L sodium aluminate. A pulsed direct current (DC) power supply with a frequency of 1000Hz was used. The process lasted for 15 minutes at current density of 0.15 A/cm^2 . The temperature of the electrolyte was maintained around 300 K using a cooling system. The surface morphology of the PEA coating was observed by a scanning electron microscope (SEM). The SEM image was used to measure the porosity of the coating. An energy dispersive X-ray detector (EDX) was used to analyze

the chemical compositions of the coating. Both the surface roughness and profiles of the PEA coating were measured using a Mitutoyo surface profiler SJ201P. Regarding the wear performance, pin-on-disc sliding wear tests were conducted. The tests were performed in a pin-on-disc tribometer to measure coefficients of friction (COFs) of the PEA-coated samples. The counterpart pins were cut from three different kinds of commercially available brake pads (ceramic, semi-metallic and NAO) and machined into cuboids (5 mm×5 mm×10 mm). The square sides (5 mm×5 mm) contacted the PEA coating in the tests. The elemental distributions of the three pad materials were analyzed through the EDX. The pin-on-disc tribometer ran with a constant applied normal force of 20 N resulted in 0.6-0.9 MPa contact pressure which was similar to that of a normal braking operation [16]. The ambient air temperature of the tests was at a room temperature of 297 K. The sliding velocity was 0.05 m/s to simulate cold friction of a brake system at low temperature. The sliding distance for every counterpart was 200m at each run of the test and repeated the test for 5 times at the same place of the coated surface, during which the COF was recorded. After the tests were completed, the height variations of the pins were determined using a digital dial indicator and these data were then used to calculate the wear of the pads. For a better comprehension of the wear and friction mechanism, the SEM and EDX were utilized again to study the surface morphology and chemical compositions of the wear tracks on the coated samples.

6.3 Results and Discussion

6.3.1 PEA Coating and Pad Materials

Figure 6.1a shows the surface image of lightly polished PEA coating on gray cast iron rotor. The surface topography exhibits a typical dimple-like morphology, while Figure

6.1b shows only the dimples of Figure 6.1a. The dimples have sizes of 1-30 μm as shown and the porosity of the coating is around 11.3%. The main constituent phase of PEA coating is Al_2O_3 phase, coupled with a smaller fraction of FeAl_2O_4 , which has been reported in previous studies [11, 17, 18].

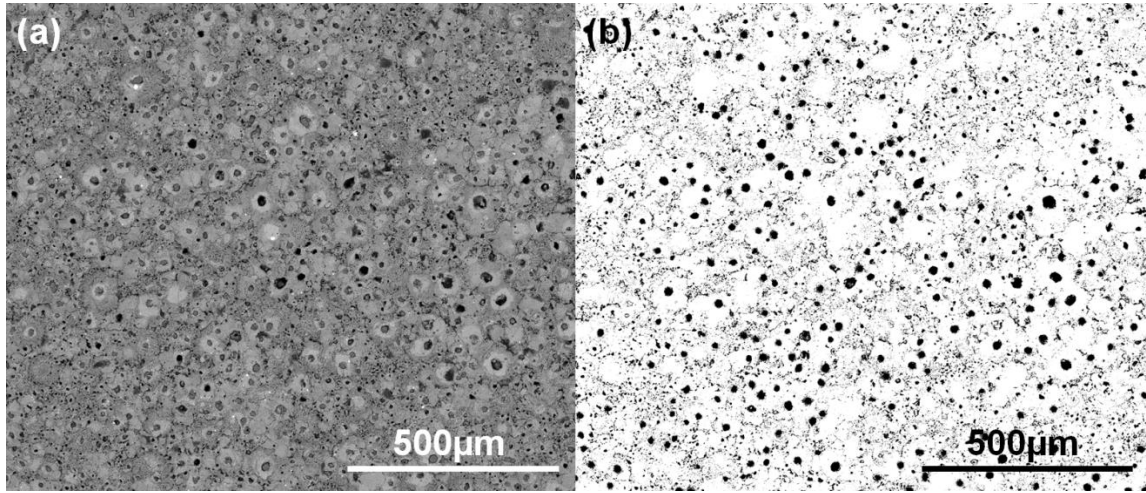


Figure 6.1. (a) SEM image showing surface morphology of lightly polished PEA coating; (b) SEM image showing dimples of the PEA coating.

Friction materials in brake pad serve a variety of functions and comprise five categories: abrasives, frictional additives or lubricants, reinforcing fibers, fillers and binders [2].

Figure 6.2-6.4 presents SEM images of the three different brake pads before and after the tribotests and elemental distribution maps of them. Main friction materials used in the three pads in this study (shown in Table 6.1) were analyzed through the elements detected in the EDX analysis. Zirconium silicate, which is abrasive material in ceramic pad, can also stabilize the COF at high temperatures. Magnesium oxide and iron oxide worked as abrasives in NAO pad: iron oxide for regulating the COF and increasing cold friction, magnesium oxide for increasing the COF. Graphite acts as lubricant in all of the

three pads to decrease the COF because an unexpectedly high friction may cause overheating of a brake system. Tin sulphide in the ceramic pad improves the COF by forming an inter-frictional layer, thus reducing pad and disc wear and preventing temperature peaks. The NAO pad was also added Zinc sulphide and Zinc oxide as solid lubricants. All of the three brake pads contain copper and mineral fibers; these are examples of reinforcing fibers which increase mechanical strength of the material. The content of the two kinds of fibers is completely different in the three pads according to the SEM images and EDX analysis, and especially, the quantities of copper fibers in the ceramic pad and mineral fibers in the semi-metallic pad are very small. There are also plenty of steel and brass fibers in the semi-metallic pad worked as reinforcing fibers. Copper and brass fibers can improve thermal conductivity and help to diffuse heat generated at the friction surface. Mineral fibers like mica, vermiculite and crystalline silica help in controlling frictional behavior and reduce noise. Baryte and antimony sulphate act as fillers in friction materials. Binders are usually made of modified phenol-formaldehyde resins and hold the components of the brake pad together to ensure the structural integrity of the pad under mechanical and thermal stress [2].

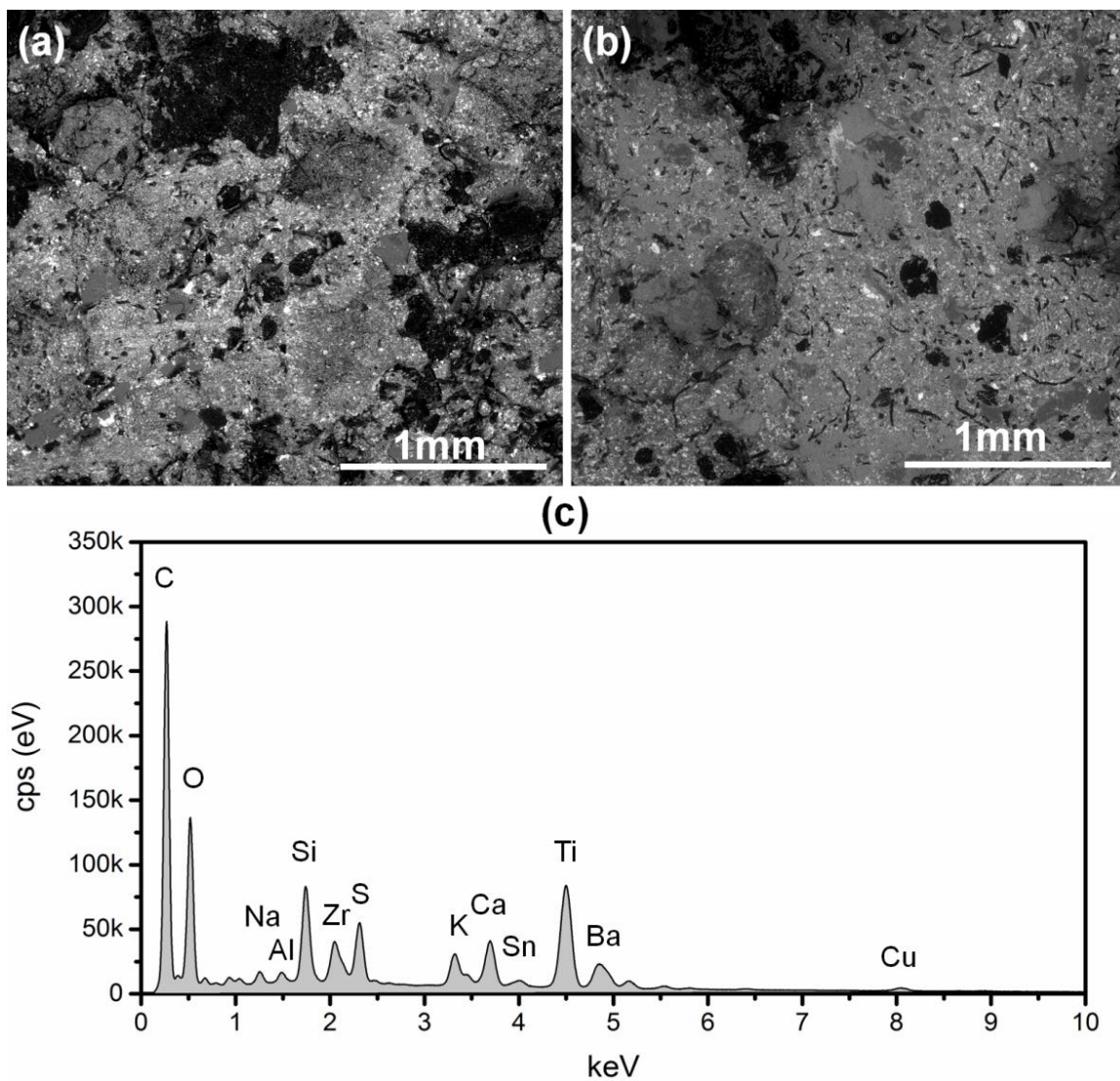


Figure 6.2. SEM images of ceramic pad surface (a) before and (b) after tribotests; (c) EDX analysis of original ceramic pad surface.

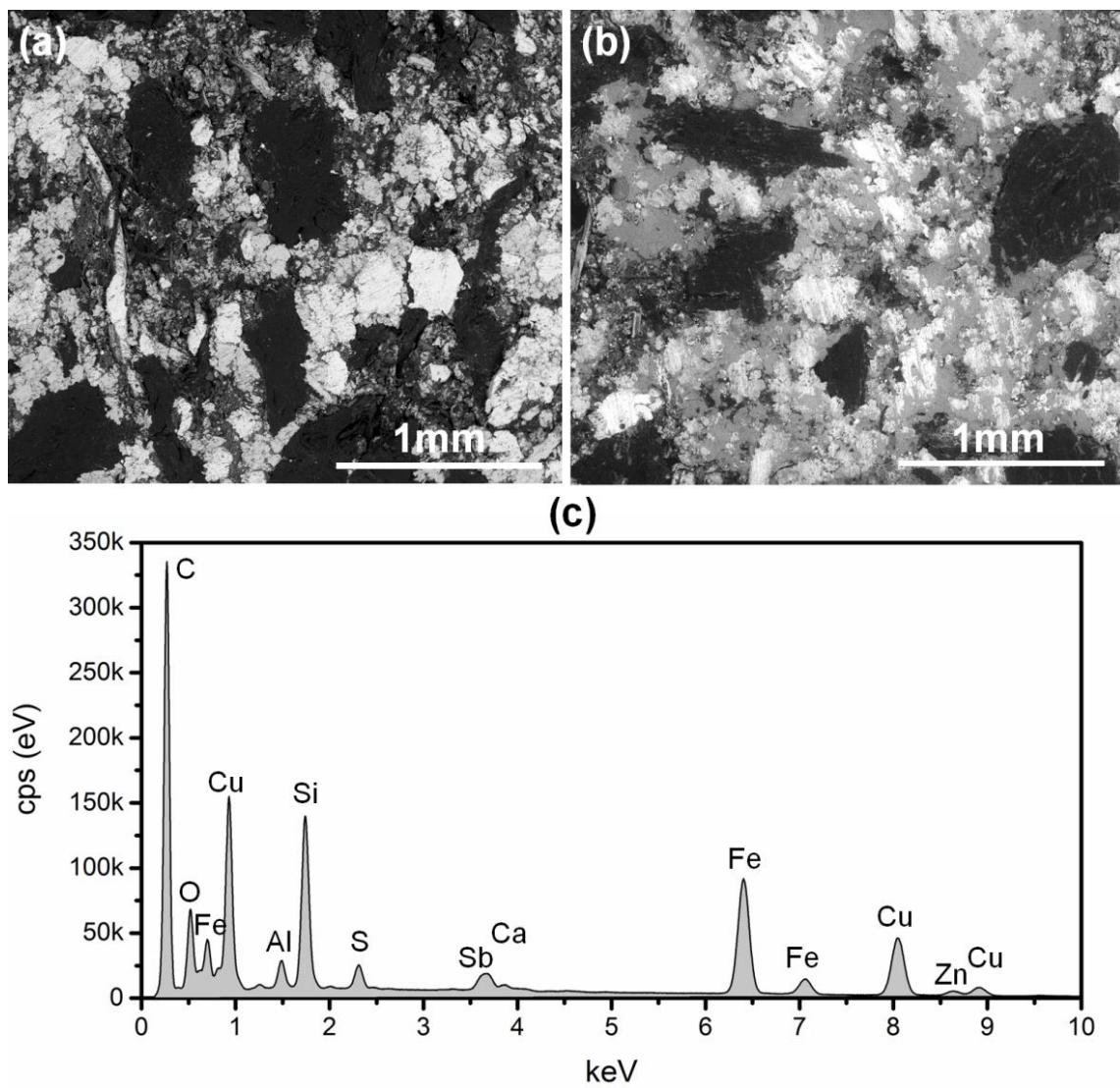


Figure 6.3. SEM images of semi-metallic pad surface (a) before and (b) after tribotests; (c) EDX analysis of original semi-metallic pad surface.

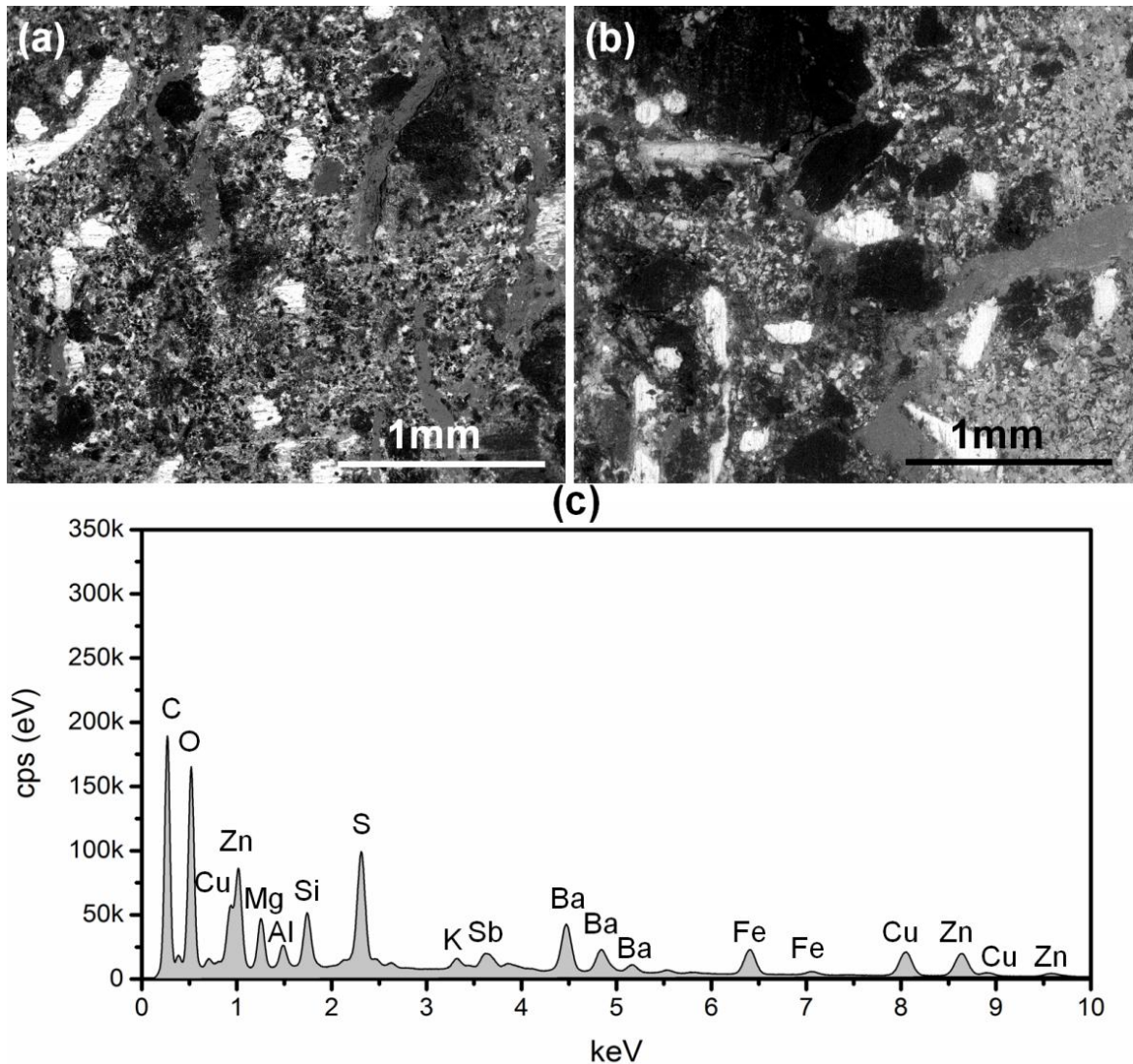


Figure 6.4. SEM images of NAO pad surface (a) before and (b) after tribotests; (c) EDX analysis of original NAO pad surface.

The SEM images in Figure 6.2-6.4, showing the surfaces of the brake pads before and after the tribotests, also demonstrate that after being tested against the PEA coating, the pads have a smoother surface (Figure 6.2b, 6.3b and 6.4b) compared to the original pads (Figure 6.2a, 6.3a and 6.4a).

Table 6.1. Main friction materials in ceramic, semi-metallic and NAO brake pads.

Friction materials	Ceramic	Semi-metallic	NAO
Abrasive	Zirconium silicate	Quartz/silica	Magnesium oxide, Iron oxide
Frictional additives/ lubricants	Graphite, Tin sulphide	Graphite	Graphite, Zinc sulphide, Zinc oxide
Reinforcing fiber	Copper fiber, Mineral fiber	Copper fiber, Brass fiber, Steel fiber, Mineral fiber	Copper fiber, Mineral fiber
Fillers	Baryte , Potassium titanate	Antimony sulphate	Baryte, Antimony sulphate

6.3.2 Surface Morphology of Wear Tracks

The surface morphology of the wear tracks on the PEA coatings after tribotests with three different counterfaces is shown in Figure 6.5. Their average roughness (R_a), reduced peak height (R_{pk}) and reduced valley height (R_{vk}) values before and after tribotests have been measured and shown in Table 6.2. Figure 6.5 shows that the thin transferred films formed and attached on the coatings in the wear tracks during the tribotests, which was also found in the previous study [17, 18]. According to the EDX analysis of the wear tracks, the thin films/layers are formed by friction materials transferred from the brake pads. The materials (i.e., wear debris) initially collected in the dimples of the coating as local islands and appear to be well adhered to the dimpled surface due to mechanical interlocking [18]. It can be stated that the dimple-like surface of the coating promotes the formation of a transferred film from the brake pad, in a manner similar to compaction galling [19].

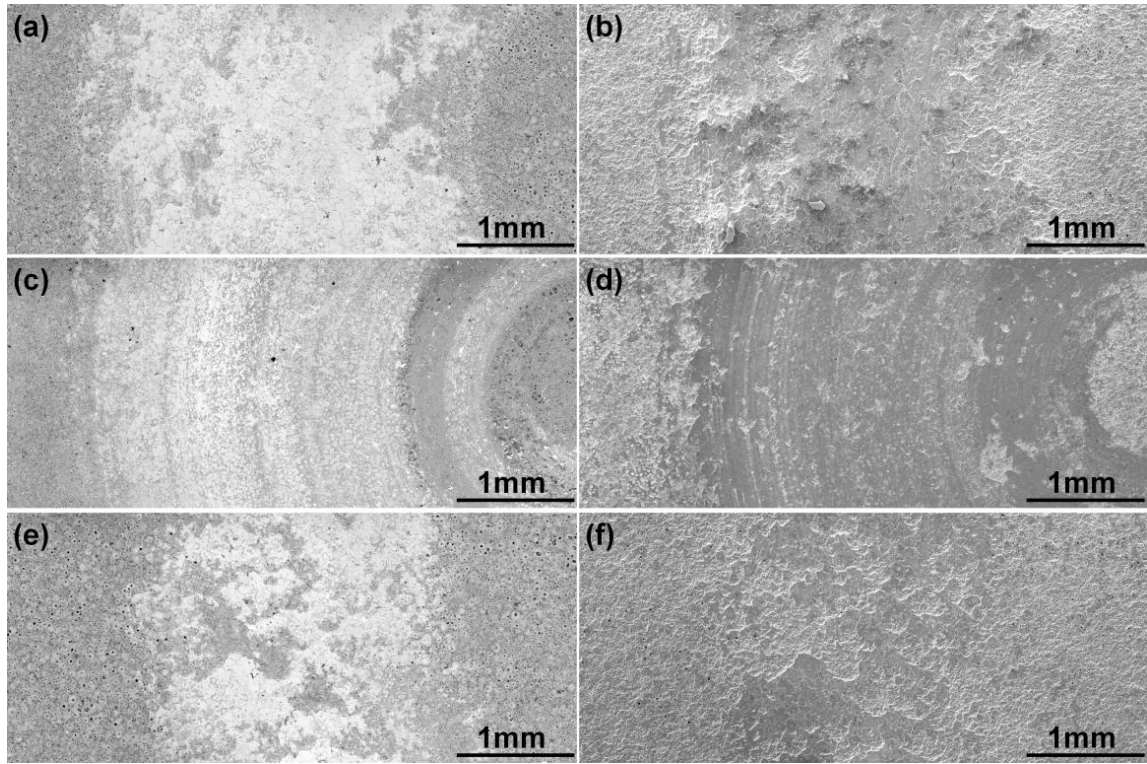


Figure 6.5. SEM images of wear tracks on the PEA coatings after tribotests against (a, b) ceramic pad, (c, d) semi-metallic pad and (e, f) NAO pad in (left) back-scattered electrons (BSE) and (right) secondary electrons (SE).

Table 6.2. Surface roughness of the samples before and after tribotests.

Sample	PEA coating			
Roughness	Initial surface	Wear track		
		Ceramic	Semi-metallic	NAO
R_a (μm)	2.20 ± 0.28	0.72 ± 0.04	1.21 ± 0.09	1.37 ± 0.13
R_{pk} (μm)	1.15 ± 0.15	0.58 ± 0.31	0.79 ± 0.11	0.85 ± 0.40
R_{vk} (μm)	2.71 ± 0.45	1.42 ± 0.14	2.37 ± 0.47	3.98 ± 0.84

All of the three transferred films caused by different brake pads are not very homogeneous, with some areas being thicker than others. The degree of the

inhomogeneity morphology of the thin films transferred from the NAO pad (Figure 6.5e, f) is higher than those transferred from the ceramic pad (Figure 6.5a, b) and the semi-metallic pad (Figure 6.5c, d). The inhomogeneous morphology of the thin films partially attributes to the second transferred layers which are developed over the first layers followed by cracking and local spalling in a dynamic manner. The second transferred layers with low completeness in the wear tracks sliding by the NAO pad are present in Figure 6.5e and f while the cracking and peeling can be found in all the wear tracks in Figure 6.5. Furthermore, morphological variations are also identified in the transverse direction of sliding wear tracks. These inhomogeneities can be related to the heterogeneous friction materials in the brake pads (Figure 6.2-6.4) which is reflected in the uneven development of the transferred films in different wear tracks and different areas in the same wear track. In the wear track caused by the semi-metallic brake pad, scratches appear along the sliding direction (shown in Figure 6.5c, d). These scratches resulted from the high metal content of the semi-metallic pad. The rather high formulation of metallic fibers of the pad may cause a frequently freshening of the surface of the thin film transferred from the pad.

It can be seen in the Table 6.2 that the roughness values of the wear track on the coating are lower after the tribotests than the original polished (initial) coating surface. In other words, the coupling surface becomes smoother after the tribological contact. This roughness reduction attributes not to material loss or asperity flattening [14] but to the aforementioned transferred films on the surface of the original dimple-like coating. It is noted that the R_{vk} value of wear track against the NAO pad seemingly increased. This is attributed to its incomplete coverage of second transferred layers of the transferred films

(Figure 6.5e, f). The surface topology of the thin films only varied in several micrometers indicated by R_{vk} in Table 6.2, which did not cause vibration and noise during the tribotests.

6.3.3 Tribological Behaviors

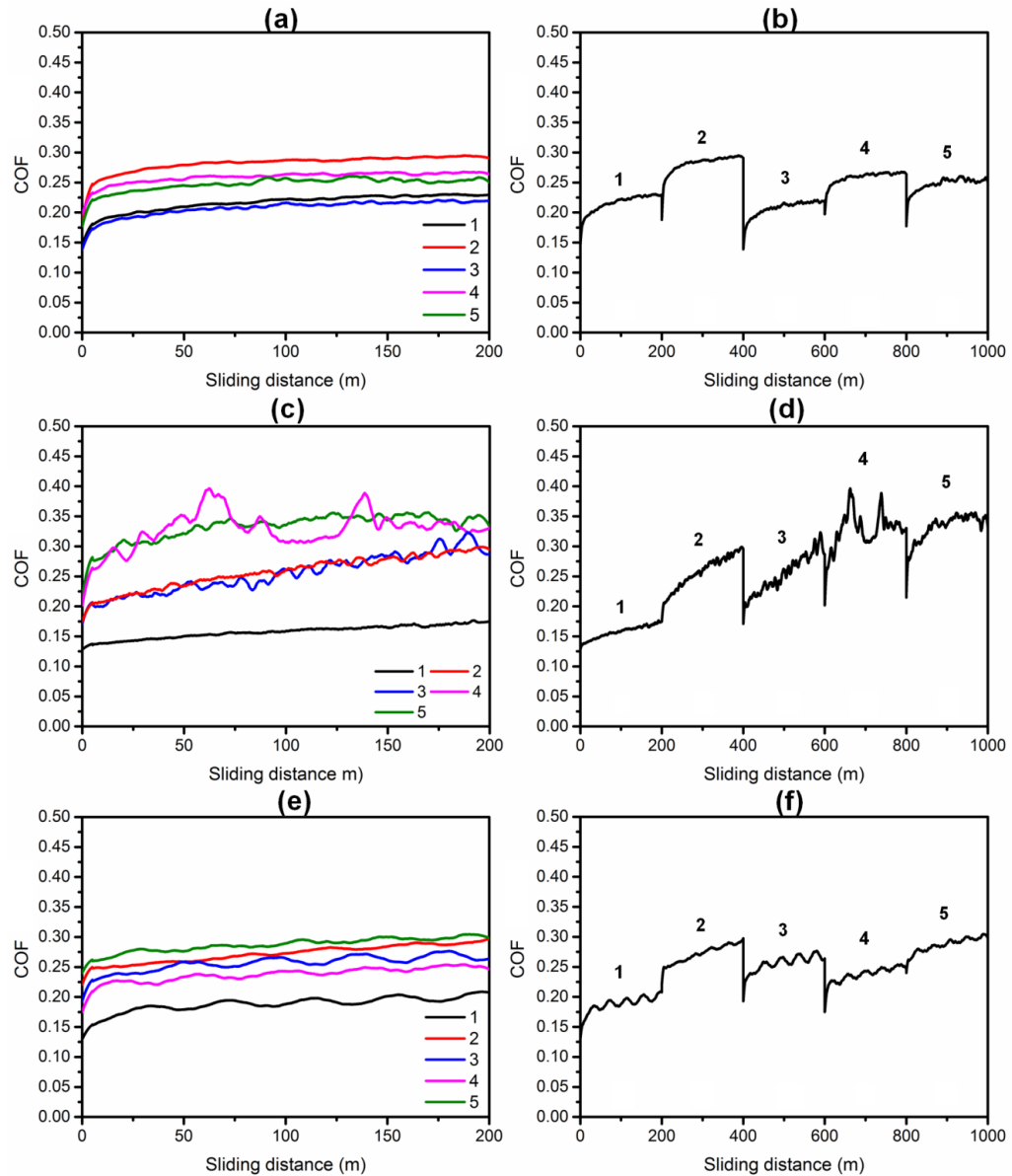


Figure 6.6. COFs of 5 repeated tribotests for PEA coating against (a, b) ceramic pad, (c, d) semi-metallic pad and (e, f) NAO pad.

Figure 6.6 presents the COFs of the tribotests where the PEA coating was run against three different brake pads. The average COFs obtained from 5 repeated tests were 0.25 ± 0.04 , 0.27 ± 0.09 and 0.26 ± 0.06 for the PEA coating coupling with ceramic, semi-metallic and NAO brake pads, respectively. It is evident that the COFs for the coating against semi-metallic pad is slightly higher than that for the coating against the ceramic pad and NAO pad. The COFs of all the test samples increased during the tribotests at varying levels, and then gradually reached a stable level to some extent.

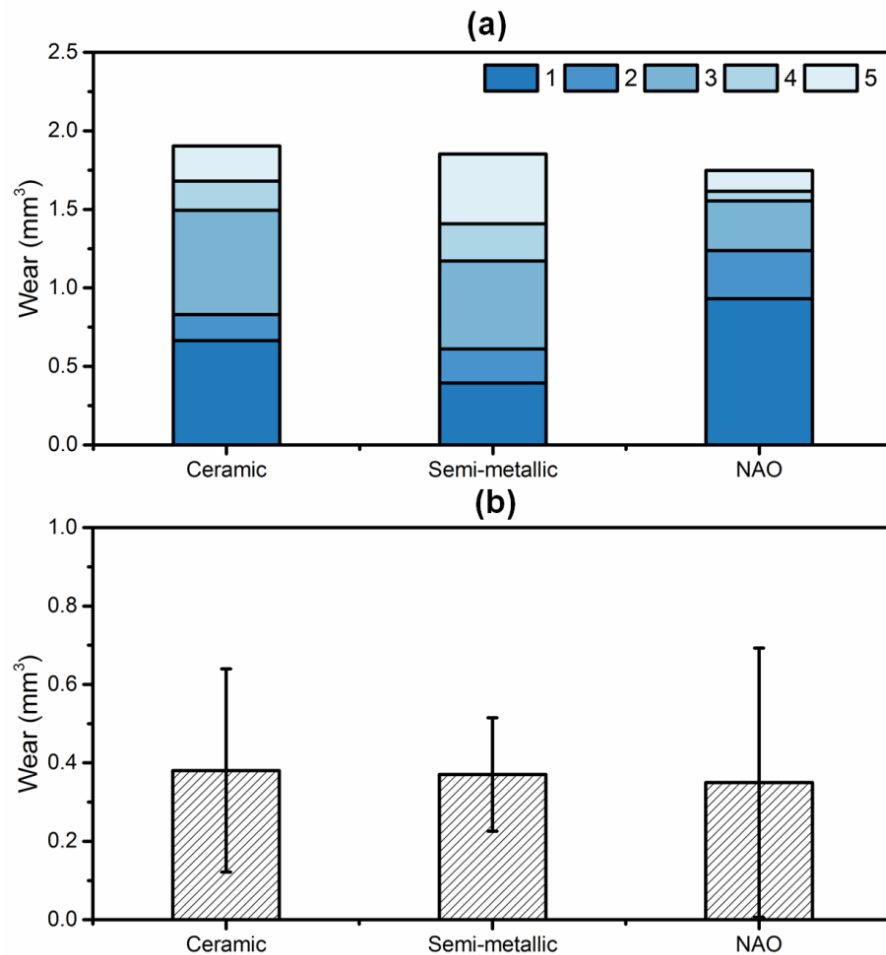


Figure 6.7. Wear of the ceramic, semi-metallic and NAO pads after tribotests against PEA coating in (a) total and (b) average.

Figure 6.7 reveals the wear results of the three different brake pads after the repeated tribotests against the PEA coating surfaces. Despite a similar total and average wear of the three pads, Figure 6.7 also shows the distinct variations (Figure 6.7a) between each 200m test for every pad itself and the large measurement error (Figure 6.7b) calculated from repeated tests. The variation and uncertainty during each of the repeated tests are likely due to arbitrary occurrence of dynamic formation or detachment of secondary plateaus [2] on the pad surfaces. Some of the wear debris was compacted and attached back to the pad contacting surface before emitting to the air. Much wear debris generated from the pad materials may be transported between the transferred films/layers on the brake rotor and the secondary plateaus on the pad surface, which leads to a longer retention for compacting and formation of larger sizes of PM before loss to the air. Large PM is usually less harmful [20]. Another benefit would come from the fact that the pad wear can also be reduced [17, 18].

Furthermore, the secondary plateaus on the pad surface also influence the variation of the COF between each of the repeated tribotests. As mentioned before, the brake pads comprise a variety of friction materials. Some of the components are hard inhomogeneities, such as reinforcing metallic fibers, embedded in soft matrix. When the wear particles produced from the brake pads reach the sliding surface during the tribotests, hard particles will be pressed into the matrix [21]. Reinforcing fibers, the contact area between which and sliding surface is called the primary plateau, provide anchors where wear particles accumulate [2, 22]. The temperature of the piled wear particles will grow up to the point that leads to mechanical alloying or even melting processes and the formation of the secondary plateaus on the surface of the pads being

possible [20]. The mechanical and thermal load results in cracks in a secondary plateau which lead to the partial destruction of the plateau. Interestingly, a less pad wear is corresponding to a relatively higher COF for such as ceramic and semi-metallic pads as shown in Test 2 and Test 4. Less wear on the pad indicates that there are more secondary plateaus, leading to a higher COF due to enhanced interfacial shear strength of the plateaus compared to original pad surface.

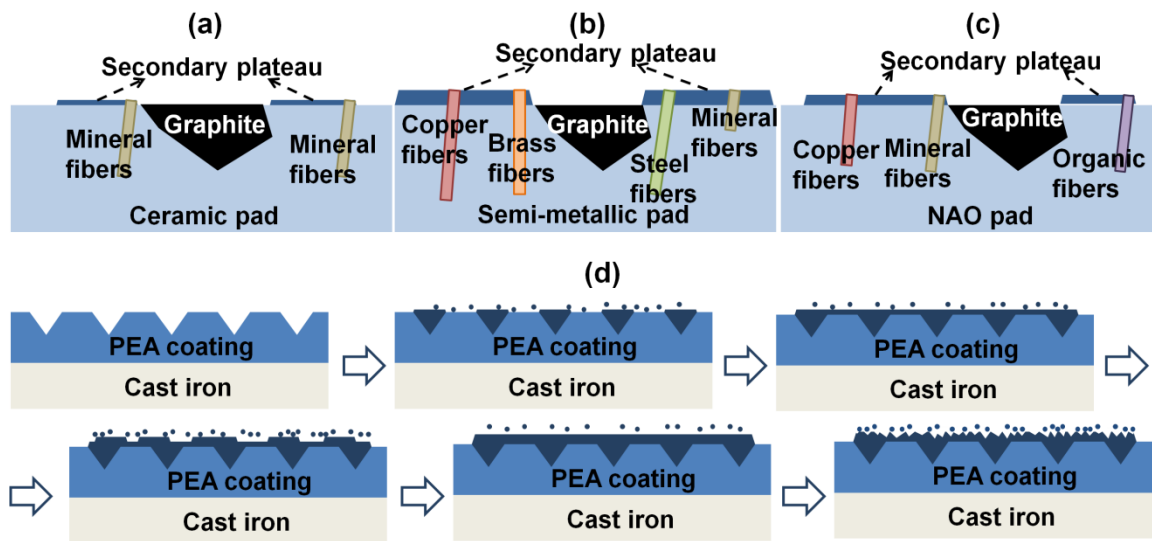


Figure 6.8. The schematic of the secondary plateaus on (a) the ceramic pad, (b) the semi-metallic pad, and (c) the NAO pad; (d) friction process model with regards to the PEA-coated brake rotor.

Figure 6.8a-c is the schematic of secondary plateau on the ceramic, semi-metallic and NAO brake pads. There are less obvious secondary plateaus on the surface of the ceramic and NAO pad which may be attributed to the relatively small amount of hard reinforcing fibers and their small shapes. The semi-metallic brake pad, which comprises large number of metallic fibers, provides more anchors for secondary plateau formation. It is

interesting to notice that there is no secondary plateau accumulating onto the graphite because of the graphite's lubricant property.

The COFs at low temperatures (or so-called cold friction performance) are quite dependent on the materials composition of the secondary plateaus on the pad contact surface. These secondary plateaus show nearly the same mechanical properties as the hard particle does with respect to wear and the friction grows up on these areas due to the plateaus' enlarged contact areas [15, 21]. Thus, it is believed that the formation of the secondary plateaus contributes to the growing of COF during the tribotests, which can explain that variation of the pad wear is in company with opposite COF alteration. Specifically speaking, the growth of the secondary plateaus lowers the wear measurement reading of the brake pads and enhances the COFs, while the detachment of the plateaus leads to the reversed results. The difference in COF at low temperature between diverse brake pads is also determined by the possible evolution in various chemical compositions of the pad top surface during the sliding contact.

More specifically, in the tribological contacts investigated here, the prepared PEA coating produces a tribological contact characterized by transferred friction materials. In this friction mechanism, the pad materials were seen to transfer onto the surface of the coated rotor, forming a compact, thin film without any loss in friction performance. We can now translate this information to a friction mechanism model as shown in Figure 6.8d. The wear debris, which is initially generated from the brake pad as abrasive particles, fills firstly the dimples and other lowland areas of the PEA coating and then is compacted to form a thin film [19]. The transferred film/layer accumulates over the whole wear track, and a transition to adherent friction mechanism occurs as a result. On the basis of the first

layer of the transferred film, wear debris transferred from pad materials continues developing over the first layer and forms second layer. The second layer of the transferred film undergoes not only cracking and local spalling but also reforming, which relates to the dynamic replenishing of the thin film. With the transition of friction mechanism achieved by the prepared dimple-like PEA coating, the thin transferred film/layer protects the rotor surface and results in no wear of the rotor. Thus, the PEA-coated gray cast iron rotor represents a promising solution for wear reduction of a brake system.

It should be noted that the PEA coating is a ceramic material which has not only excellent wear resistance but also corrosion resistance [11]. When it is used as a coating on friction surface of a brake rotor, it prevents the rotor from wear and corrosion. The current coating technologies apply paint, Zn, Zn-Al or Al-Si galvanized coatings for the corrosion protection on brake rotor. However, those polymer or metallic coatings cannot survive on the rotor friction surface due to their relatively low hardness. Therefore, the PEA process could be used to eliminate corrosion and emission of brake rotor for conventional and electrical vehicles.

6.4 Conclusions

A PEA process can produce a dimple-like ceramic coating on gray cast iron brake rotor. This dimple-like morphology provides convenience for the initiation and growth of a transferred film. The wear debris generated from the brake pad accumulates in the dimples first and then form a replenishable thin film over the entire wear track. As the transferred film sticking on the PEA coating well, the friction mechanism of the coated brake rotor and pad was changed away from the abrasive wear mode that is usually

observed for uncoated gray cast iron rotor. This transition resulted in almost no wear on the PEA-coated cast iron rotor. The wear debris is likely transported between the secondary plateaus on the pad and the transferred film on the rotor before the debris is worn off, which would reduce the pad wear and also reduce the debris emissions in fine PM form. All three kinds of pads showed a similar wear rate and friction level at the room temperature testing condition, even though the semi-metallic pad seemed to be more aggressive. The dynamic formation and detachment of the secondary plateaus are likely responsible to the variation of COFs. Therefore, this work underlines a potential strategy of preparing surface coating using PEA process for minimizing wear and in turn debris emissions of gray cast iron brake rotors. Further tests such as brake dynamometer tests will help confirm the validity of PEA applications in actual automotive brake systems for conventional and electrical vehicles.

REFERENCES

- [1] Aranke, Omkar, Wael Algenaid, Samuel Awe, and Shrikant Joshi. "Coatings for automotive gray cast iron brake discs: A review." *Coatings* 9, no. 9 (2019): 552. doi:10.3390/coatings9090552.
- [2] Grigoratos, Theodoros, and Giorgio Martini. "Brake wear particle emissions: a review." *Environmental Science and Pollution Research* 22, no. 4 (2015): 2491-2504. doi:10.1007/s11356-014-3696-8.
- [3] Mandich, Nenad V., and Donald L. Snyder. "Electrodeposition of chromium." *Modern Electroplating* 5 (2010): 205-241.
- [4] Lal, Roop, and Ramesh Chandra Singh. "Experimental comparative study of chrome steel pin with and without chrome plated cast iron disc in situ fully flooded interface lubrication." *Surface Topography: Metrology and Properties* 6, no. 3 (2018): 035001. doi:10.1088/2051-672X/aac60a.
- [5] Ocel k, Vaclav, Uazir O.B. De Oliveira, M. De Boer, and Jeff Th M. De Hosson. "Thick Co-based coating on cast iron by side laser cladding: Analysis of processing conditions and coating properties." *Surface and Coatings Technology* 201, no. 12 (2007): 5875-5883. doi:10.1016/j.surfcoat.2006.10.044.
- [6] Liu, Yan, Ying Wu, Yuanming Ma, Wei Gao, Guiying Yang, Hao Fu, Naiyuan Xi, and Hui Chen. "High temperature wear performance of laser cladding Co06 coating on high-speed train brake disc." *Applied Surface Science* 481 (2019): 761-766. doi:10.1016/j.apsusc.2019.02.235.

- [7] G éard, Barbezat. "Application of thermal spraying in the automobile industry." *Surface and Coatings Technology* 201, no. 5 (2006): 2028-2031.
doi:10.1016/j.surfcoat.2006.04.050.
- [8] Federici, Matteo, Cinzia Menapace, Alessandro Moscatelli, Stefano Gialanella, and Giovanni Straffelini. "Effect of roughness on the wear behavior of HVOF coatings dry sliding against a friction material." *Wear* 368 (2016): 326-334.
doi:10.1016/j.wear.2016.10.013.
- [9] Federici, Matteo, Cinzia Menapace, Alessandro Moscatelli, Stefano Gialanella, and Giovanni Straffelini. "Pin-on-disc study of a friction material dry sliding against HVOF coated discs at room temperature and 300 °C." *Tribology International* 115 (2017): 89-99.
doi:10.1016/j.triboint.2017.05.030.
- [10] "IDisc Brake Disc." Bosch Mobility Solutions. <https://www.bosch-mobility-solutions.com/en/highlights/automated-mobility/idisc/>.
- [11] Zhao, Chen, Wei Zha, Ran Cai, Xueyuan Nie, and Jimi Tjong. "A New Eco-friendly Anticorrosion Strategy for Ferrous Metals: Plasma Electrolytic Aluminating." *ACS Sustainable Chemistry & Engineering* 7, no. 5 (2019): 5524-5531.
doi:10.1021/acssuschemeng.8b06839.
- [12] Yerokhin, Aleksey L., Xueyuan Nie, Adrian Leyland, Allan Matthews, and Stephen J. Dowey. "Plasma electrolysis for surface engineering." *Surface and Coatings Technology* 122, no. 2-3 (1999): 73-93. doi:10.1016/S0257-8972(99)00441-7.

- [13] Nie, Yining, Carol Kalapos, Xueyuan Nie, Monica Murphy, Riyad Hussein, and Jing Zhang. "Superhydrophilicity and antibacterial property of a Cu-dotted oxide coating surface." *Annals of Clinical Microbiology and Antimicrobials* 9, no. 1 (2010): 25. doi:10.1186/1476-0711-9-25.
- [14] Clyne, Trevor William, and Samuel Christopher Troughton. "A review of recent work on discharge characteristics during plasma electrolytic oxidation of various metals." *International Materials Reviews* 64, no. 3 (2019): 127-162. doi:10.1080/09506608.2018.1466492.
- [15] Cai, Ran, Chen Zhao, and Xueyuan Nie. "Effect of plasma electrolytic oxidation process on surface characteristics and tribological behavior." *Surface and Coatings Technology* 375 (2019): 824-832. doi:10.1016/j.surfcoat.2019.06.104.
- [16] Shorowordi, Kazi Md, Abdul S. Md Abdul Haseeb, and Jean-Pierre Celis. "Velocity effects on the wear, friction and tribochemistry of aluminum MMC sliding against phenolic brake pad." *Wear* 256, no. 11-12 (2004): 1176-1181. doi:10.1016/j.wear.2003.08.002.
- [17] Cai, Ran, Chen Zhao, and Xueyuan Nie. "Alumina-Based Coating with Dimples as Enabling Sustainable Technology To Reduce Wear and Emission of the Brake System." *ACS Sustainable Chemistry & Engineering* 8, no. 2 (2019): 893-899. doi:10.1021/acssuschemeng.9b05302.
- [18] Cai, Ran , Jingzeng Zhang, Xueyuan Nie, Jimi Tjong, and David T.A. Matthews. "Wear Mechanism Evolution on Brake Discs for Reduced Wear and Particulate Emissions." *Wear* (2020): 203283. doi:10.1016/j.wear.2020.203283.

- [19] Venema, Jenny, Javad Hazrati, David T. A. Matthews, R. A. Stegeman, and A. H. Van Den Boogaard. "The effects of temperature on friction and wear mechanisms during direct press hardening of Al-Si coated ultra-high strength steel." *Wear* 406 (2018): 149-155. doi:10.1016/j.wear.2018.04.006.
- [20] Lelieveld, Jos, Andrea Pozzer, Ulrich Pöschl, Mohammed Fnais, Andy Haines, and Thomas Münzel. "Loss of life expectancy from air pollution compared to other risk factors: a worldwide perspective." *Cardiovascular Research* (2020). doi:10.1093/cvr/cvaa025.
- [21] Müller, Michael, and Georg Peter Ostermeyer. "Cellular automata method for macroscopic surface and friction dynamics in brake systems." *Tribology International* 40, no. 6 (2007): 942-952. doi:10.1016/j.triboint.2006.02.045.
- [22] Persoon, Fernao, Desirée Tegels, Diego Adolfo Santamaria Razo, and Arno Kerssemakers. "Bio-soluble Mineral Fibres: Alternative Chemical Compositions and the Effect in Disc Pad Applications." Paper presented at EuroBrake 2016, Milan, Italy, June 13-15, 2016.

CHAPTER 7

CONCLUSIONS AND FUTURE WORK

7.1 PEA Coating on Cast Iron

An alumina-based coating on cast iron rotors can be obtained by a PEA (plasma electrolytic aluminating) process. The surface topography exhibits a typical dimple-like morphology. The dimples have sizes of 1-50 μm and the porosity of the coating is around 10-12 %. The interfacial region between the substrate and the coating exhibits small pores, and larger pores appear at the upper region in the coating. The XRD data reveals the main constituent phase of surface coating is Al_2O_3 phase, coupled with a smaller fraction of FeAl_2O_4 , which has been reported. The coating includes dense ceramic microstructures and pores. The phase FeAl_2O_4 identified in the XRD analysis indicates that there is a metallurgical bonding between the PEA coating and the cast iron substrate. The surface of the PEA-coated cast iron was 2-3 times harder than the uncoated one. The cross-sectional hardness of the PEA coating was reported to be in a range of 750-800 HV, depended on the locations away from the surface.

7.2 Effects of PEA Coating on Cast Iron Rotors

7.2.1 Surface Morphology of PEA-coated Cast Iron Rotors

Due to its dimple-like texturing surface, the mildly polished PEA coating is characterised by comparatively higher roughness values than the uncoated polished original cast iron. A thin film filled in the dimples, formed and attached on the coating surface in the wear track during the Pin-on-Disc tribotest, while no material build-up and only scratches in the wear track was identified on the uncoated cast iron. The thin films/layers are formed

by friction materials transferred from the brake pads. Unlike large and deep dimples on the original coating, the coating surface became smoother than prior to testing on its wear track area due to coverage of the transferred layer while the surface of the uncoated cast iron sample roughened due to the scratches. It can be stated therefore that the dimple-like coating surface promotes the formation of a transfer layer from the brake pad, in a manner similar to compaction galling, while the pore-free surface of the cast iron, combined with the free carbon (graphite) prevents material sticking. The loss of roughness on PEA-coated cast iron is attributed to the aforementioned material transfer.

The transferred films/layers are not very homogeneous, with some areas being thicker than others. When the sliding distance of the test increased, the transfer layer became thicker to some extent and a secondary transfer layer seemingly formed on the top of the first thin layer. The inhomogeneous morphology of the thin films partially attributes to the second transferred layers. Cracks and local spalling in a dynamic manner are identified in the second layer. Furthermore, morphological variations are also identified in the transverse direction of sliding wear tracks. These inhomogeneities can be related to the heterogeneous friction materials in the brake pads which is reflected in the uneven development of the transferred films in different wear tracks and different areas in the same wear track. The rather high formulation of metallic fibers of the pad may cause a frequently freshening of the surface of the thin film transferred from the pad and even scratches appear along the sliding direction.

7.2.2 Wear of PEA-coated Cast Iron Rotors

The wear rate of PEA-coated cast iron rotors is negative. The negative wear rate is predominantly due to the material transfer to the surface dimples, resulting in a stable

surface layer. Subsequently, the transfer layer thickness hardly increased with sliding distances; newly generated wear debris from the brake pad is added to the rotor's transfer layer through compaction galling as fine PM and sequentially released to the air as large PM at a similar rate in terms of mass or volume loss.

The PEA coating is a ceramic material which has not only excellent wear resistance but also corrosion resistance. When it is used as a coating on friction surface of a brake rotor, it prevents the rotor from wear and corrosion.

7.3 Effects of PEA Coating on Brake Pads

7.3.1 Surface Morphology of Brake Pads

When the wear particles produced from the brake pads reach the sliding surface during the tribotests, hard particles will be pressed into the matrix of the pad. Reinforcing fibers in the pad, the contact area between which and sliding surface is called the primary plateau, provide anchors where wear particles accumulate. The temperature of the piled wear particles will grow up to the point that leads to mechanical alloying or even melting processes and the formation of the secondary plateaus on the surface of the pads being possible. The mechanical and thermal load results in cracks in a secondary plateau which lead to the partial destruction of the plateau. There are less obvious secondary plateaus on the surface of the ceramic and NAO pad which may be attributed to the relatively small amount of hard reinforcing fibers and their small shapes. The semi-metallic brake pad, which comprises large number of metallic fibers, provides more anchors for secondary plateau formation. It is interesting to notice that there is no secondary plateau accumulating onto the graphite because of the graphite's lubricant property. Furthermore,

after being tested against the PEA coating, the brake pad has a smoother surface compared to not only the original pad but also the pad tested against the uncoated cast iron disc.

7.3.2 Wear of Brake Pads

The variations of brake pad wear during each of the repeated tests are likely due to arbitrary occurrence of dynamic formation or detachment of secondary plateaus on the pad surfaces. Some of the wear debris was compacted and attached back to the pad contacting surface before emitting to the air. Much wear debris generated from the pad materials may be transported between the transferred films/layers on the brake rotor and the secondary plateaus on the pad surface, which leads to a longer retention for compacting and formation of larger sizes of PM before loss to the air. The PEA coating caused a significantly lower wear to the brake pads compared to bare cast iron.

7.4 Effects of PEA Coating on Wear Particles

The dimples of the PEA coating surface act as reservoirs and accommodate the fine particles to reduce airborne emission. After the stable transfer layer was formed, the wear particle sizes increased before the non-exhaust emission could occur. The enlarged size and local compaction of PM seen in the case of PEA-coated cast iron discs would cause less harm to human health. The small wear debris on the uncoated cast iron disc was generated from both the worn pad friction materials and the disc itself and then centrifugally ejected from the wear track, which indicates a higher airborne PM emission in terms of particle number and mass.

7.5 Tribological Effects of PEA Coating

7.5.1 Pad Wear Variation and COF Alteration

The formation of the secondary plateaus contributes to the growing of COF during the tribotests, which can explain that variation of the pad wear is in company with opposite COF alteration. The COFs at low temperatures (or so-called cold friction performance) are quite dependent on the materials composition of the secondary plateaus on the pad contact surface. These secondary plateaus show nearly the same mechanical properties as the hard particle does with respect to wear and the friction grows up on these areas due to the plateaus' enlarged contact areas. Less wear on the pad indicates that there are more secondary plateaus, leading to a higher COF due to enhanced interfacial shear strength of the plateaus compared to original pad surface. The difference in COF at low temperature between diverse brake pads is also determined by the possible evolution in various chemical compositions of the pad top surface during the sliding contact.

7.5.2 Wear Mechanism on PEA Coating

This dimple-like morphology of the PEA coating provides a mechanical key for the initiation and growth of a transfer layer. Through the application of coating on the cast iron disc, a step change in brake performance is seen, and more significantly a transition to adhesive-like friction is observed. In this friction mechanism, the pad materials were seen to transfer onto the surface of the treated disc, forming a compact, thin layer without any loss in friction performance. The wear debris, which is initially generated from the brake pad as abrasive particles, fills firstly the dimples and other lowland areas of the PEA coating and then is compacted to form a thin film as in compaction galling. The transferred film/layer accumulates over the whole wear track, and a transition away from

abrasive friction mode occurs as a result. The development of the transfer film, in turn means that both surfaces in the contact are effectively the same or similar materials. The friction generated in this contact is now achieved by rupture or shear of bonds identical to those in the pad material.

7.6 Future Work

This work therefore underlines the potential importance of an alumina-based coating strategy for minimizing wear and in turn debris emissions in future brake systems for sustainable and environmental benefit. However, the tribological tests in this study are not enough to assess the performance of the PEA-coated rotors completely. An adjustable high speed Pin-on-Disc tribometer can be used in high speed Pin-on-Disc tribotests. Cast iron substrate machined to have a shape of a ring could be coated by the PEA process. An uncoated cast iron ring will also be prepared as a reference. The counterface material could be the same brake pads as which in the study. During tribotest on a ring, the speed will be increased step by step. We can study the morphology and tribological performances of both PEA-coated cast iron and various types of brake pads with the change of speed in the tests. A heating element can also be added in the tribotests. The temperature of the tests can be adjusted much higher than the tribotests conducted in the room temperature in the current research. The performances of the transfer layer on the PEA coating surface in a heating situation can be studied using the heating element. The tribological behavior of the PEA coating against brake pads in the same conditions could also be studied.

The PEA coatings on commercial cast iron brake rotors are also currently preparing for brake dynamometer tests to satisfy many brake standards. There are various automotive

test standards are being used to assess the performance of the brakes such as Society of Automotive Engineers (SAE) J2522 (dynamometer global brake effectiveness), SAE J2521 (dynamometer squeal noise matrix of disc and drum brakes), SAE 2928 (brake rotor thermal cracking procedure), United Nations Economic Commission for Europe (UNECE) Regulation No. 90 (uniform provisions concerning the approval of replacement brake pad assemblies and drum brake pads for power-driven vehicles and their trailers), Federal Motor Vehicle Safety Standards (FMVSS) for disc brake NVH (noise, vibration and harshness), Type P Test for dynamic performance, Type F Test for heat fade and Type W Test for water fade of Indian Standard (IS) 14664:1999, Japan Safety Standard 12-61 and Australian Design Rule 33/00. These have various sections detailing the requirements and procedures for different types of vehicles, though the approach and methodology in general remain common. Further tests will help confirm the validity of PEA applications in actual automotive brake systems for conventional and electrical vehicles.

APPENDICES

Appendix A



RightsLink



Home

Help

Email Support

Sign in

Create Account



Alumina-Based Coating with Dimples as Enabling Sustainable Technology To Reduce Wear and Emission of the Brake System

Author: Ran Cai, Chen Zhao, Xueyuan Nie

Publication: ACS Sustainable Chemistry & Engineering

Publisher: American Chemical Society

Date: Jan 1, 2020

Copyright © 2020, American Chemical Society

PERMISSION/LICENSE IS GRANTED FOR YOUR ORDER AT NO CHARGE

This type of permission/license, instead of the standard Terms & Conditions, is sent to you because no fee is being charged for your order. Please note the following:

- Permission is granted for your request in both print and electronic formats, and translations.
- If figures and/or tables were requested, they may be adapted or used in part.
- Please print this page for your records and send a copy of it to your publisher/graduate school.
- Appropriate credit for the requested material should be given as follows: "Reprinted (adapted) with permission from (COMPLETE REFERENCE CITATION). Copyright (YEAR) American Chemical Society." Insert appropriate information in place of the capitalized words.
- One-time permission is granted only for the use specified in your request. No additional uses are granted (such as derivative works or other editions). For any other uses, please submit a new request.

[BACK](#)

[CLOSE WINDOW](#)

Appendix B



RightsLink



Home



Help



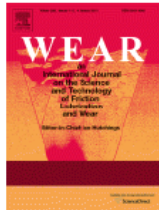
Email Support



Sign in



Create Account



Wear mechanism evolution on brake discs for reduced wear and particulate emissions

Author: Ran Cai, Jingzeng Zhang, Xueyuan Nie, Jimi Tjong, D.T.A. Matthews

Publication: Wear

Publisher: Elsevier

Date: Available online 4 April 2020

© 2020 Elsevier B.V. All rights reserved.

Please note that, as the author of this Elsevier article, you retain the right to include it in a thesis or dissertation, provided it is not published commercially. Permission is not required, but please ensure that you reference the journal as the original source. For more information on this and on your other retained rights, please visit: <https://www.elsevier.com/about/our-business/policies/copyright#Author-rights>

[BACK](#)

[CLOSE WINDOW](#)

© 2020 Copyright - All Rights Reserved | [Copyright Clearance Center, Inc.](#) | [Privacy statement](#) | [Terms and Conditions](#)
Comments? We would like to hear from you. E-mail us at customercare@copyright.com

VITA AUCTORIS

NAME: Ran Cai

PLACE OF BIRTH: Jingmen, Hubei, China

YEAR OF BIRTH: 1996

EDUCATION: Longquan High School, Jingmeng, Hubei, China
2014

Beijing Institute of Technology, B.Eng., Beijing,
China, 2018

University of Windsor, M.A.Sc., Windsor, ON,
Canada, 2020